KU LEUVEN

Biomedical Sciences Group
Faculty of Medicine
Department of Neurosciences
Laboratory for Cognitive Neurology

Graph Analysis of the Associative-Semantic Network

Yu Wang

Supervisor:
Prof. dr. Patrick Dupont
Co-supervisor:
Prof. dr. Rik Vandenberghe

Dissertation presented in partial fulfillment of the requirements for the degree of Doctor in Biomedical Sciences

September 2015

Graph Analysis of the Associative-Semantic Network

Yu WANG

Examination committee:
Prof. dr. Wim Vanduffel, chair
Prof. dr. Patrick Dupont, supervisor
Prof. dr. Rik Vandenberghe, co-supervisor
Prof. dr. Rufin Vogels
Prof. dr. Stephan Swinnen
Prof. dr. Steven Dymarkowski
Prof. dr. Daniele Marinazzo
Prof. dr. Martijn van den Heuvel

Dissertation presented in partial fulfillment of the requirements for the degree of Doctor in Biomedical Sciences

September 2015

Uitgegeven in eigen beheer, Yu Wang, Herestraat 49, B-3000 Leuven (Belgium)

Contents

List of Figures

List of Tables

Summary

Analysing networks extracted from functional imaging data has proven to be a valuable technique to investigate the complex functional structure of the human brain that influences the dynamics underlying cognition. A promising tool to rigorously study the network is graph analysis which provides a framework to characterize and to quantify the network. This thesis describes the application of graph analysis of the associative semantic network obtained using task based fMRI data and addresses some important issues in graph analysis. More specifically, we focused on explicit associative-semantic processing of words and pictures which activates a distributed set of brain areas.

First, the unweighted associative semantic network was constructed at the group-level. We applied graph analysis to characterize a system level view of this network in chapter 3. We selected regions which are activated in the main contrast of associative semantic processing versus visuoperceptual judgements and used partial correlation to quantify functional connections between nodes based on the fMRI time series. A group-level network was then constructed by given the value one to connections which are significantly different from zero ($p_{corr} < 0.05$) and zero to the remaining connections. A modularity analysis discerned two main communities: one corresponding to the classical perisylvian language system, including the superior temporal sulcus (STS), middle temporal gyrus (GTm) and pars triangularis of the inferior frontal gyrus (GFi), among other nodes. A second subsystem consisted of the left ventral occipital temporal transition zone (vOT) and the anterior fusiform gyrus along with hippocampus and the intraparietal sulcus. The two subsystems were linked through a unique connection between vOT and GTm, which were both considered as hubs of the network . In addition, the binary network exhibited small-world characteristics, which is a sign of economical and efficient information exchange.

Further, we have studied the reproducibility and robustness of various graph measures in group based and in individual binary and weighted networks for an independent group in chapter 4. The nodes of the network were taken the same as these defined in chapter 3 and the connectivity was based on the partial correlation of the time series between any pair of nodes. The network was binarized

by applying equi-density thresholds across a range of densities in this chapter to avoid network density differences which relate to different graph properties. The results showed that in case of binary networks defined at the group level, global graph measures exhibit a good reproducibility and robustness for networks which are not too sparse and these figures of merit depend on the graph measure and on the density of the network. Furthermore, these group based binary networks should be derived from groups of sufficient size and the lower the density the more subjects are required to obtain robust values. Local graph measures are very variable in terms of reproducibility and should be interpreted with care. For weighted networks, we found good reproducibility (average test-retest variability $< 5\%$ and ICC values > 0.4) when using subject specific networks and this will allow us to relate network properties to individual subject information. These findings redirected our focus to weighted global graph metrics in the following chapters.

Because of the limitations of existing weighted generalizations for the clustering coefficient and local efficiency in weighted networks, we then proposed in chapter 5 new weighted generalizations which also apply in case of a fully weighted network. Our approach outperformed existing generalizations in terms of general versatility, weight-scale invariance, continuity and overall robustness.

We then investigated in chapter 6 the effect of granularity of the associative semantic network on the resulting graph measures as well as on the modular structure and the identification of hubs. Fully weighted network analysis based on partial correlations between fMRI time series was conducted. We found that graph measures are depending on the granularity level. However, this dependency on the granularity level can be greatly diminished by normalizing the networks by equivalent random networks. Small world topology of the associative semantic network was found across all levels of granularity which has been investigated. Part of the modular structure and some hubs are consistent as well across levels of granularity.

In chapter 7 we used the data obtained in early Alzheimer's disease patients to examine possible global alterations related to the disease compared to elderly normal controls. To improve the between group comparison with individual specificity, we adapted the parcellation algorithm used in the previous chapter to study the granularity effect so that the group based parcellation can be taken from an independent study while allowing subject specific adaptations of the parcellations. In this way, the AD group and the normal control group were analysed in the same way while allowing for different adaptations of the parcels. We found that the fully weighted task-based associative-semantic network demonstrated an increased connectivity, preserved global network topology characteristics in early-stage AD compared to matched healthy elderly controls.

Finally, in chapter 8 we will give a general discussion and formulate the conclusions of this thesis.

Samenvatting

De analyse van netwerken afkomstig van functionele beeldvormingdata laat ons toe om de complexe functionele structuur van de menselijke hersenen te bestuderen. Die organisatie bepaalt uiteindelijk ook de onderliggende dynamica van cognitieve processen. Graafanalyse is een veelbelovende techniek, aangezien het een kader biedt waarbij netwerken gekarakteriseerd en gekwantificeerd kunnen worden. Deze thesis biedt een beschrijving van de applicatie van graafanalyse van het associatief-semantisch netwerk. Dat netwerk werd verkregen aan de hand van van taakgebaseerde functionele magnetische resonantiebeeldvorming, waarbij woorden en beelden werden gebruikt. Daarnaast werd tijdens dit proces een gedistribueerde verzameling van verschillende hersengebieden geactiveerd. Verder worden enkele belangrijke punten behandeld die specifiek van toepassing zijn op de graafanalyse.

Allereerst werd een ongewogen associatief-semantisch netwerk gecreerd op het niveau van de groep. In hoofdstuk drie wordt dat netwerk gekarakteriseerd op systeemniveau. Hierbij werden regios geselecteerd die geactiveerd werden tijdens de vergelijking van associatieve semantische verwerking van woorden of beelden, met de visuoperceptuele beoordeling van de stimuli. Die regios werden als knooppunten van het netwerk gebruikt en de connectie hiertussen werd berekend op basis van de partile correlaties van de tijdreeksen in die knooppunten. Op groepsniveau werd bepaald of deze connectie significant verschilde van nul en in dat geval werd de connectiviteit op 1 gezet. De andere connecties kregen de waarde 0. Bij de modulariteitsanalyse werden twee belangrijke modules gevonden. Een ervan kwam overeen met het klassieke perisylvische taalsysteem, waarin naast nog enkele andere knooppunten ook de superieure temporale sulcus (STS), de middelste temporale gyrus (GTm) en de pars triangularis van de inferieure frontale gyrus (GFi) waren inbegrepen. De tweede module bestond uit de linkse ventrale occipitale temporale transitiezone (vOT), de anterieure fusiforme gyrus, de hippocampus en de intraparietale sulcus. De twee subsystemen worden verbonden door een unieke connectie tussen vOT en GTm en beide knooppunten werden bovendien gedentificeerd als hubs in het netwerk. Daarenboven vertoonde het binair netwerk small world karakteristieken, wat een teken is van economische en efficinte informatie-uitwisseling.

Verder werden de reproduceerbaarheid en de robuustheid van de verschillende graafmaten bestudeerd. Dat gebeurde niet enkel voor binaire groepgebaseerde netwerken, maar ook voor de individuele gewogen netwerken. Deze studie werd uitgevoerd bij een andere groep van proefpersonen en kan teruggevonden worden in hoofdstuk vier. Tijdens deze analyse werden dezelfde knooppunten gedefinieerd als in hoofdstuk drie, waarbij de connectiviteit opnieuw gebaseerd was op de partile correlaties tussen tijdsreeksen in de verschillende knooppunten. De netwerken werden gebinariseerd door het toepassen van meerdere drempelwaardes en elk ervan kwam overeen met een bepaalde dichtheid. Op die manier werd voorkomen dat de graafmaten van netwerken met verschillende dichtheid vergeleken zouden worden. In het geval van binaire netwerken, die op groepsniveau werden gedefinieerd, toonden de resultaten aan dat de globale graafmaten een goede reproduceerbaarheid en robuustheid vertoonden indien het netwerk voldoende dicht was en de groep voldoende groot. De kwaliteit van deze eigenschappen hing af van de graafmaat en de dichtheid van het netwerk. Zo waren er meer subjecten nodig om een robuust en reproduceerbaar netwerk te definiren wanneer de dichtheid lager was. Lokale graafmaten varieerden in reproduceerbaarheid en dienen dan ook met enige voorzichtigheid te worden genterpreteerd. Voor gewogen individuele netwerken werd een goede reproduceerbaarheid gevonden met een test-retest variabiliteit kleiner dan 5% en ICC waarden groter dan 0.4. Dat laat toe om graafmaten te relateren aan andere subjectspecifieke informatie. Als gevolg van die bevinding, werd in de volgende hoofdstukken de aandacht gericht op gewogen globale graafmaten.

Aangezien de bestaande gewogen uitbreidingen van de clusteringcofficint en lokale efficintie onvoldoende zijn voor gewogen netwerken, werden in hoofdstuk vijf nieuwe veralgemeningen van deze maten voorgesteld die toepasbaar zijn in het geval van volledig gewogen netwerken. Die uitbreidingen zijn superieur ten opzichte van bestaande op het vlak van veralgemening, schaalinvariantie van de gewichten, continuteit en algemene robuustheid.

Vervolgens werd in hoofdstuk zes het effect van de granulariteit van het associatief-semantisch netwerk op de graafmaten bestudeerd. Dat effect werd ook nagegaan voor de modulaire structuur van het netwerk en voor de identificatie van hubs. De granulariteit werd bepaald door het detail van de opdeling van alle voxels in regios op basis van een datagedreven techniek, die voorheen beschreven was in de literatuur voor toepassingen bij rust fMRI. Het volledig gewogen netwerk was gebaseerd op de partile correlaties tussen de gemiddelde tijdsreeksen in de verschillende regios. Er werd gevonden dat graafmaten afhingen van de granulariteit, maar dit effect verdween grotendeels na normalisatie van graafmaten door equivalente willekeurige netwerken. Bovendien werd de small world topologie van het associatief-semantisch netwerk behouden voor de verschillende niveaus van granulariteit die onderzocht werden. Daarnaast waren een deel van de modulaire structuur en een aantal hubs consistent tussen de verschillende niveaus van de granulariteit.

In hoofdstuk zeven werd het associatief-semantisch netwerk, verkregen in Alzheimerpatinten, bestudeerd met graafanalyse om eventuele veranderingen ten

gevolge van de ziekte te bepalen door de vergelijking te maken met oudere, normale proefpersonen. Om de resultaten van beide groepen goed te kunnen vergelijken, werd het parcellatie-algoritme, gebruikt in vorig hoofdstuk, aangepast. Hierdoor kon er gestart worden met een groep-gebaseerde parcellatie, verkregen in een onafhankelijke groep van proefpersonen, maar waarbij subjectspecifieke aanpassingen van deze parcellaties mogelijk waren. Zo werd de groep van Alzheimerpatinten en de groep van oudere normale controles op dezelfde manier verwerkt. In deze studie werd, in vergelijking met gezonde oudere controlepersonen, een verhoogde connectiviteit gevonden van het volledig gewogen associatief-semantisch netwerk in vroegtijdige Alzheimerpatinten. De globale netwerktopologie bleef behouden. Ten slotte wordt in hoofdstuk acht een algemene discussie vooropgesteld en worden conclusies over de bevindingen van deze thesis geformuleerd.

1 Introduction

This chapter aims at introducing the associative semantic processing in the human brain and the advantages of using graph theoretic approaches to study this process. Section 1.1 therefore focuses on providing the reader with some general background about the different aspects relating to this thesis. First, a general description is given about the associative semantic processing and functional magnetic resonance imaging. Subsequently, we introduce connectivity and graph theory as the main methodology in this thesis. In addition to this background, the general aims of the thesis are defined in section 1.3 and the structure of the thesis is outlined in section 1.4.

1.1 Background

There are several steps to take to conduct a graph theoretical analysis of associative semantic networks (Figure 1.1). For better understanding of the analyses conducted in this thesis, some basic background of associative semantic processing and the employed neuroimaging methods is indispensable. This background thus touches briefly several of these physiological and methodological aspects.

1.1.1 Associative Semantic Processing

Our brain is not wired to understand everything. Semantic processing is the process to encode information in the mind and wove into meaning. Where and how information is coded and interpreted in our brain is an important question for mankind, especially for those who are suffering a neurodegenerative disease. A huge amount of studies have put their effort to decipher this puzzle. In our lab, the paradigm used to study associative-semantic processing was derived from the pyramids and palm trees test (Howard and Patterson, 1992; Adamczuk et al., 2014). During the associative semantic task, the stimuli within each triplet belonged to the same category, and subjects matched the stimuli for meaning.

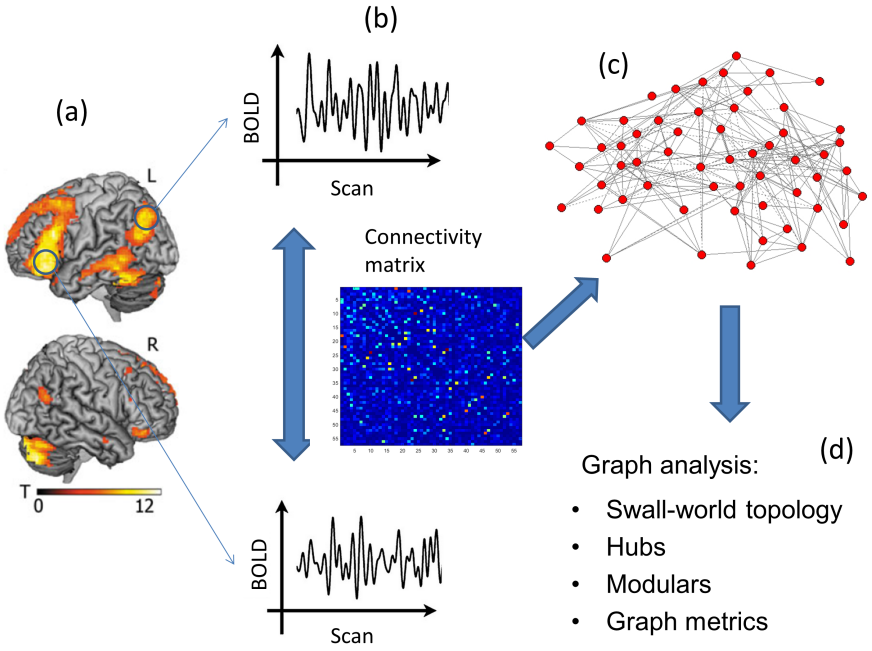

Figure 1.1: Schematic illustration of the graph network analysis. The first step (a) consists of obtaining fMRI data and defining the nodes of the graph. The second step (b) quantifies the temporal interactions between the filtered fMRI BOLD time-series of all nodes and constructs a connectivity matrix. (c) This connectivity matrix is then transformed to a binary or weighted graph. (d) Finally, graph theoretical tools are applied to investigate network properties, small world topology, hubs, modules etc.

During the baseline condition (visuoperceptual task), they matched stimuli for physical size. The stimuli were either shown as words or pictures (Figure 1.2).

Univariate statistics (see 1.1.2) revealed a systematic activation of regions for associative semantic tasks versus the visuoperceptual conditions (main effect of task, Figure 1.3a) in the left ventral occipital temporal transition zone (vOT) (Vandenberghe et al., 1996; Buckner et al., 2000; Van Doren et al., 2010; Seghier and Price, 2011), the left posterior middle temporal gyrus (Vandenbulcke et al., 2007; Whitney et al., 2011), the anterior temporal pole (Vandenberghe et al., 1996), the left ventral anterior temporal cortex (Visser et al., 2012a) and the left anterior inferior frontal gyrus (Goldberg et al., 2007). Some of the regions which may be invoked during a wider variety of tasks are also activated: the inferior frontal sulcus (Wagner et al., 1997; Van Doren et al., 2010), the middle frontal gyrus (Vandenberghe et al., 1996), and the intraparietal sulcus.

The interaction between task and input modality revealed word-specific acti-

vation during the semantic compared with the visuoperceptual task in the left superior temporal sulcus (STS) (Vandenberghe et al., 1996; Vandenbulcke et al., 2007) (Figure 1.3b). Picture-specific semantic activation occurred bilaterally in the ventral occipitotemporal cortex extending to the superior occipital gyrus and in the right inferior frontal gyrus (Adamczuk et al., 2014) (Fig. 1.3c).

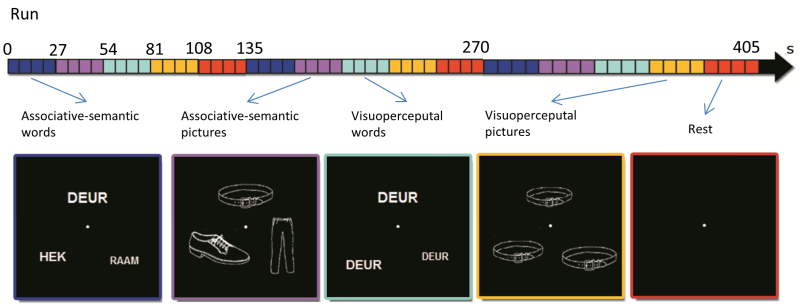

Figure 1.2: Stimuli and tasks in the fMRI experiment using the associative-semantic paradigm. The arrow in top of the figure shows a timeline of 1 fMRI run, with five condition indicated in different colours: associative-semantic task with words (blue) and with pictures (purple); visuoperceptual task with words (cyan) and pictures (yellow); resting baseline with fixation point (red). Subjects were asked to press a left- or right-hand button depending on which of the 2 lower stimuli matched the upper stimulus more closely in meaning (blue, purple) or in size (cyan, yellow) on the screen. A given concept triplet was presented in either the word or the picture format, and this was counterbalanced across subjects. The order of conditions was randomized for each run and subject. Translation: deur = door, hek = fence, raam = window. Figure adapted from (Adamczuk et al., 2014).

The brain utilizes a complex web of circuits to perform semantic processing, mostly in the left hemisphere. Until recently, these studies were mainly focusing at the regional level and less is known about how information is integrated and transferred between regions.

1.1.2 Functional magnetic resonance imaging

By virtue of its non-invasive nature and relative good spatial resolution, functional magnetic resonance imaging (fMRI), primarily based on the blood oxygenation level dependent (BOLD) effect, is the most widely used method in the field of mapping brain functions (Buxton, 2009). The BOLD effect, a local increase of the MR signal during increased neuronal activity, arises due to two phenomena (Figure 1.4). The first is the subtle change in magnetic field when haemoglobin

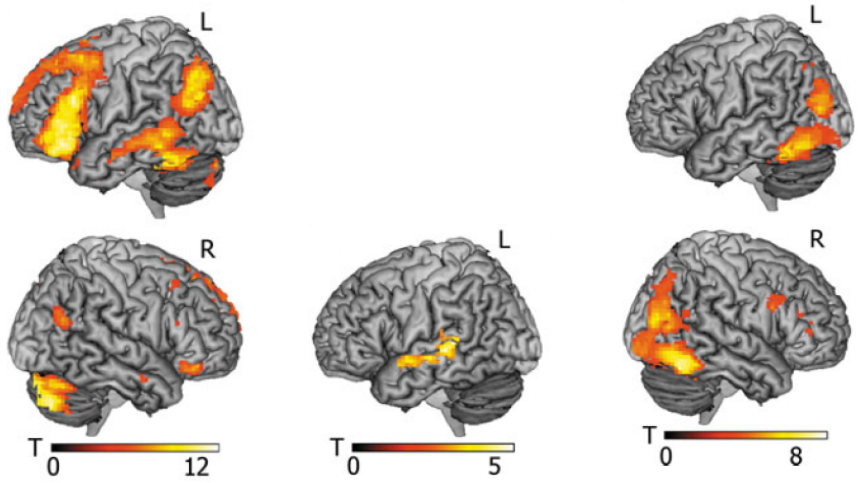

(a) (b) (c)

Figure 1.3: (a) Main effect of associative-semantic task minus visuopercetual task. (b) Effect of semantic words ([associative-semantic task with words - visuoperceptual task with words] - [associative-semantic task with pictures - visuoperceptual task with pictures]). (c) Effect of semantic pictures ([associative-semantic task with pictures - visuoperceptual task with pictures] - [associative-semantic task with words - visuoperceptual task with words]). Shown activations are significant at the threshold of voxel-level $P_{uncorr} = 0.001$ combined with cluster-level $P_{corr} = 0.05$. The colour scales indicate the T-values for the contrasts. Figure adapted from (Adamczuk et al., 2014).

becomes deoxyhaemoglobin after supplying oxygen to the brain regions depending on their need: the MR signal decreases when the blood becomes less oxygenated. The second is the increased oxygenation in venous blood despite the increase of the oxygen metabolic rate ($CMRO_2$) when an area of brain is activated. This is due to the fact that blood flow increases much more than $CMRO_2$. MR images capturing BOLD effect will therefore be brighter in active brain regions with the gradient echo planar imaging (EPI) sequence.

However, detecting activations with fMRI is complicated due to the fact that increase in BOLD response related to neuronal activations is limited (2-5 % of the total signal). That's why careful preprocessing and statistical analyses are important.

Preprocessing refers to a series of steps aimed at increasing signal to noise ratio, correcting for sampling error and preparing data for later analysis. Noise can arise from different sources such as movement, subject, scanner etc. Preprocessing of fMRI data typically contains motion correction, slice timing correction, coregistration with a structural MRI scan, normalization to a common space and smoothing.

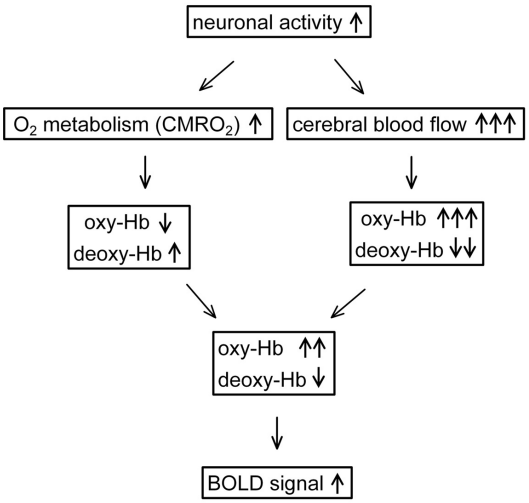

Figure 1.4: Physiology of the hemodynamic response during increased neuronal activity. Figure adopted from (Lindauer et al., 2010)

Statistical analysis can be implemented with different pipelines (Figure 1.5) which can be differentiated primarily based on whether a pre-defined model is involved (model-based vs. model-free) and whether the analysis is conducted independently for each voxel (univariate vs. multivariate).

Currently, the dominant pipeline is the model-based univariate analysis as implemented within the General Linear Model (GLM). GLM models the BOLD response and specifies the parameters of the model. The result of the GLM analysis is a statistical map for the measured change in BOLD in response to a certain experimental manipulation. By thresholding the statistical map, brain regions which are activated can be revealed (Figure 1.3). Although GLM studies have enabled us to make considerable progress, our understanding is partly contingent upon the assumptions made by the model (Turk-Browne, 2013). The GLM approach is applied to all voxels and assumes independence between them, whereas the underlying areas and tissues are not (Turk-Browne, 2013).

Multivariate pattern analysis (MVPA) is a model-free approach and it captures patterns of activation across voxels (Figure 1.5) (Bruffaerts et al., 2013b,a; Liuzzi et al., 2015). However, one limitation of MVPA is that it remains focusing on activation and thus ignores interactions in the brain.

Connectivity studies, which are primarily based on the internal structure of the data and which do not have to be linked to the experimental design, will be discussed in a later section.

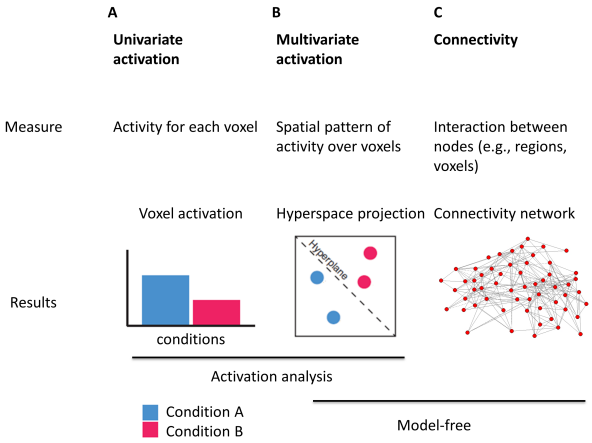

Figure 1.5: Types of fMRI statistical analysis. (A) Univariate activation refers to the average amplitude of BOLD activation evoked by an experimental condition. (B) Multivariate classifiers are trained on patterns of activation over voxels to decode distributed representations for specific events. (C) Connectivity is the temporal interaction (e.g. correlation) between nodes, which can be defined as regions or voxels in the brain. Figure adapted from (Turk-Browne, 2013).

1.1.3 Connectivity network

The debates regarding functional specialization/segregation versus functional integration have a long history (Poldrack et al., 2011); that is whether our mental functions reside in specific brain regions or instead recruit regions distributed over the entire brain. Whereas functional specialization is the dominant view in neuroimaging studies, there is also increasing recognition that the function of each of these regions should be integrated in order to achieve a coherent mental function and behaviour. Brain connectivity analysis, which provides a framework to understand the interaction of spatially remote brain regions in a non-invasive way, stimulates an enormous amount of researches recently. Connectivity studies can be conducted at the structural (diffusion tensor imaging, structural MRI etc.) and at the functional (electroencephalography, fMRI etc.) level. Functional connectivity (FC) studies have documented reliable changes in human functional brain maturity over development (Dosenbach et al., 2010). An increasing number of pathologic conditions are found to be related to the alterations in the functional connectivity between certain brain regions (Power et al., 2011; Brown et al., 2011).

Resting-state functional connectivity is the most common application of functional connectivity by examining low-frequency interactions in BOLD signals while participants are at rest. Distinct resting-state networks have been identified, such as the default mode network (DMN), hearing, language, and salience networks (Power et al., 2011). DMN is a set of brain regions that typically deactivate during

performance of cognitive tasks (Greicius et al., 2009). The popularity of resting-state analysis roots in the fact that resting-state data can be easily collected and compared across research sites, especially for patients with neurodegeneration (Turk-Browne, 2013). Despite these advantages, resting state fMRI cannot replace task-based fMRI when studying cognitive processes in the brain.

In contrast with the general consensus on processing fMRI data with a pre-defined model (e.g. GLM), the field of model-free connectivity analysis is still in a highly creative period. Constructing the brain's connectivity networks often consist of identifying a set of nodes and estimating the connections or edges or "links" between these nodes. Henceforth we will briefly scratch the surface of the two aspects.

Nodes

Defining nodes which represent brain regions with coherent patterns of extrinsic anatomical or functional connections is the first step in network analysis. Ways to define nodes vary. Region-based nodes obtained from activation in task-fMRI or from brain atlases such as the automatic anatomic labelling atlas (AAL) (van den Heuvel et al., 2010; Achard et al., 2006) is one option. While region based networks represent a coarser macroscopic organization of the brain, a voxel-based analysis by treating each voxel as a node can give insight into the functional connectivity of the brain in a microscopic view (Buckner et al., 2009; Cecchi et al., 2007; Eguluz et al., 2005). An alternative is to apply connectivity-based parcellation to identify functionally homogeneous regions using methods such as Independent component analysis (ICA). However, the difficulty in matching ICA components across subjects and the ignorance of subject specific idiosyncratic effects in group ICA makes this technique difficult to use in network analysis. In addition, group ICA analysis is often performed by concatenating or averaging time across subjects. Although modelling the same biological system, the human brain, striking differences have been reported between different approaches (Rubinov and Sporns, 2010). For example, voxel-based network analysis by treating each voxel as a node (Hayasaka and Laurienti, 2010) are reported to be better in further localization of highly connected nodes or hubs within the anatomical areas identified by region-based analysis.

Edges

Given a set of nodes, the next step is to quantify the interaction between these nodes by neurobiological interpretable quantities. Many approaches have been used to define the synchrony between signal responses in spatially distinct brain regions: (1) Correlation coefficient between time course of brain regions (or with that of the seed region) (Schwarz and McGonigle, 2011; Hayasaka and Laurienti, 2010; van den Heuvel et al., 2008); (2) Correlation between wavelet components (Wang et al., 2013; Achard et al., 2006; Achard and Bullmore, 2007); (3) Mutual information (Smith et al., 2011); (4) Beta-series correlation to investigate trial-by trial fluctuation (Rissman et al., 2004).

However, there are some issues with the methods above. First, a third-party involvement may exist and can lead to spurious connections. For example, if two disconnected regions both connect with a third region, then the third region can drive the correlation between the two other regions. This can be avoided by applying partial correlations instead. Partial correlations isolate the signal specific to a pair of regions to disambiguate direct links from indirect effects and turns out to be an effective way to model the connectivity (Smith et al., 2011). Second, although functional connectivity elucidates the interactions between brain regions, the directionality of the information flow is still unknown. Methods have been proposed to investigate directed connectivity, such as structural equation modelling (SEM) (Smith et al., 2011; Karunanayaka et al., 2014), dynamic causal modelling (DCM) (Smith et al., 2011; Seghier and Friston, 2013; Di and Biswal, 2014), granger causality (Smith et al., 2011; Wen et al., 2013) and so on.

Despite these fancy ideas of understanding the brain in a better way, there are aspects of fMRI rendering inference of directionality very challenging. The signal measured in fMRI depends on the blood oxygenation level dependent (BOLD) signal, which has noise and systematic distortions (such as hemodynamic delays) and a slow response to the neuronal activity and therefore, it can be problematic in estimating directionality (Ramsey et al., 2010). Take granger causality for example, it quantifies the temporal precedence to predict the current values of various brain regions based on their past values. Thus latency differences across different brain regions, low-sampling rates and noise of fMRI hinder its neural interpretability (Wen et al., 2013). Furthermore, the powerful inference from directionality of effective connectivity comes at the cost of making much stronger assumptions (both SEM and DCM assume a priori specification of a structural model). The major shortcoming of the field thus concerns with the validity of the assumptions, which are often poorly specified and difficult to check.

1.1.4 Graph theory

> *"The origins of graph theory are humble, even frivolous. Whereas many branches of mathematics were motivated by fundamental problems of calculation, motion, and measurement, the problems which led to the development of graph theory were often little more than puzzles, designed to test the ingenuity rather than to stimulate the imagination. But despite the apparent triviality of such puzzles, they captured the interest of mathematicians, with the result that graph theory has become a subject rich in theoretical results of a surprising variety and depth."*
>
> –N. L. Biggs, E. K. Lloyd, and R. J. Wilson (Biggs et al., 1986)

As a mathematical technique, graph theory dates back to over two hundred years, when Leonhard Euler solved a popular puzzle on the Königsberg bridges in 1735 (Euler, 1741; Biggs et al., 1986; Alexanderson, 2006; Fornito et al., 2013). Königsberg (now Kaliningrad) was an East Prussian city with Pregolya River passing through. The branches of the river subdivided the city into several isolated

sections which were connected by seven bridges (Figure 1.6a). The puzzle posed was this: is it possible to devise a path crossing each of the seven bridges exactly once and return to the starting point?

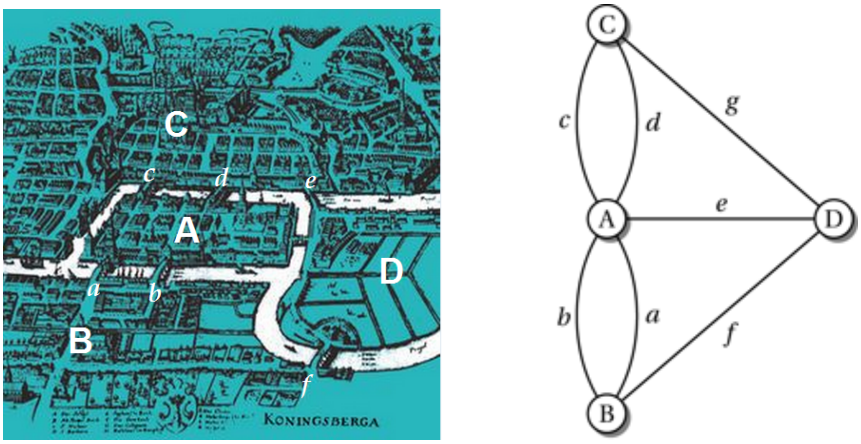

(a) (b)

Figure 1.6: Königsberg Bridge problem. (a) shows the river Pregel and its branches subdivided the city into four separate parts (A-D) which were connected by seven bridges (a-f). (b) is the graphical representation of (a). Figure adopted from (Biggs et al., 1986; Sporns, 2011).

In 1735, Euler presented his solution by using locations as nodes and bridges as edges of a graph (figure 1.6b). He proved mathematically that it is impossible to have a path crossing the seven bridges in a single journey and generalized the scenario: a connected graph has a path traversing each edge exactly once if exactly zero or exactly two nodes have odd degree. Euler's work has been published as "Solutio problematis ad geometriam situs pertinentison" (translation: The solution of a problem relating to the geometry of position) later in 1741.

Since then, graph theory has been applied in fields ranging from computer science to physics, biology, chemistry and social sciences. The advancing technique in analysing a wide range of complex systems has led to a fundamental insight: many complex systems often share certain topological characteristics, and these can be captured by graph theoretical metrics (Barabasi and Oltvai, 2004; Amaral and Ottino, 2004; Bullmore and Sporns, 2009; Fornito et al., 2013). A detailed description of graph theoretical measures will be provided in chapter 2.

Small worldness

A hallmark of many current graph studies is the influx of interests in the small-world topology. Originally described in social networks, the small world concept describes the fact that despite their often large size, in most networks there is a relatively short distance between any two nodes (Watts and Strogatz, 1998; Albert

and Barabási, 2002). The distance is the number of connections that must be traversed to connect two nodes. In other words, all nodes in a small-world system can be reached through relatively few intermediate steps, despite the fact that only a few direct connections are attached to most nodes. Small-world organization is intermediate between random and regular (lattice) networks. A Regular network embodies a high-level of clustering with a long distance between nodes, while a random network features low-level of clustering with a short distance.

The small-world topology is an attractive model for the organization of brain anatomical and functional networks because it entails both specialized and integrated information processing. Moreover, small-world topology is economical, featuring a reduced cost of maintaining many connections with the ability to support efficient information exchange (Achard and Bullmore, 2007).

Evidence for small-world attributes has been reported in a wide range of studies of genetic, signalling, communications, Internet, computational and neural networks (Achard et al., 2006; Micheloyannis et al., 2006, 2009; He et al., 2007b; Batalle et al., 2012). These studies indicate that many networks in natural systems have non-random/non-regular or small-world architectures.

Segregation: communities

Another appealing picture is the network segregation: a graph can be decomposed into communities or modules with larger number of intra-modular connections compared with inter-modular connections (Figure 1.7). Given a network, detecting communities refers to finding groups of nodes that are more closely related internally than with the rest of the network. Such arrangement of connections in networks tends to generate statistical dependence of signals within communities and independence between modules, and hence promotes functional segregation (Sporns, 2013). Such architectures are hallmarks of many complex systems (Simon, 1996). Communities within networks are usually unknown, can be of unequal size and with hierarchies. Partitioning a network into communities can give information about the underlying structure. The concept can also be used for a more compact representation of the network, for instance for visualizations.

Integration: hubs

Hubs, in an intuitive sense, are pivotal in facilitating network traffic and maintaining network integration (Figure 1.7): routers connecting many computers are more important in the Internet system; high-volume airfields are more powerful in facilitating air transportation. Hubs gain their influence in the network by virtue of the number and positioning of their contacts. Losing such nodes will have catastrophic consequences to network functions. The manner in which individual nodes are embedded within the overall network is thus evaluated. Hubs can also be classified as provincial and connector hubs by their roles in the modularity structure (Sporns et al., 2007; Power et al., 2013). Provincial hubs are local hubs with most of its connection within their own module. Connector hubs, on the other hand, are global hubs bridging different modules.

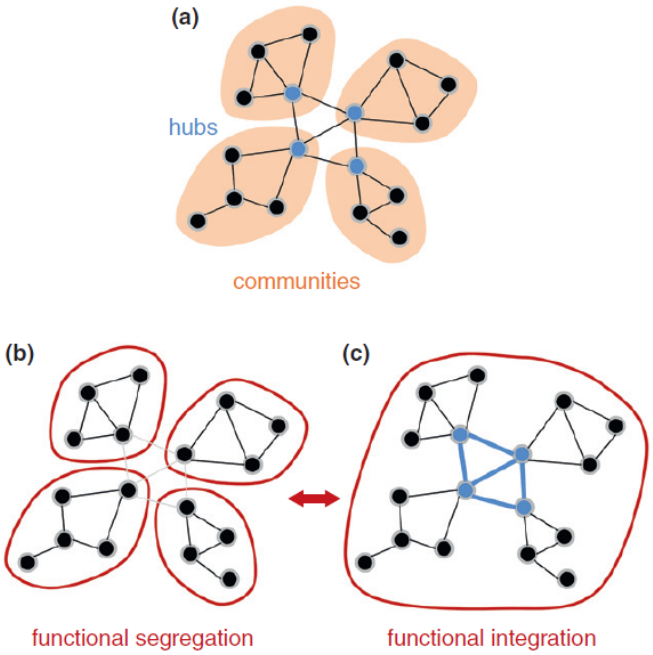

Figure 1.7: Communities and hubs, segregation and integration. (a) Schematic diagram showing a set of nodes and edges arranged into a network comprised of four network communities (orange) interconnected by highly connected and highly central network hubs (blue). (b) Functional segregation indicated by strong functional coupling within communities (red) with little or no functional coupling across communities. (c) Functional integration indicated by globally strong functional coupling, including strong information flow across network hubs and their mutual interconnections (blue). Figure adopted from (Sporns, 2013)

.

Application to neuroscience

The use of graph theoretical tools to study brain connectivity has proceeded at a phenomenal rate in recent years. Applying graph theory to networks extracted from functional imaging data has proven to be a promising tool to investigate the complex functional structure of the human brain that influences the dynamics underlying cognition and emotion. The potential to characterize the entire brain connectivity in a way that is both biologically meaningful and related to normal and disordered function makes these graph theoretical approaches attractive to clinical and basic research. This provides a framework to characterize and to quantify networks. Many non-trivial graph characteristics, such as small-worldness, modularity and hubs have been observed with some consistency in human brain networks in all modalities of neuroimaging data and over a range of spatial and temporal scales (Achard et al., 2006; Micheloyannis et al., 2006, 2009; van den

Heuvel et al., 2008; He et al., 2007b; Meunier et al., 2009b). Network metrics have been found to be heritable and to change with normal ageing (Wang et al., 2010; Micheloyannis et al., 2009). Clinical studies have identified abnormalities of network configuration in patients (Bassett and Bullmore, 2009). Differences in graph properties have been found in people with Alzheimer's disease (Wang et al., 2013) and schizophrenia (van den Heuvel et al., 2010; Micheloyannis et al., 2006; Ma et al., 2012). Changes in graph measures were also found during motor learning (Heitger et al., 2012) and taking nicotine (Wylie et al., 2012). The functional-segregation structure highlights sub-systems that match well the known brain networks and reveals the functional interactions between sub-systems (Power et al., 2011; Meunier et al., 2009b). All these studies suggest that graph analysis can be a promising tool in clinical and basic research to characterize brain connectivity.

1.2 Aims of the thesis

As should be clear from the above background, the associative-semantic network is complex not only for the distributed brain regions involved in the process but also because of the even more connections between them. The aim of this thesis is to apply graph theoretical tools to investigate associative-semantic network. More specifically: (1) To characterize the associative-semantic network in terms of graph metrics; (2) To determine the reproducibility and robustness of the network; (3) To perform a network granularity analysis; and (4) To compare network properties between elderly normal controls and patients.

1.3 Chapter-by-chapter overview

The contents of the chapters nicely follow the different aims of the project.
Chapter 2 focuses on the technical background of graph analysis and some extensions we proposed.
In Chapter 3, we apply graph analysis to the associative-semantic network and we identify the modular structure and hubs of the network.
In Chapter 4, we evaluate the reproducibility and reliability of the graph analysis for the associative-semantic network.
In Chapter 5, we propose new weighted generalizations of clustering coefficient and local efficiency for the fully-weighted network.
In Chapter 6, we analyse the effect of granularity on the graph analysis.
In Chapter 7, the methods we developed so far are applied to AD patients and we compare the network properties between normal controls and patients.
In Chapter 8, we give a general discussion of the work presented in this thesis and formulate the conclusion. Finally, suggestions for future work are formulated.

2

Graph theoretical measures

Graph theoretical measures may characterize one or several aspects of global and local network properties. In this chapter, we describe measures that capture aspects of network integration and segregation, quantify importance of individual nodes and characterize patterns of local connectivity. Networks have many variants: it can be constructed as binary or weighted, directed or undirected networks. This chapter will focus on binary and weighted undirected graphs with no self-connections.

2.1 Binary Graph characterization

The connections in the binary undirected network either exist or not. Let G denote the set of nodes in the network and N represent the number of nodes in the network. A is the adjacency matrix where a_{ij} shows the connection status between node i and j and $a_{ij} = 1$ if the a connections exists $a_{ij} = 0$ otherwise. Nodes which have a non-zero connection to node i are called the neighbours of i.

2.1.1 Binary Graph measures

A basic and important graph measure to start with is the node degree. The degree k_i of an individual node i is the sum of the number of connections attached to that node, which is also the count of neighbours of that node:

$$k_i = \sum_{j \in G} a_{ij} \tag{2.1}$$

It has a straightforward interpretation: nodes with a high degree are interacting more with many other nodes in the network. The mean network degree is directly related to the density, which is the ratio of the number of existing connections to the total number of possible connections in the network. Density can also be referred to as wiring cost.

The local clustering coefficient C_i for an individual node i is quantified as the fraction of triangles (for example triangle $N_2 - N_1 - N_3$ in Figure 2.1) divided by the total number of possible triplets around i (in our example $N_4 - N_1 - N_3$, $N_2 - N_1 - N_3$ and $N_4 - N_1 - N_2$ in Figure 2.1):

$$C_i = \frac{2t_i}{k_i(k_i - 1)} \tag{2.2}$$

where t_i indicates the number of triangles around i and k_i is the degree of i. Averaging C_i over all nodes of the network hence reflects, on average, the degree in which nodes in a graph tend to cluster together.

Paths are sequences of distinct nodes and edges and represent potential routes of information flow between pairs of nodes. The shortest path length d_{ij}, which amounts to the shortest geodesic distance between nodes i and j, consequently estimate the potential for information integration.

$$d_{ij} = \sum_{a_{uv} \in g_{i \to j}} a_{uv} \tag{2.3}$$

where $g_{i \to j}$ is the shortest geodesic path between nodes i and j, $d_{ij} = \infty$ for all disconnected pairs (i, j). The average path length L_i of node i is defined as the average of the shortest path from i to all other nodes:

$$L_i = \frac{\sum_{j \in G, j \neq i} d_{ij}}{N - 1} \tag{2.4}$$

The characteristic path length L, calculated as the average of L_i over all nodes thus quantifies the network's integration globally (Watts and Strogatz, 1998).

Averaging the inverse shortest path lengths gives a measure known as the global efficiency (Latora and Marchiori, 2001).

$$E = \frac{1}{N} \sum_{i \in G} E_i = \frac{1}{N} \sum_{i \in G} \frac{\sum_{j \in G, j \neq i} d_{ij}^{-1}}{N - 1} \tag{2.5}$$

where E_i is the efficiency of node i.

Although the inverse of the characteristic path length can be a good approximation of E, there is a fundamental difference between the two. E is the efficiency of a parallel system (i.e. packets of information is exchanging concurrently in parallel), while $\frac{1}{L}$ measures the efficiency of a sequential system (i.e. only one packet of information is transferring) (Latora and Marchiori, 2001). Furthermore, the global efficiency is considered as a superior measure of integration over characteristic path length by some authors (Achard and Bullmore, 2007). Because paths to disconnected nodes will be set to infinite, the global efficiency is consequently meaningful for disconnected networks, which is not the case for the characteristic path length. This can be solved by calculating the characteristic path length for the connected network without taking into consideration the isolated nodes as well. Furthermore, the global efficiency is primarily driven by short paths whereas

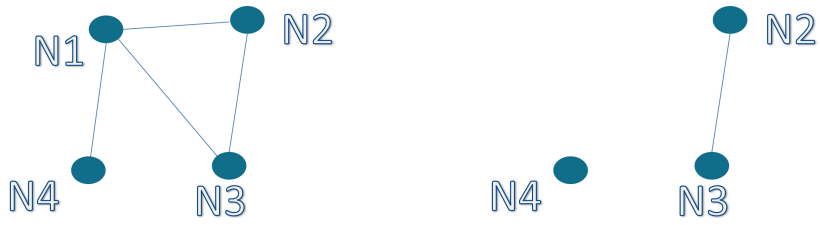

(a) (b)

Figure 2.1: Example of a simple graph. (a) The network consists of four nodes and four edges. (b) The subgraph G_{N_1} of node N_1.

the characteristic path length is influenced more by long paths (Rubinov and Sporns, 2010).

The local efficiency of a node i is defined as the global efficiency of the local subgraph (G_i) (fig. 2.1b), which contains only the neighbours of i:

$$E_{loc,i} = E(G_i) = \frac{1}{k_i(k_i-1)} \sum_{j,h;j\neq h} a_{ij}a_{ih}[d_{jh}(G_i)]^{-1} \tag{2.6}$$

where G_i is the subgraph, $d_{jh}(N_i)$ is the shortest distance between j and h in subgraph G_i. Local efficiency, which shows how fault-tolerant the system is at a local level, measures the averaged efficiency of the first-order neighbourhoods (Latora and Marchiori, 2003). Local efficiency plays a role similar to the clustering coefficient C, which is the intuitive measures of how well connected a cluster is (Newman, 2001). It has been shown that C is a good approximation of E_{loc} for graphs where most of the subgraphs G_i are non-sparse.

Node betweenness centrality is the fraction of all shortest paths in the network that pass through a given node (Freeman, 1977; Kintali, 2008).

$$b_i = \frac{1}{(N-1)(N-2)} \sum_{j,h\in G, h\neq j, h\neq i, i\neq j} \frac{\rho_{hj}(i)}{\rho_{hj}} \tag{2.7}$$

where ρ_{hj} is the number of shortest paths between h and j, and $\rho_{hj}(i)$ is the number of shortest paths between h and j that pass through i. Nodes with high values of betweenness centrality participate in building a large number of shortest paths. Bridging nodes that connect disparate parts of the network often have a high betweenness centrality.

2.2 Weighted graph characterization

In the weighted network, edge (i, j) is associated with weight w_{ij}. Henceforth, weights are assumed to be normalized ($0 \leq w_{ij} \leq 1$ for all i and j) (Rubinov and Sporns, 2010). The elements of a_{ij} in adjacency matrix A will be set to zero if $w_{ij} = 0$ and to one otherwise.

Besides the node degree, we can define the node strength in a straightforward way:

$$s_i = \sum_{j \in G} w_{ij} \tag{2.8}$$

The shortest weighted path length between i and j can be obtained by

$$d_{ij}^w = \sum_{a_{uv} \in g_{i \xrightarrow{w} j}} f(w_{uv}) \tag{2.9}$$

where $g_{i \xrightarrow{w} j}$ is the shortest weighted path between nodes i and j, f is a map (e.g. an inverse) from weight to length. Note that $d_{ij}^w = \infty$ for all disconnected pairs (i, j) (Rubinov and Sporns, 2010). The generalization of weighted shortest path length can then be used to generalize the weighted characteristic path length, global efficiency and betweenness centrality:

$$L^w = \frac{1}{N} \sum_{i \in G} L_i^w = \frac{1}{N} \sum_{i \in G} \frac{\sum_{j \in G, j \neq i} d_{ij}^w}{N - 1} \tag{2.10}$$

$$E^w = \frac{1}{N} \sum_{i \in G} E_i^w = \frac{1}{N} \sum_{i \in G} \frac{\sum_{j \in G, j \neq i} d_{ij}^w}{n - 1} \tag{2.11}$$

$$b_i^w = \frac{1}{(N-1)(N-2)} \sum_{j,h \in G, h \neq j, h \neq i, i \neq j} \frac{\rho_{hj}^w(i)}{\rho_{hj}^w} \tag{2.12}$$

where $\rho_{hj}^w(i)$ and ρ_{hj}^w are based on weighted shortest paths.

Onnela et al. proposed a weighted clustering coefficient based on how much the triangles weight are compared to the network maximum (Onnela et al., 2005), and this algorithm is used in the brain connectivity toolbox (Rubinov and Sporns, 2010):

$$C^O(i) = \frac{\sum_{j,h} (w_{ij} w_{ih} w_{jh})^{1/3}}{k_i (k_i - 1)} \tag{2.13}$$

where k_i is the binary node degree.

Rubinov and Sporns (Rubinov and Sporns, 2010) gave the generalization of local efficiency as

$$E_{loc}^R(i) = \frac{\sum_{j,h} (w_{ij} w_{ih} [d_{jh}^w(N_i)]^{-1})^{1/3}}{k_i (k_i - 1)} \tag{2.14}$$

where k_i is the binary node degree and $d_{jh}^w(N_i)$ is the shortest distance between j and h, that contains only neighbours of i.

2.3 Small world topology

A small world network is intermediate between regular and random networks (Figure 2.2). The small world property of a network is often characterized by comparing the clustering coefficient and characteristic path length between the network at hand with equivalent random networks: $C/C_{rand} > 1$ and $\lambda/\lambda_{rand} \approx 1$, where C is the clustering coefficient and λ is the characteristic path length (Watts and Strogatz, 1998; He et al., 2007b). The equivalent random network has a random topology but shares the same size and degree (strength) distribution with the original network.

Besides this, a more general criterion is that the small world network should satisfy (Achard and Bullmore, 2007; Batalle et al., 2012): $E_{glob}^{latt} < E_{glob} < E_{glob}^{rand}$ and $E_{loc}^{latt} > E_{loc} < E_{loc}^{rand}$, where E_{glob}^{latt} and E_{loc}^{latt} are global and local efficiency of the lattice surrogate and E_{glob}^{rand} and E_{loc}^{rand} of the random surrogate.

2.4 Modularity structure

Various algorithms have been developed to identify the modular structure: the generalized Louvain algorithm (Blondel et al., 2008), InfoMap (Rosvall and Bergstrom, 2008), WalkTrap (Pons and Latapy, 2005), Markov Cluster (Shih and Parthasarathy, 2012), etc. Most of them are identifying non-overlapping communities based on nodes. There are also algorithms which can partition overlapping communities, for instance CFinder (Palla et al., 2007, 2005). Link communities can also be defined based on the hierarchical structure of the connections (Ahn et al., 2010). To determine the community structure of the network, we used the algorithm of Newman (Newman, 2006a) as implemented in the Brain Connectivity Toolbox. The algorithm starts from a random order of the nodes which lead to a slightly different community structure each time the algorithm is applied. To generate a consensus assignment of nodes to communities, we used a two step procedure (Barnes et al., 2012). In the first step, we computed a co-assignment matrix represented as an N x N matrix, where cell (i, j) was equal to 1 if node i and node j were assigned to the same community. During the second step, a probabilistic co-assignment matrix is then obtained by averaging different realizations of the co-assignment matrices.

2.5 Hub distribution

Hubs are often identified solely on the basis of their high degree, which is the number of edges attached to them (Buckner et al., 2009; van den Heuvel et al., 2008). This is the simplest and most intuitive way to define hubs in the network. Betweenness centrality, which measures the role a node plays in the shortest path between other nodes, is another option. Betweenness centrality puts emphasis on the importance of the node to others in building the shortest path of the network. The shortest path length can also be used to identify hubs by focusing on the

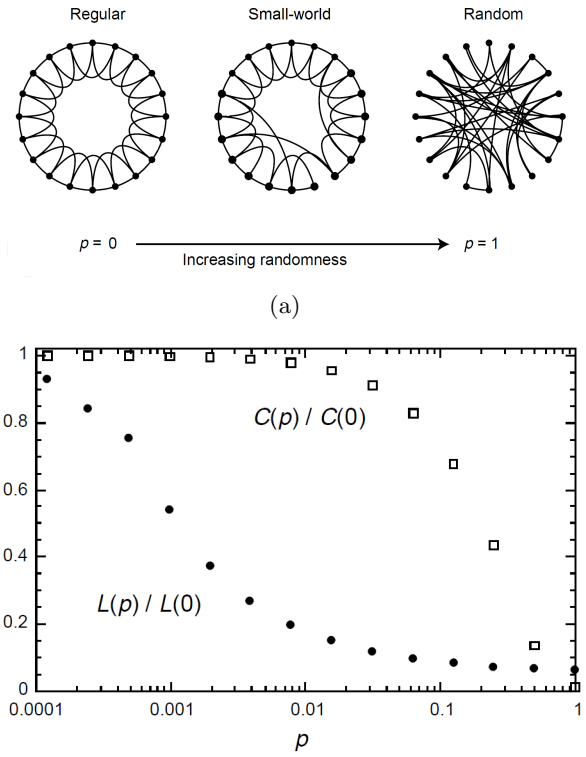

Figure 2.2: A small world network is intermediate between regular and random networks. (a) The computational model of small-world networks began by connecting nodes with their nearest neighbours (spatially when organized on a ring), producing a regular graph that is locally clustered. By randomly rewiring the edges in the regular network at a probability p, the amount of disorder is then increased. Thus p = 0 represent an unchanged original ring; as p increases, the graph becomes increasingly disordered until for p = 1, all edges are rewired randomly. (b) A regular graph (when the rewire probability p is low) has a high clustering coefficient C and average path length L. On the other hand, a random network (when p is high) entails low C and L. A small-world network with intermediate values of p is highly clustered like a regular graph, yet with small characteristic path length like a random network. $C(0)$ and $L(0)$ are the corresponding values from a regular network. Figure adapted from (Watts and Strogatz, 1998).

accessibility of that node. Hub nodes display a low level of clustering coefficient as well (Bullmore and Sporns, 2009; van den Heuvel et al., 2010). Furthermore, the hub score which is the sum of dummy values for four criteria is also used to identify hubs (van den Heuvel et al., 2010; Vandenberghe et al., 2013; Heitger et al., 2012; Bullmore and Sporns, 2012; Wu et al., 2013; Shi et al., 2013; Fornito and Bullmore, 2015). We gave a score of 1 or 0 depending on whether or not the node belongs to the top 20% of nodes with 1) the highest node degree, 2) the highest betweenness centrality, 3) the lowest local cluster coefficient (limited to nodes with a degree > 2), and 4) the lowest average path length. Nodes with a hub score ≥ 2 were considered hubs.

3

The Associative-semantic Network for Words and Pictures: Effective Connectivity and Graph Analysis

Abstract

Explicit associative-semantic processing of words and pictures activates a distributed set of brain areas that has been replicated across a wide range of studies. We applied graph analysis to examine the structure of this network. We determined how the left ventral occipitotemporal transition zone (vOT) was connected to word-specific areas. A modularity analysis discerned 4 communities: one corresponded to the classical perisylvian language system, including superior temporal sulcus (STS), middle temporal gyrus (GTm) and pars triangularis of the inferior frontal gyrus (GFi), among other nodes. A second subsystem consisted of vOT and anterior fusiform gyrus along with hippocampus and intraparietal sulcus. The two subsystems were linked through a unique connection between vOT and GTm, which were hubs with a high betweenness centrality compared to STS and GFi which had a high local clustering coefficient. Graph analysis reveals novel insights into the structure of the network for associative-semantic processing.

This chapter has been published as: Rik Vandenberghe, Yu Wang, Natalie Nelissen, Mathieu Vandenbulcke, Thijs Dhollander, Stefan Sunaert, Patrick Dupont. The associative-semantic network for words and pictures: Effective connectivity and graph analysis. *Brain and Language* 127(2): 264-72.

3.1 Introduction

Until recently, the vast majority of functional imaging data were based on univariate voxelwise comparisons between conditions. The maps of significant differences were often described as 'systems' or 'networks' but this commonly went beyond the actual data analysis. In the current paper we will apply a graph theoretical approach (Bullmore and Sporns, 2009; Buckner et al., 2009; He and Evans, 2010; Bullmore and Bassett, 2011) to characterize the network for associative-semantic processing. As a mathematical technique, graph theory has been known for long. Its application however to imaging data is of a more recent date and has steadily increased in popularity. Graph analysis has been applied to a number of imaging modalities: structural (He et al., 2007a, 2008) and resting-state MRI (Nelson et al., 2010), diffusion-tensor imaging (DTI) (Gong et al., 2009) as well as task-related fMRI (Buckner et al., 2009). Compared to dynamic causal modelling (DCM) (Penny et al., 2004), graph analysis does not require the a priori definition of a restricted set of models (nodes, intrinsic feedforward and feedback connections, modulations) by the experimenter. The associative-semantic network consists of a large number of nodes and an even exponentially larger number of possible functional connections. Given the extent of the network and the significant lacunes that remain in our knowledge about its internal connectivity structure, graph analysis was optimally suited for this research purpose.

A highly consistent pattern of activation in functional imaging can be obtained when explicit associative-semantic judgments are compared to lower-level tasks such as visuoperceptual judgments of size for words and pictures (Vandenberghe et al., 1996; Vandenbulcke et al., 2005, 2007; Nelissen et al., 2009, 2011). Regions activated both for words and pictures include the left ventral occipitotemporal transition zone (vOT) (Vandenberghe et al., 1996; Buckner et al., 2000; Van Doren et al., 2010; Seghier and Price, 2011), left posterior middle temporal gyrus (Chertkow et al., 1997; Vandenbulcke et al., 2007; Whitney et al., 2011), the anterior temporal pole (Hodges et al., 1992; Vandenberghe et al., 1996; Rogers and McClelland, 2004), left ventral anterior temporal cortex (Jefferies and Lambon Ralph, 2006; Visser et al., 2012a) and left anterior inferior frontal gyrus (Goldberg et al., 2007). Other areas are activated more during semantic processing specifically for words compared to pictures or vice versa. Such areas include the triangular and opercular part of the inferior frontal gyrus, the posterior third of STS for words (Vandenberghe et al., 1996; Vandenbulcke et al., 2007) and the right fusiform gyrus for pictures (Vandenbulcke et al., 2006; Thierry and Price, 2006). It also contains more domain-general (Binder et al., 2009) regions such as the inferior frontal sulcus (Wagner et al., 1997; Van Doren et al., 2010), middle frontal gyrus (Demb et al., 1995; Vandenberghe et al., 1996), and intraparietal sulcus. In this context, we use the term 'domain-general' to refer to cognitive processes that may not be exclusive for tasks involving language or semantic processing and that may be invoked during a wider variety of tasks, e.g. due to their role in selective attention or executive control. A similar distribution of activations has been reported across a wide variety of experiments of semantic processing (Binder et al., 2009). To our knowledge, this set of activations has not

been analyzed mathematically at the systems level until now. The first aim of the current study was to apply a graph theoretical approach to this activity pattern to investigate the network structure.

At a more local level, we were mainly interested in how the junction between left ventral occipital and posterior inferior temporal cortex (ventral occipitotemporal transition zone (vOT)) is connected with the perisylvian word-specific system. vOT is activated across a wide variety of language (Cohen et al., 2000, 2002; Jobard et al., 2003; Price and Devlin, 2003; Démonet et al., 2005; Vinckier et al., 2007; Seghier and Price, 2011; Price and Devlin, 2011; Woodhead et al., 2011; Hellyer et al., 2011) as well as picture processing paradigms (Buckner et al., 2000; Price and Devlin, 2003; Seghier and Price, 2011; Price and Devlin, 2011). It lies at the transition between ventral occipital and ventral temporal cortex and contains the mid-fusiform gyrus (Seghier and Price, 2011; Price and Devlin, 2011; Woodhead et al., 2011; Hellyer et al., 2011). It overlaps with the visual word form area (Cohen et al., 2000, 2002; Vinckier et al., 2007). Its y coordinate (-58 $\pm$ 5 mm) lies slightly posterior to the basal temporal language area (-41 $\pm$ 6 mm) area, the anterior fusiform gyrus and the inferior temporal gyrus (Jobard et al., 2003; Démonet et al., 2005). It is neuroanatomically and functionally distinct from the ventral anterior temporal cortex that lies at a distance more anteriorly and has been implicated in multimodal processing of conceptual representations (Visser and Ralph, 2011; Visser et al., 2012a). Rather than an anatomically or functionally well-delineated area, vOT is a conglomerate of areas fulfilling different functions, with a posterior-anterior gradient (Jobard et al., 2003; Démonet et al., 2005; Seghier and Price, 2011).

Many functional interpretations of vOT implicitly assume a connectivity pattern with the language network but this has not been directly tested empirically. For instance, if one considers vOT as an 'entry point' to the word-specific system (Démonet et al., 2005), one would expect functional connectivity between vOT and language-specific areas such as posterior STS. Likewise, if vOT integrates top-down predictions from the language system with bottom-up visual input (Price and Devlin, 2011) or reflects the interaction between the 'triangular network' of orthography, phonology and semantics (Woodhead et al., 2011; Hellyer et al., 2011), one would expect a high degree of connectivity with word-specific areas in posterior temporal or inferior frontal cortex. Alternatively, left vOT has also been implicated in more 'generic' functions (Van Doren et al., 2010, 2012). According to one hypothesis, it belongs to a long-distance feedback loop together with the inferior frontal sulcus that mediates visual short-term memory, enhancing perceptual identification, conscious perception and episodic memory encoding (Van Doren et al., 2010, 2012). According to a related hypothesis, based on a meta-analysis of reading studies (Jobard et al., 2003), it is implicated in segmentation and classification of visual stimuli in familiar units. The second aim therefore of the current study was to evaluate how vOT is connected with word-specific areas, such as STS.

3.2 Subjects and Methods

3.2.1 Subjects

Thirty-three healthy elderly subjects, aged between 54 and 89 years of age (19 M/14 F; mean age 67.2 yr +/- 8.5 years), without neurological or psychiatric history, participated. All were strictly right-handed, free of psychotropic or vasoactive drugs, had a normal structural MRI and scored within the published norms on a standard conventional neuropsychological assessment. This sample has already been published as control group for fMRI studies of language and semantic processing in primary progressive aphasia (Vandenbulcke et al., 2005), stroke (Vandenbulcke et al., 2006), amnestic mild cognitive Impairment (Vandenbulcke et al., 2007) and Alzheimer's disease (Nelissen et al., 2007, 2011).

3.2.2 Experimental paradigm

Stimuli were projected onto a screen 28 cm in front of the subjects' eyes. The design of the fMRI experiment was factorial (Vandenberghe et al., 1996; Vandenbulcke et al., 2005, 2006; Nelissen et al., 2009). The first factor, task, had two levels: Associative-semantic versus visuoperceptual judgment. The second factor, input modality, also had two levels: Pictures versus printed words. The associative-semantic condition consisted of a modified version of the Pyramids and Palm Trees test (Hodges et al., 1992). During a trial, a triplet of stimuli was presented for 5250 ms, one stimulus on top (the sample stimulus) and one in each lower quadrant (the test stimuli). Subjects had to press a left- or right-hand key depending on which of the two test stimuli matched the sample stimulus more closely in meaning. A given triplet was presented in either the picture or the word format and this was counterbalanced across subjects. In the visuoperceptual control condition, a stimulus was presented in three different sizes. Subjects had to press a left or right-hand key depending on which of the two test stimuli matched the sample stimulus more closely in size on the screen. Two successive trials were separated by a 1500 ms interval. Each epoch, i.e. a block of trials of the same type, consisted of 4 trials (total duration 27 s).

Stimuli were presented at 3.8 deg eccentricity. The pictures were taken from the Snodgrass-Vanderwart set. Mean picture size was 5.6 deg and letter size 1.5 deg.

3.2.3 Image acquisition

A 1.5 tesla Siemens Sonata system (Siemens Medical Solutions, Erlangen, Germany) equipped with an 8-channel receive-only head coil (MRI Devices Corp., Waukesha, USA) provided a T1-weighted structural volume (coronal inversion recovery prepared three-dimensional gradient echo images; Inversion time 800 ms, TE/TR 3.93/1950 ms) as well as T2* echo-planar images (EPI) (42 sagittal slices; voxel size 3.6x3x3 mm^3; TE/TR 40/3000 ms). Usage of the GeneRalized Autocalibrating Partially Parallel Acquisitions (GRAPPA) method (Griswold

et al., 2002) maximized sensitivity for anterior temporal activity changes and minimized susceptibility artefacts. Scans were acquired between 2003 and 2007 (Vandenbulcke et al., 2005, 2006, 2007; Nelissen et al., 2007), prior to the development of Spin-Echo EPI as a means to reduce anterior temporal susceptibility artefact (Visser and Ralph, 2011; Visser et al., 2012a). A total of 108 volumes were acquired during each run. Each run consisted of 3 replications of each of the 4 conditions. Subjects underwent 4 to 6 runs each.

3.2.4 Image preprocessing

We used the normalized and smoothed data from previous studies (Vandenbulcke et al., 2005, 2006, 2007; Nelissen et al., 2007) which were spatially transformed using Statistical Parametric Mapping (SPM2; Wellcome Department of Cognitive Neurology, London, UK; http://www.fil.ion.ucl.ac.uk/spm). In brief, EPI images were realigned and the anatomical MRI was coregistered to the mean realigned EPI image, the coregistered MRI was normalized to a custom-made T1 template of elderly subjects (Nelissen et al., 2007) in Montreal Neurological Institute (MNI) space, and the normalization matrix was subsequently applied to all individual EPI images. These images (voxel size of 3x3x3 mm^3) were smoothed with a Gaussian kernel (6x6x6 mm^3). Using SPM8, we applied high-pass filtering (FWHM = 270 s) and low-pass filtering consisting of a canonical hemodynamic response function (hrf) to the data. The epoch related response was modelled by a canonical hrf convolved with a boxcar.

3.2.5 Network nodes and time series

A random effects analysis was performed for the main effect of task (associative semantic judgment > visuoperceptual judgment). We used a statistical threshold at the voxel level of uncorrected $P < 0.001$ combined with a family wise error (FWE) corrected $p < 0.05$ at the cluster level. Suprathreshold clusters were ordered according to decreasing size and within each cluster, all suprathreshold local maxima were ordered according to decreasing t value. Next, we selected the MNI coordinates of local maxima which were located at least 20 mm apart from each other, starting from the coordinates of the first local maximum in our ordered list. In each coordinate, we defined a sphere with a radius of 6 mm and intersected this sphere with the underlying cluster. This gave us a set of voxels which constitute the volume of interest (VOI) of the network node around that coordinate. Note that for all subjects the same VOIs derived from the group analysis were used. Alternative approaches to define the nodes are to start from VOIs based on a priori atlases (He et al., 2007a, 2008) or to include each gray matter voxel (Buckner et al., 2009).

To assess the between-subject variability of the nodes, we calculated for each node the percentage subjects for which a voxel with an uncorrected $P < 0.05$ was found within a distance of 6 mm from the group local maximum. We also calculated the contribution coefficient (Seghier et al., 2007). If every subject

contributed equally to the group spm T map, the contribution coefficient equals - in our case - 1/33.

In each voxel of the VOI, we extracted the time series after whitening, filtering and removing effects of no interest (session specific effects) using SPM8 code. Finally, the average time series in the network node was calculated as the mean of the time series in the voxels belonging to the corresponding VOI. Time series of the different runs were concatenated.

3.2.6 Partial correlation coefficients

The effective connectivity [1] between nodes was determined by the partial correlations between the network nodes, quantifying the unique relationship between each pair of nodes. The calculation of the partial correlations was based on calculating the inverse of the covariance matrix. After applying Fisher's r-to-Z transformation to each partial correlation a random effects analysis was performed to identify those connections which were significantly different from zero at the group level. The significance level was set at $p < 0.05$ Bonferroni corrected for the total number of possible connections. Significant partial correlations are closely related to effective connectivity (Marrelec et al., 2006, 2009).

3.2.7 Graph analysis

Graph analysis was performed using the brain connectivity toolbox (https://sites.google.com/a/brain-connectivity-toolbox.net/bct/Home (Rubinov and Sporns, 2010)).

Prior to graph analysis, we binarized the connections based on the statistical significance (He et al., 2007a) of the partial correlation coefficients. The statistical threshold was set to $P < 0.05$ corrected for the number of possible connections. This threshold determines the 'density' of the network, i.e. the number of supra-threshold connections over the total number of possible connections.

We calculated two global network measures: the characteristic path length of the graph and the mean clustering coefficient. The path length of node i is the average distance to each other node excluding isolated nodes. The distance between two nodes is the shortest path length between these nodes. The characteristic path length of the graph is the path length averaged over all nodes. The mean clustering coefficient of the graph is the clustering coefficient averaged over all nodes. The clustering coefficient of node i is the fraction of neighbours of node i that are neighbours of each other. We will also report the normalized values of the characteristic path length and the mean clustering coefficient, i.e. the values divided by the value obtained in an equivalent random network. A normalized mean clustering coefficient > 1 and a normalized characteristic path length of approximately 1 are commonly considered to indicate small-world characteristics of the network.

[1] Here, the term effective connectivity refers to undirected functional connectivity using partial correlations since both concepts are closely related (Marrelec et al., 2006, 2009).

To evaluate the robustness of our graph analysis, we examined the impact of sample size on the global graph measures. We calculated the difference between the global graph measures as a function of the number of subjects included, compared to using the full sample (n = 33). We randomly selected a subset of cases. The relative error was the average of the relative error over all realizations of this random sample (with a maximum of 500 realizations) (Fig. 3.2).

Apart from path length and local clustering coefficient, typical graph measures at the local level are also degree and betweenness centrality. The degree of node i is the number of edges (connections) linked to node i. The betweenness centrality of node i is the fraction of shortest paths within the graph that pass through node i. Betweenness centrality is a measure of how pivotal a given node is in the overall network. Hubs are typically characterized by a high degree, a high betweenness centrality, a short average path length and a low clustering coefficient (Sporns et al., 2007; Bullmore and Sporns, 2009). To identify such hubs, we calculated a hub score. The hub score is the sum of the dummy values for 4 criteria (each set at 1 or 0 depending on whether or not the criterion is fulfilled, with a maximum of 4) (van den Heuvel et al., 2010; Heitger et al., 2012). These criteria are whether the node belongs to the top 20% of nodes

1. showing the highest degree
2. showing the lowest path length
3. showing the lowest local cluster coefficient
4. showing the highest betweenness centrality.

When a node had a hub score of 2 or more, it was marked as a hub (van den Heuvel et al., 2010). The hub scores will be provided for each node in Table 3.1.

Graph analysis also allows one to detect of which 'modules' or 'communities' a network is built. Communities are non-overlapping groups of nodes with a high number of within-community connections and a low number of between-community connections. We used the algorithm of Newman (Newman, 2006a,b) as implemented in the Brain Connectivity Toolbox to determine the community structure of the network. In this modularity analysis, the algorithm starts from a random order of the nodes. Across different iterations (realizations) of the analysis this order is randomized, in our instance for a total of 100 realizations. We evaluated how systematically the same community structure recurred between these different realisations of the community structure. If two nodes were assigned to a same community structure in 80% of these realizations, the assignment was considered relatively stable. Nodes that were assigned to a same community across 95% or more of realizations, will be considered most robust and be the main focus of this report.

As a further means to determine the robustness of our modularity analysis, we also examined the impact of network density on the community structure. One of the factors determining network density is the threshold applied when the connections are binarized. Network density therefore can be manipulated by varying the statistical threshold for binarizing the connections. We varied this

threshold between 3 different possibilities: $P < 0.1$, $P < 0.05$ and $P < 0.01$. All P values are corrected for the number of possible connections.

The network will be visualized using Pajek (http://pajek.imfm.si) and a Kamada-Kawai energy layout (Kamada and Kawai, 1989; Batagelj and Mrvar, 1998). In this approach, two nodes are considered as connected by a spring with a length equal to the strength of the partial correlation. The final layout is then given by minimization of the energy of the layout.

3.3 Results

3.3.1 Nodes

The thresholded t map of the main effect of task is shown in figure 3.1A. The median size of the intersection of the sphere (with radius 6 mm around the center coordinate) and the thresholded group spmT map was 29 voxels (range 3 - 33 voxels). The number of subjects with at least one voxel with an uncorrected $p < 0.05$ (for the main effect of task) within the sphere was 88% (median value; range 58-100%). The contribution coefficient of every subject is given in figure 3.1B.

3.3.2 Global graph measures

The mean clustering coefficient of the associative-semantic network was 0.32 and the characteristic path length 3.17. The corresponding values for an equivalent random network (with 57 nodes and 124 connections) using 1000 randomizations were 0.07 and 2.84, respectively. The normalized values therefore for mean clustering coefficient and characteristic path length were 4.57 and 1.12, respectively. The network therefore exhibits small-world characteristics.

To evaluate the impact of sample size on these estimates, we calculated the error of these global graph measures as function of sample size, relative to using the full sample (n = 33). Error linearly decreased as a function of sample size, with values of 10% for 31 or more subjects (Fig. 3.2).

3.3.3 Local graph measures and community structure

The final network is shown in Fig. 3.3. The local network measures (degree, path length, local clustering coefficient, betweenness centrality and hub score) are given in Table 3.1 for nodes with a degree > 3.

Analysis of the community structure revealed 6 subsystems (Figure 3.3, table 3.1). The composition of 4 of these subsystems was highly robust: it was present in 95% of realisations (Table3.1, symbol +). These communities were also robust when we manipulated the network density by varying the statistical threshold either to a corrected $P < 0.1$ (density 9.1%) or $P < 0.01$ (density 6.3%) instead of $P < 0.05$ (density of 7.8%) (table 3.1, symbol *). We will mainly focus on these 4 most robust communities.

x	y	z	anatomical location	degree	path length	clustering coefficient	betweenness centrality	hub score	community
-48	**-69**	**30**	**L angular gyrus**	**8**	**2.6**	**0.14**	**0.12**	**4**	**red *+**
-63	**-39**	**-6**	**L posterior GTm**	**7**	**2.7**	**0.33**	**0.10**	**2**	**red *+**
-60	-54	9	L posterior STS	6	3.1	0.47	0.03	0	red *+
-51	21	24	L GFi pars triangularis	5	3.0	0.40	0.03	0	red +
-60	-45	27	L supramarginal gyrus	5	3.0	0.30	0.03	0	red *+
-54	27	-3	L GFi pars orbitalis	5	3.2	0.50	0.01	0	red +
-57	-12	-9	L anterior STS	4	3.5	0.50	0.01	0	red *+
-39	39	-18	L anterior GFi	4	3.1	0.67	0.00	0	red +
-30	**-66**	**60**	**L intraparietal sulcus (IPS)**	**6**	**2.6**	**0.40**	**0.11**	**2**	**yellow *+**
-54	**-57**	**-18**	**L vOT**	**5**	**2.6**	**0.20**	**0.11**	**2**	**yellow *+**
-39	**-87**	**0**	**L middle occipital gyrus (GOm)**	**8**	**2.5**	**0.29**	**0.10**	**3**	**yellow *+**
-15	**-93**	**-9**	**L lingual gyrus**	**7**	**2.5**	**0.19**	**0.10**	**3**	**yellow *+**
-36	**-42**	**-24**	**L anterior fusiform**	**8**	**2.5**	**0.25**	**0.08**	**3**	**yellow *+**
-24	-66	39	L intraparietal sulcus (IPS)	6	2.6	0.40	0.04	0	yellow *+
-30	-33	-6	L hippocampus	4	3.1	0.33	0.02	0	yellow *+
33	-39	-24	R anterior fusiform	6	3.6	0.33	0.04	0	green *+
27	-96	-3	R inferior occipital gyrus	5	3.1	0.40	0.03	0	green *+
42	-78	-9	R inferior occipital gyrus	5	3.1	0.40	0.02	0	green *+
30	-69	-54	R cerebellum	5	3.6	0.30	0.02	0	green +
30	-93	18	R middle occipital gyrus (GOm)	4	3.1	0.67	0.01	0	green *+
-39	**6**	**33**	**L inferior frontal junction (IFJ)**	**7**	**2.8**	**0.19**	**0.10**	**2**	**blue *+**
-3	**15**	**54**	**dorsomedial prefrontal**	**8**	**2.6**	**0.25**	**0.09**	**3**	**blue *+**
-24	24	54	L superior frontal sulcus (SFS)	7	2.8	0.29	0.04	1	blue *+
-9	54	45	L superior frontal gyrus (GFs)	6	2.9	0.47	0.04	0	blue *+
-33	6	60	L superior frontal gyrus (GFs)	5	2.8	0.40	0.03	0	blue *+
-9	30	33	L anterior cingulate	6	3.0	0.40	0.02	0	blue *+
-9	36	60	L superior frontal gyrus (GFs)	6	3.1	0.47	0.02	0	blue *+
-3	-57	15	precuneus	6	2.6	0.33	0.07	1	purple *+
-12	-3	9	L anterior thalamus	6	2.9	0.33	0.03	0	purple
12	3	12	R caudate	4	3.1	0.50	0.01	0	purple +
-3	**-33**	**3**	**posterior thalamus**	**7**	**2.6**	**0.29**	**0.08**	**3**	**cyan**
-15	**-54**	**-18**	**L cerebellum**	**6**	**2.6**	**0.07**	**0.08**	**2**	**cyan +**
45	**21**	**27**	**R GFi pars triangularis**	**4**	**2.6**	**0.00**	**0.08**	**3**	**cyan**
-21	-33	-51	L cerebellum	4	3.0	0.00	0.06	1	cyan +
-3	-63	45	precuneus	6	2.7	0.27	0.05	0	cyan
6	-54	-42	vermis	4	3.1	0.00	0.03	1	cyan +

Table 3.1: Ranking of nodes per community according to betweenness centrality and, next, degree. Only local graph measures of nodes with a degree > 3 are shown. x,y,z are the MNI coordinates of the centre of the nodes; degree is the degree of the node, path length is the average shortest path length of the node to any other node (excluding 3 nodes which were isolated in the graph), community refers to the colour coding used in figure 3.3. Hubs (with a hub score of 2 or more) are indicated in bold. * denotes robustness of community structure when varying the density of the network. Nodes marked with '+' are assigned to a given community in 95% of the realizations. *Abbreviations:* vOTC: ventral occipitotemporal transition zone; GTm: middle temporal gyrus; STS: superior temporal sulcus; GFi: inferior frontal gyrus; L: left.; R: right.

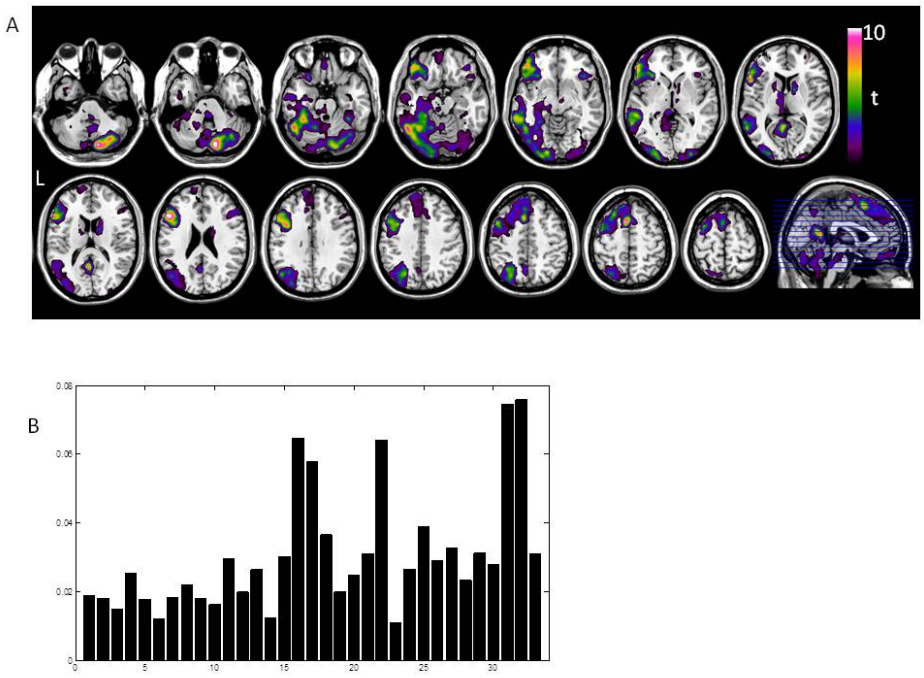

Figure 3.1: **A.** spmT map on transverse sections, corresponding to the contrast of associative-semantic versus visuoperceptual judgment, thresholded at voxel-level uncorrected $P<0.001$ and cluster-level FWE corrected $P<0.05$. **B.** Contribution coefficient for each of the 33 subjects (Seghier et al., 2007).

Three were nearly exclusively left-hemispheric, the fourth was mainly right-sided and located more posteriorly. Among the left-sided communities, one was mainly perisylvian, the second community extended from IPS to vOT extending ventromedially to the parahippocampal gyrus and the hippocampus, and the third covered the dorsolateral prefrontal and medial prefrontal cortex. Its most inferior component was the inferior frontal junction.

The perisylvian community (Figure 3.3, red dots) consisted of posterior STS and anterior STS, middle temporal gyrus and the anterior temporal pole, pars orbitalis of the frontal operculum and the anterior inferior frontal gyrus, as well as the left angular and left supramarginal gyrus. The left angular gyrus and the left posterior middle temporal gyrus were the hubs of this network (Figure 3.3 red, Table 3.1).

Left vOT belonged to a different subsystem together with left anterior fusiform gyrus, left middle occipital gyrus (GOm), left intraparietal sulcus (IPS) and ventromedially the left parahippocampal gyrus and hippocampus (Figure 3.3, yellow dots). This system clearly lay at a distance from the sylvian fissure, more or less concentrically to the perisylvian community. This module contained a

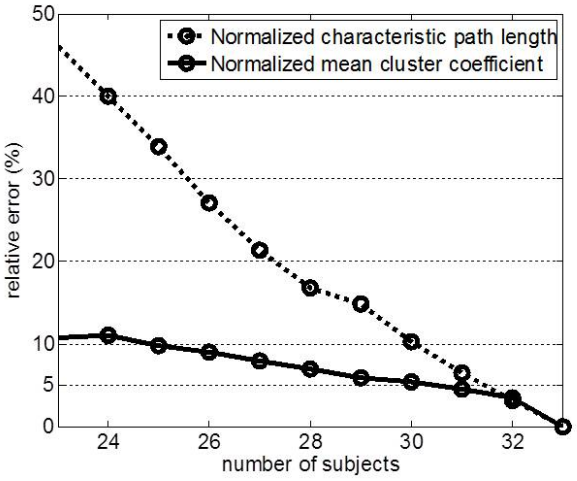

Figure 3.2: Relative error as a function of sample size. The relative error is the difference between the observed value and the value obtained in the full dataset (n = 33) divided by the value of the full dataset. X axis: sample size. Y axis: relative error in %.

total of 5 hubs: IPS, vOT, GOm, lingual gyrus and the anterior fusiform gyrus (Figure 3.3 yellow, Table 3.1).

A third system (Figure 3.3, blue dots) consisted almost entirely of foci in middle and superior frontal gyrus, both lateral and medial wall as well as cingulate. Two hubs were located in this module: one in the left inferior frontal junction (IFJ) and one in the dorsomedial prefrontal cortex (Figure 3.3 yellow, Table 3.1).

Graph analysis also extracted a fourth, mainly right-sided community. It contained the right mid- and anterior fusiform gyrus (Vandenbulcke et al., 2006), as well as the right middle occipital gyrus (Figure 3.3, green dots). One of the nodes was located in the left hemisphere, i.e. hippocampus.

3.3.4 Connectivity between vOT and STS

Given our primary research question regarding the connectivity between vOT and STS, we also provide more detail about the partial correlations of left vOT $(-54, -57, -18)$ and left posterior STS $(-60, -54, 9)$ (Table 3.2A and B, respectively): Both nodes had a relatively strong connection with left posterior

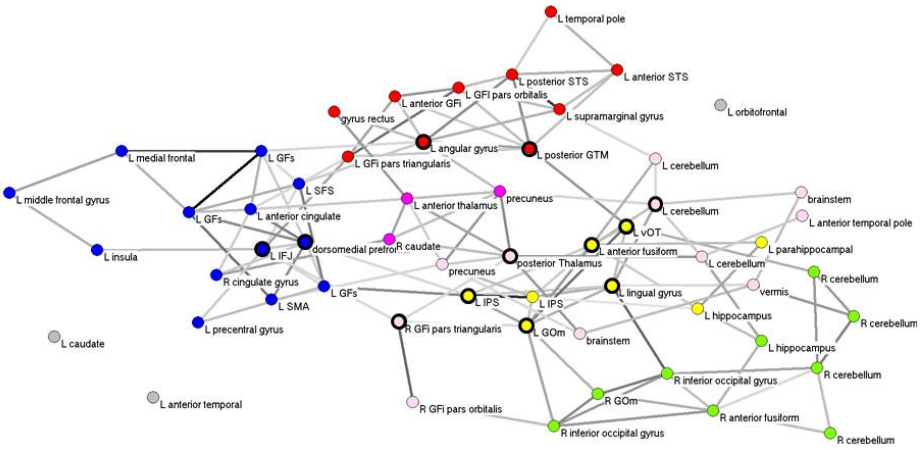

Figure 3.3: Graph of the associative-semantic network. The connection strength is determined by the partial correlation. Only connections which are significant at corrected $p < 0.05$ are shown. Nodes belonging to a same 'community' are given a same colour. The two communities most pertinent to the current purposes are: (red) the left perisylvian module including posterior and anterior STS, posterior GTm, the anterior temporal pole, angular and supramarginal gyrus, GFi (anterior, pars orbitalis and pars triangularis), gyrus rectus and the orbitofrontal gyrus and (yellow) the left ventral occipitotemporal module including vOT, IPS, anterior fusiform, lingual and parahippocampal gyrus, GOm, hippocampus and caudate). The 4 additional communities are coloured in blue, purple, green and cyan, respectively. Nodes encircled with a black border are considered as hubs in the network.

GTm but no direct connections with each other. Except for the posterior GTm, no other overlap in neighbours was found between posterior STS and vOT (Table 3.2). This strongly suggests that vOT and STS are connected with each other through their mutual connection with posterior GTm. The striking difference in connectivity pattern also suggests that they may belong to different communities (Figure 3.3, yellow versus red dots).

3.4 Discussion

Graph analysis allowed us to mathematically decompose the distributed network activated by the contrast of associative-semantic with visuoperceptual processing (Vandenberghe et al., 1996; Vandenbulcke et al., 2005, 2006; Nelissen et al., 2009, 2011) into subsystems, or in graph terminology, 'communities'. In a strictly data-driven manner, our modularity analysis dissected the perisylvian network out of the distributed set of activations with remarkable precision. Left temporal and occipital activations fell into two separate communities: this perisylvian

	x	y	z	corrected p-value	partial correlation
A. Cortical connectivity of left vOT (-54,-57,-18)					
L middle occipital gyrus (GOm)	-39	-87	0	8.9E-05	0.13
L posterior GTm	-63	-39	-6	4.8E-02	0.10
L anterior fusiform	-36	-42	-24	1.2E-03	0.07
R cerebellum	36	-69	-30	5.4E-04	0.07
L lingual gyrus	-15	-93	-9	3.6E-03	0.06
B. Cortical connectivity of left posterior STS (-60,-54,9)					
L supramarginal gyrus	-60	-45	27	4.4E-10	0.19
L angular gyrus	-48	-69	30	9.1E-08	0.12
L posterior GTm	-63	-39	-6	6.9E-05	0.11
L anterior STS	-57	-12	-9	7.0E-05	0.08
L GFi pars orbitalis	-54	27	-3	5.3E-03	0.06
L anterior temporal pole	-54	12	-21	7.4E-03	0.05

Table 3.2: Cortical nodes with a significant partial correlation with left vOT (A) and left posterior STS (B), respectively, ranked based on the strenght of the partial correlation coefficient. *Abbreviations:* vOTC: ventral occipitotemporal transition zone; GTm: middle temporal gyrus; STS: superior temporal sulcus; GFi: inferior frontal gyrus; L: left.; R: right.

subsystem containing STS, pars triangularis, and GTm along with angular gyrus and a second, more or less concentric subsystem extending from IPS to vOT and ventromedially towards the parahippocampal gyrus and the hippocampus. The interface between these two communities consisted of a unique direct connection of vOT with the posterior third of the middle temporal gyrus (Table 3.2).

All nodes were defined on the basis of a same contrast, preventing any bias that could be induced in our connectivity analysis by differences in contrasts used to define nodes. Neither can proximity between nodes explain the connectivity pattern: To define nodes, we applied a criterion of minimally 2 cm Euclidean distance and, furthermore, many connections that reached significance bridged relatively large distances, e.g. left posterior STS to left pars orbitalis GFi (Table 3.2).

The data were acquired prior to the advent of Spin-Echo EPI which substantially increases sensitivity in anterior temporal cortex (Visser et al., 2010; Visser and Ralph, 2011). This may explain why we did not obtain activation in the ventral anterior temporal cortex (Visser et al., 2010; Visser and Ralph, 2011). The most anterior temporal region we reliably imaged was at y = -12 (anterior STS). More anterior temporal activity foci were rather scarce and usually had a low degree, probably for reasons of fMRI susceptibility. Our data therefore do not allow for any conclusions regarding the position of the anterior temporal regions in the network. This is a shortcoming as some of these anterior temporal nodes may function as hubs (Ralph et al., 2010).

Among the distributed set of activations (Fig. 3.1) our modularity analysis

dissected out the perisylvian network (Mesulam, 1998, 2008) with remarkable accuracy (Fig. 3.3). Two of the nodes belonging to the perisylvian community, the posterior middle temporal gyrus and the left angular gyrus were assigned a hub status. Most of the other nodes of this module had a relatively high local clustering coefficient (Table 3.1). The posterior middle temporal gyrus and the angular gyrus have been found in numerous studies of semantic processing (for a review see (Binder et al., 2009)) and have been previously described as network hubs (Buckner et al., 2009). Both have been implicated in multimodal integration and semantic access (Jobard et al., 2003). Their high betweenness centrality may fit with the hypothesis that they play a role in 'semantic executive control' (Whitney et al., 2012), a process similar to what has been previously denoted as 'semantic access' (Lauro-Grotto et al., 1997). If a region plays a role in semantic control, one would predict a high betweenness centrality since semantic control requires coordination of and interaction with regions that are widely distributed over the cortical surface (Jefferies and Lambon Ralph, 2006; Noonan et al., 2010; Corbett et al., 2009, 2011). GTm is activated mainly in tasks that require explicit responses related to the identity or the semantic category of the stimuli (Van Doren et al., 2010). The effect of TMS on posterior GTm depends on task demands, in terms of degree of strategic control required during semantic knowledge retrieval (Whitney et al., 2012). The similarity between TMS effects in posterior GTm and GFi fit with the observation that both nodes belonged to the same subsystem (Fig. 3.3, Table 3.1). In contrast, TMS of IPS using the same paradigm yields qualitatively different effects, with a domain-independent selection deficit (Whitney et al., 2012). This is consistent with our observation that IPS belongs to a separate subsystem involved in more generic processes (Fig 3.3, table 3.1). The distinction between the perisylvian subsystem and a more general-purpose subsystem including vOT and IPS, among other nodes, is also in agreement with fMRI data directly contrasting orienting based on spatial versus semantic cues. Semantic cueing specifically activates the areas which our graph analysis assigned to the perisylvian subsystem, such as the posterior STS, posterior GTm, GFi and angular gyrus (Cristescu et al., 2006). In contrast, IPS was generally involved in both spatial and semantic cueing (Cristescu et al., 2006), in accordance with its assignment to a more general-purpose community in our graph analysis (Fig. 3.3).

The angular gyrus had the highest betweenness centrality of all nodes tested. In patients with aphasic stroke in the middle cerebral artery territory, semantic control is impaired and the angular gyrus is one of the areas that is regularly damaged under such conditions (Jefferies and Lambon Ralph, 2006; Noonan et al., 2010; Corbett et al., 2009, 2011). Other communities outside the perisylvian subsystem, such as the prefrontal subsystem, may also be involved in executive control, but the angular gyrus differed from these control regions as it was immersed in the perisylvian community according to our graph analysis. This may indicate that its role in regulatory control is specifically related to language and semantic processing, at least under the current experimental paradigm. Its function has been interpreted in terms of multimodal integration and it has been

implicated in semantic access (Jobard et al., 2003). The perisylvian subsystem also contained a second inferior parietal node in the supramarginal gyrus. This node corresponded with 50% probability with human cytoarchitectonic area PF (Caspers et al., 2006, 2008), an area that has been implicated in dictation and repetition, as well as gesture discrimination and imitation (Nelissen et al., 2010).

The perisylvian community also contained several nodes with a high local clustering coefficient but a relatively low betweenness centrality. The local clustering coefficient of a given node x reflects how frequently the neighbours of node x are connected also directly with each other. Using a social-life metaphor, it constitutes a measure of 'cliquishness'. Apart from the left anterior inferior frontal gyrus (Goldberg et al., 2007), the nodes with the highest local clustering coefficients have been typically implicated in word-specific processing, such as the pars orbitalis of the frontal operculum, and left anterior and posterior STS (all above 0.45, table 3.1). The posterior third of the left STS showed a high local clustering coefficient (0.47) with relatively low betweenness centrality (0.03), which clearly differed from the posterior middle temporal gyrus (0.33 and 0.10, respectively). Its connectivity profile was also clearly different (Fig.3.3, Table 3.2B). These observations confirm the functional dissociation between these 2 juxtaposed posterior temporal regions (Vandenbulcke et al., 2007). Left posterior STS was principally connected with nodes within the perisylvian subsystem, including the angular and supramarginal gyrus, anterior STS, anterior temporal pole, the orbital part of the frontal operculum and posterior GTm. Left posterior STS hypoactivity is associated with slowing of visual word identification speed as well as naming deficits, suggestive of a role of posterior STS in lexical-semantic retrieval (Vandenbulcke et al., 2007). Alternatively, the association between STS activity and word identification speed could also be explained by a role of posterior STS in graphophonological conversion (Jobard et al., 2003). Activity level in left posterior STS also increases with increasing rates of hearing or retrieving words and in noun and verb generation versus rest, which may indicate a role in transient representation of phonological sequences (Wise et al., 2001). From an anatomical perspective, fascicles that form the structural basis for the dense interconnectedness within the perisylvian system are probably the arcuate fascicle, the middle longitudinal fascicle and the extreme capsule (Schmahmann and Pandya, 2009).

A second highly robust system was located distally and concentrically to the perisylvian module. vOT was part of this subsystem rather than the perisylvian subsystem. This has implications for the function attributed to vOT. If vOT were an area of interaction between a triangular network of orthography, phonology, and semantics (Woodhead et al., 2011; Price and Devlin, 2011), one would rather expect it to belong to the perisylvian language subsystem containing the lateral temporal, inferior frontal and inferior parietal nodes. This was not the case. Instead, vOT belonged to a subsystem that also contained IPS, typically implicated in attentional selection (Vandenberghe et al., 2005; Molenberghs et al., 2008; Vandenberghe and Gillebert, 2009) and hippocampus, typically implicated in episodic memory. In our interpretation, the contribution of this ventral occipitotemporal

system relates more to conscious perception, visuoperceptual identification, attentional selection, access of perceptual units to visual short-term memory, and long-term memory (Bundesen et al., 2005). Identification ('categorization') of perceptual units is determined by sensory evidence, relevance and expectancy which determine access of the perceptual units to visual short-term memory (Bundesen and Habekost, 2008). The interaction account of vOT (Price and Devlin, 2011) with prediction error is closely related to this proposal. According to this hypothesis, vOT integrates top-down predictions from the language system with bottom-up visual input (Price and Devlin, 2011). Based on a meta-analysis of reading studies, Jobard et al. (2003) implicated vOT in segmentation and classification of visual stimuli in familiar units. At the moment we do not attribute a specific semantic role to this community but rather a general-purpose function that is not necessarily exclusively related to language or semantic processing. We propose that this system functions as an 'amplifier' of inner representations of perceptual units, mediating conscious perception and enhancing access of these units to other cognitive systems, e.g. involved in episodic memory (Van Doren et al., 2010, 2012). This hypothesis is also compatible with the observation that this community contains a remarkably high proportion of hub nodes. It is important to distinguish vOT from the ventral anterior temporal region that has been implicated in multimodal conceptual representations specifically (Visser and Ralph, 2011; Visser et al., 2012a). Neuroanatomically, an important structural basis for this community may be provided by the inferior longitudinal fascicle, which runs from IPS over ventral occipital cortex and also connects to medial temporal cortex (Schmahmann and Pandya, 2009).

Complementary to the analysis of the community structure our approach also allowed us to define the connections between the perisylvian and the ventral occipitotemporal subsystem. The two subsystems were connected through a unique link between left vOT and the posterior third of left GTm. This indicates the pivotal role of both vOT and GTm at the interface between these two communities. vOT was one of the regions with highest betweenness centrality, similarly to GTm and angular gyrus, confirming its pivotal role in the network. According to neurosurgical dissection of postmortem brains, these two structures are joined through the superficial layer of the inferior fronto-occipital fascicle, which connects superior parietal and basal temporal cortex with middle temporal gyrus and the inferior frontal gyrus (Martino et al., 2010; Sarubbo et al., 2013).

Apart from the perisylvian and the ventral occipitotemporal subsystem, the community structure revealed 4 additional communities (Fig. 3.3). The only node with high betweenness centrality lying outside the perisylvain or ventral occipitotemporal communities was the left inferior frontal junction. Left IFJ was part of a prefrontal subsystem with multiple nodes in inferior frontal sulcus, middle and superior frontal gyrus, both at the lateral convexity and to the medial side. It is plausible to attribute to this subsystem (Fig. 3.3, blue dots) a role in cognitive control (Derrfuss et al., 2005). Several of these nodes have been identified as hubs in previous studies (Buckner et al., 2009).

To conclude, the temporal and occipital constituents of the 'associative-

semantic network', defined by contrasting an explicit associative-semantic task with a visuoperceptual task with words and pictures, can be decomposed into two subsystems: a lateral temporal pathway that runs along the posterior third of the temporal gyrus and the superior temporal sulcus and is connected with inferior frontal areas and the angular gyrus, and, secondly, a lateral and ventral occipital pathway that runs anteriorly towards medial temporal cortex and is connected dorsally with the intraparietal sulcus. The transition zone between ventral occipital and temporal cortex, region vOT, belonged to the latter subsystem. These two systems are uniquely connected with each other through a link between GTm and vOT. Together, these two regions constitute the interface between these two communities.

4

Reproducibility and Robustness of Graph Measures of the Associative-Semantic Network

Abstract

Graph analysis is a promising tool to quantify brain connectivity. However, an essential requirement is that the graph measures are reproducible and robust. We have studied the reproducibility and robustness of various graph measures in group based and in individual binary and weighted networks derived from a task fMRI experiment during explicit associative-semantic processing of words and pictures. The nodes of the network were defined using an independent study and the connectivity was based on the partial correlation of the time series between any pair of nodes. The results showed that in case of binary networks, global graph measures exhibit a good reproducibility and robustness for networks which are not too sparse and these figures of merit depend on the graph measure and on the density of the network. Furthermore, group based binary networks should be derived from groups of sufficient size and the lower the density the more subjects are required to obtain robust values. Local graph measures are very variable in terms of reproducibility and should be interpreted with care. For weighted networks, we found good reproducibility (average test-retest variability $< 5\%$ and ICC values > 0.4) when using subject specific networks and this will allow us to relate network properties to individual subject information.

This chapter has been published as: Yu Wang, Natalie Nelissen, Katarzyna Adamczuk, An-Sofie DeWeer, Mathieu Vandenbulcke, Stefan Sunaert, Rik Vandenberghe, Patrick Dupont. Reproducibility and Robustness of Graph Measures of the Associative-Semantic Network. *Plos One* 9: e115215.

4.1 Introduction

There is a surge of interest in mapping and modelling the complicated networks within the brain. Functional connectivity analyses of neuroimaging data are based on the concept of synchrony between the signal responses in spatially distinct brain regions (Niu and He, 2013). Analysing networks extracted from functional imaging data has proven to be a promising tool to investigate the complex functional structure of the human brain that influences the dynamics underlying cognition (Bullmore and Sporns, 2012, 2009; Rubinov and Sporns, 2010).

A promising tool to rigorously study the problem is graph analysis. This provides a framework to characterize and to quantify networks (Achard et al., 2006; Micheloyannis et al., 2006, 2009; van den Heuvel et al., 2008; He et al., 2007b). Many non-trivial graph characteristics, such as small-worldness, modularity and highly connected hubs, have been observed in human brain networks. Differences in graph properties have been found in people with Alzheimer's disease (Wang et al., 2013) and schizophrenia (van den Heuvel et al., 2010; Micheloyannis et al., 2006; Ma et al., 2012), and also in association with age (Wang et al., 2010; Micheloyannis et al., 2009). Changes in graph measures were also found during motor learning (Heitger et al., 2012) and taking nicotine (Wylie et al., 2012). All these studies suggest that graph analysis can be a promising tool in clinical and basic research to characterize brain connectivity in a way that is both biologically meaningful and related to normal and abnormal function. However, an essential requirement when using this type of quantification is that the different measures are reproducible and robust.

The reproducibility of graph measures has already been investigated in a number of studies looking at binarized networks derived from structural MRI (Bernhardt et al., 2011; Tijms et al., 2012), diffusion-weighted MRI (Vaessen et al., 2010; Bassett et al., 2011; Li et al., 2012; Liu et al., 2013), resting state fMRI (Telesford et al., 2010; Weber et al., 2013; Wang et al., 2013), MEG (Deuker et al., 2009) and resting-state functional near infrared spectroscopy (Niu et al., 2013). Only one study has looked at the reproducibility of graph measures when using task fMRI (Weber et al., 2013). Graph measures using task fMRI is expected to be different compared to resting state fMRI since functional connectivity between two nodes depend on the context (i.e. resting state versus a specific task context). Furthermore, the reproducibility of weighted graph measures has received very little attention: only two studies are available which addressed this problem and both were using graphs derived from diffusion-weighted MRI (Owen et al., 2013; Buchanan et al., 2014). Therefore, we investigated the reproducibility and the robustness of graph measures of weighted and binarized networks derived from a task fMRI during explicit associative-semantic processing of words and pictures. This task activates a distributed set of brain areas that has been replicated across a wide range of studies (Vandenberghe et al., 1996; Vandenbulcke et al., 2007; Nelissen et al., 2007, 2011; Buckner et al., 2000; Van Doren et al., 2010; Seghier and Price, 2011; Whitney et al., 2011; Goldberg et al., 2007; Binder et al., 2009; Wagner et al., 1997). Previously, we have applied graph analysis to examine the

structure of this network (Vandenberghe et al., 2013).

4.2 Materials and Methods

4.2.1 Participants

A group of 54 healthy elderly participants (age (mean ± std): 65.2 ± 5.6 yrs; 31 male) (Adamczuk et al., 2013) performed an associative-semantic judgement task. Twenty-eight subjects were scanned on a 3T Philips Intera system equipped with an 8-channel receive-only head coil (Philips SENSitivity Encoding head coil). Twenty-six subjects could not undergo the fMRI in the Intera system due to space limitation in the scanner lumen in combination with the screen. These subjects were scanned on a 3T Philips Achieva system equipped with a 32-channel receive-only head coil (Philips 10 SENSitivity Encoding head coil) which used a screen placed behind the individual's head for the projection.

The protocol was approved by the Ethics Committee University Hospitals Leuven (EudraCT: 2009-014475-45) and written informed consent was obtained from all subjects in accordance with the Declaration of Helsinki.

4.2.2 Experimental design

Stimuli were projected onto a screen (resolution of 1024 x 768 pixels, refresh rate 60 Hz) using Presentation 14.8 (NeuroBehavioural Systems, Albany, CA, USA). The design of the fMRI experiment was factorial (Vandenberghe et al., 1996; Vandenbulcke et al., 2007; Nelissen et al., 2007, 2011). The first factor, task, had two levels: associative-semantic versus visuoperceptual judgement. The second factor, input modality, also had two levels: pictures versus printed words. During a trial of the associative-semantic condition, a triplet of stimuli was presented for 5250 ms, one stimulus on top (the sample stimulus) and one in each lower quadrant (the test stimuli), at 4.6° eccentricity, followed by a 1500 ms interstimulus interval. Subjects had to press a left- or right-hand key depending on which of the two test stimuli matched the sample stimulus more closely in meaning. A given triplet was presented either as pictures or as words and this was counterbalanced across subjects. In the visuoperceptual control condition, a picture or word stimulus was presented in three different sizes (mean picture size was 3.7° and mean letter size 1.2°). Subjects had to press a left- or right-hand key depending on which of the two test stimuli matched the sample stimulus more closely in size on the screen. An epoch, i.e. a block of trials belonging to the same condition, consisted of four trials (total duration 27 s). The fifth condition consisted of a resting baseline condition during which a fixation point was presented in the centre of the screen. During each fMRI run (5 runs in total), a series of the 5 epoch types, was replicated 3 times. The order of conditions was pseudorandom and differed across runs of the same subject. Subjects received a practice session before entering the scanner. In this session we determined which size difference (9%, 6%, 3%, or 1%) for the visuoperceptual conditions was needed for each individual subject to

obtain comparable accuracies as for the associative-semantic conditions.

4.2.3 Preprocessing of the data

Image analysis was performed using Statistical Parametric Mapping (SPM8, Wellcome Department of Cognitive Neurology, London, UK. http://www.fil.ion.ucl.ac.uk/spm). Functional images of each subject were realigned to correct for small head motion during each run. The anatomical T_1-weighted image was coregistered to the average of the realigned functional volumes and non-linearly normalized to Montreal Neurological Institute (MNI) space using the unified segmentation approach (Ashburner and Friston, 2005) and the resulting transformation was used to spatially normalize the functional images. The voxel size of the images in MNI space was 3x3x3 mm^3. Images were smoothed using a 6x6x6 mm^3 Full Width at Half Maximum (FWHM) Gaussian kernel. We also applied a temporal high-pass filter (cut-off 270s) and a low-pass filter consisting of the canonical hemodynamic response function. The epoch-related response was modelled by a canonical hemodynamic response function convolved with a boxcar.

4.2.4 Network construction

Volumes of interests (VOI) were taken from a previously published study on the associative-semantic network (Vandenberghe et al., 2013), namely fifty-seven spheres (radius 6 mm) located at least 20 mm apart. The spheres were centred on group-specific activation maxima (from the main effect of task) determined from this previous study. Note that the position of the VOIs was identical as in the previous study, i.e. the functional information in the current study was not used to position the VOIs. We have previously shown that the nodes of the associative semantic network have a low anatomical inter-subject variability (Dupont et al., 2008).

For each subject, we applied each of these VOIs to the current dataset and we extracted the time series after whitening, filtering and removing effects of no interest (session specific effects) using code from statistical parametric mapping software (SPM8; Wellcome Department of Cognitive Neurology, London, UK; http://www.fil.ion.ucl.ac.uk/spm). Finally, the average time series in the VOI was calculated as the mean of the time series over all voxels in the VOI. Time series of different runs were concatenated. It is important to note that we used the whole time series, i.e. it includes all the different conditions as well as the null condition.

Based on the average time series, partial correlation coefficients between volumes of interest were calculated. Partial correlation was used to obtain the degree of association between regions, with the effect of other regions removed (Marrelec et al., 2006; Smith et al., 2011). Among the methods evaluating functional interdependencies between functional MRI time courses in different regions, partial correlations have a high sensitivity to network connection detection (Smith et al., 2011). An association matrix was defined in which each element represents the association strength between two regions. The association strength

is defined as the absolute value of the z-score which is calculated from the partial correlation using the Fisher r-to-z transform (Finn, 1974):

$$z = \frac{\sqrt{n-3-(p-2)}}{2} \ln \frac{1+r}{1-r} \tag{4.1}$$

in which r is the partial correlation, n the number of data points in the time series and p the number of nodes.

The great majority of network analysis in systems neuroscience relies on the construction of undirected and unweighted graphs through thresholding of the association matrix (Bullmore and Sporns, 2009; Rubinov and Sporns, 2010). The thresholded association matrix represents a binary adjacency matrix with 1 indicating the presence and 0 indicating the absence of an edge (connection) between two vertices (nodes/regions). A possible approach to define the threshold is to fix the network's edge density (also referred to as wiring cost), i.e. the number of existing edges divided by the number of possible edges. In order to investigate changes in the network topology as a function of network density, we thresholded the association matrix at network densities ranging from 5% to 45%, in steps of 5%. Densities below 5% are considered too sparse and densities above 50% are less likely to be biological (Kaiser and Hilgetag, 2006; Hosseini et al., 2013). Furthermore, we also included a density of 7.8% corresponding to the density of the associative-semantic network in the previously published study (Vandenberghe et al., 2013).

The binarization of connections has one major drawback: it enhances scale contrast by underrating (overrating) connections because connections around the threshold may vary considerably between subjects. To avoid this problem, weighted graph analysis (Li et al., 2014; van den Heuvel et al., 2010; Schwarz and McGonigle, 2011; Wang et al., 2011; Van Wijk et al., 2010), which preserves all the edge information, is also used. To obtain weights W with $0 \leq W \leq 1$, we applied a nonlinear mapping of z score to weight:

$$W = 2\Phi(|z|) - 1 \tag{4.2}$$

where Φ is the cumulative distribution function of the standard normal distribution.

4.2.5 Graph-theoretical analysis

Local and global graph measures were calculated for the binary network (at different densities) as well as for the weighted network using the brain connectivity toolbox version 2013_12_25
(https://sites.google.com/a/brain-connectivity-toolbox.net/bct/Home; (Rubinov and Sporns, 2010)). We calculated the following local graph measures for node i: node degree k_i, average path length L_i, local clustering coefficient C_i, local efficiency $E_{loc,i}$, efficiency E_i and betweenness centrality b_i. Global measures included characteristic path length λ, mean clustering coefficient C, mean local efficiency E_{loc}, global efficiency E and mean betweenness centrality b. For the

definition of these network measures, we refer to (Rubinov and Sporns, 2010). It should be noted that isolated nodes can be present when the density of the network is very low. In that case, these nodes were not taking into account when calculating the network measures.

The network itself was either defined at the individual level (for every subject separately) or at the group level (after averaging the association matrices across the subjects belonging to that group).

4.2.6 Reproducibility at the individual level

To look at the intra-subject reproducibility, two groups were constructed by evenly splitting each subject's time series into two parts by randomly assigning four of the five runs to one of the two even parts. This corresponds to the situation in which each subject is measured twice under the same conditions. In this way we constructed two groups of paired subjects. We refer to this situation as the *split-half* case. A partial correlation based network and corresponding graph measures were obtained for each subject in each group across a range of densities or using the weights of the network.

The intraclass correlation coefficient (ICC) was used to analyse reproducibility of the network (Telesford et al., 2013). More specifically, values were merged into a 2 x 54 matrix (number of measurements x subjects). The total variance was split into the between-subject (BMS) and the residual (EMS) variance. ICC values were calculated according to the equation (Shrout and Fleiss, 1979):

$$ICC(3,1) = \frac{BMS - EMS}{BMS + EMS}. \tag{4.3}$$

By randomly switching (100 random realizations) time series parts between the two measurements, we can calculate the mean and variance of the ICC for each graph measure. ICC > 0.4 is usually considered as a cut-off for a fairly reliable measure (Faria et al., 2012).

We also calculated the test-retest value between the two measurements of the same subject and averaged this over all subjects to obtain the average test-retest value. The test-retest TRT was calculated as:

$$TRT = 100 \left| \frac{m_2 - m_1}{\frac{m_1 + m_2}{2}} \right|, \tag{4.4}$$

where $|.|$ denotes the absolute value and m_1 and m_2 are the values of the graph measure under investigation obtained in the first and second measurement respectively.

4.2.7 Reproducibility for group-based graph measures

Averaging the association matrices across subjects summarizes the overall characteristics of the group (Rubinov and Sporns, 2011; Power et al., 2011). To study the reproducibility for group-based graph measures, we looked at the test-retest

TRT calculated as equation 4.4 except that m_1 and m_2 represent the measures obtained for the first and second group. Mean and variance of each graph measure were calculated based upon the 100 random realizations of switching time series parts.

However, a more challenging situation occurs when we want to compare two independent groups which are scanned on MR scanners with different field strength and which differ slightly in the fMRI paradigm. This is the case when we want to compare the results of the current group with the results of our previous study (Vandenberghe et al., 2013). In that study we used the same paradigm (except that we did not include a null condition in our measurement). Furthermore, the data of this group ($n = 33$) were acquired on a 1.5 T Siemens Sonata. Age (67.2 $\pm$ 8.5 years) and gender (19 M/14 F) were similar to the current study. We refer in the remaining of the paper to the comparison of these two studies as the *between-independent groups* case. The test-retest values were calculated according to equation 4.4.

4.2.8 Hubs and community structure

We also assessed the reproducibility of the community structure and the identification of hubs for binary and weighted networks at the individual and the group level.

The identification of hubs was based on a hub score (van den Heuvel et al., 2010; Vandenberghe et al., 2013; Heitger et al., 2012; Bullmore and Sporns, 2012; Wu et al., 2013; Shi et al., 2013; Fornito and Bullmore, 2015), which is the sum of dummy values for four criteria. We gave a score of 1 or 0 depending on whether or not the node belongs to the top 20% of nodes with 1) the highest node degree, 2) the highest betweenness centrality, 3) the lowest local cluster coefficient (limited to nodes with a degree > 2), and 4) the lowest average path length. Nodes with a hub score ≥ 2 were considered hubs.

We evaluated the consistency of hubs by measuring the co-occurrence of hubs (H_C) across networks. If H_A is a list of hubs in network A and H_B in network B, the co-occurrence is calculated as

$$H_C = \frac{2\,|H_A \cap H_B|}{|H_A| + |H_B|} \tag{4.5}$$

where $|.|$ denotes the cardinality of the set. A value of 1 corresponds to a perfect agreement of hubs while 0 reflects no agreement at all.

To determine the community structure of the network, we used the algorithm of Newman (Newman, 2006a) as implemented in the Brain Connectivity Toolbox. The algorithm starts from a random order of the nodes which lead to a slightly different community structure each time the algorithm is applied. To generate a consensus assignment of nodes to communities, we used a two step procedure (Barnes et al., 2012). In the first step, we computed a co-assignment matrix represented as an $N * N$ matrix, where cell (i, j) was equal to 1 if node i and node j were assigned to the same community. During the second step, a probabilistic co-

assignment matrix is then obtained by averaging 100 realizations of co-assignment matrices.

The consistency of the community structure of the network was assessed by probabilistic scaled inclusivity (pSI), a metric quantifying the consistency of communities across multiple networks and which is an extension of the scaled inclusivity SI (Steen et al., 2011; Moussa et al., 2012). SI is calculated by measuring the overlap of modules across multiple networks while penalizing for disjunction of modules. For example, a node i is part of module A_i in network A and module B_i in network B. Then SI for node i, denoted as SI_i, is calculated as

$$SI_i = \frac{|S_{A_i} \cap S_{B_i}|}{|S_{A_i}|} \frac{|S_{A_i} \cap S_{B_i}|}{|S_{B_i}|} \tag{4.6}$$

where S_{A_i} and S_{B_i} denote sets of nodes in modules A_i and B_i and $|.|$ denotes the cardinality of a set. If the two modules A_i and B_i consist of an identical set of nodes, then $SI_i = 1$. The SI value between two networks is a value between 0 and 1; if $SI = 1$ at a particular node, it means that the node is in the same module with exactly the same set of nodes in the two networks. A problem with this way of calculating the SI value is that it requires a final assignment of nodes to a community. This can be done based upon the probabilistic co-assignment matrix but may lead to different results depending on the algorithm to assign the final community to each node. An alternative is to use the probabilistic co-assignment matrix directly to calculate a probabilistic SI value. This is done as follows:

$$pSI(i) = \frac{(\sum_{j=1}^{N} P_A(i,j).P_B(i,j))^2}{\sum_{j=1}^{N} P_A(i,j). \sum_{j=1}^{N} P_B(i,j)} \tag{4.7}$$

in which $P_A(i,j)$ and $P_B(i,j)$ are the probability co-assignment between nodes i and j in network A and network B.

To further characterize the consistent parts of the communities, we averaged the co-assignment matrices for the two groups in the *between-independent groups* case or across every possible pair in the *split-half* case.

There's no established rule to define which H_C and pSI are sufficiently high to ensure consistency between networks but we can determine if it is significantly different from the value obtained under random conditions by comparing it to the distribution of values obtained from null networks, i.e. networks with the same number of nodes and connections which were generated by randomly (1000 realizations) rewiring the observed network (Zalesky et al., 2012). The weighted null network is obtained by randomly rewiring connections with the same distribution of weights.

4.2.9 Robustness of the data

Group size effect

We applied a bootstrapping procedure (100 realizations) to calculate graph measures as a function of group size. More specifically, we created random subsamples

from our 54 subjects, each time creating a subgroup with a certain number of subjects, and we repeated this for subgroup sizes ranging from 10 to 53. Results were calculated as the relative change (in %) taking the values of the complete group of 54 subjects as the reference.

Network robustness

When we identify the nodes of the network, we may not have captured all nodes. The question then arises, in how far this is affecting the quantification of the network. To address this question, we assume that the 57 nodes represent all nodes of the underlying network and we removed nodes from this network to investigate the impact when nodes were not captured. The procedure is similar to network robustness analysis against random failures and targeted attacks (Bernhardt et al., 2011; Albert and Barabási, 2002; Achard et al., 2006) although the interpretation is clearly different. Since it is more likely to miss the least significant nodes, we conducted our analysis by removing nodes based on their significance in the main effect of task in the fMRI study starting by removing the least significant ones. The degree of tolerance will be expressed as the relative change of the graph measures compared to values of the network with all 57 nodes.

4.2.10 Statistics

To evaluate if ICC values were significantly higher than 0.4, we performed a one-sample t-test. The same test was used to evaluate if the test-retest variability was $< 5\%$ or $< 10\%$. The comparison between subject-specific graph measures obtained in two independent groups was assessed by a two-sample t-test. To test the relation between test-retest variability of global graph measures and density, we first log-transformed the test-retest values and performed a linear regression.

The statistical threshold to reach significance was set to $p_{cor} < 0.05$. We corrected for the number of densities under investigation in case of global graph measures and additionally for the number of nodes in case of local graph measures.

4.3 Results

In table 4.1 a summary of the main findings is given.

4.3.1 Reproducibility at the individual level (subject-specific networks)

Averaged global ICC across all randomizations are shown in figure 4.1 for binary (over a range of densities) and weighted networks. For binary networks, global efficiency E, characteristic path length λ and mean betweenness centrality b show significant ($p_{cor} < 10^{-4}$) reproducibility ($ICC > 0.4$) when the network density is high ($\geq$40%). This is not the case for the mean cluster coefficient and the mean

Table 4.1: Summary of the main findings.

Subject-specific networks

Binary networks

- Global efficiency, characteristic path length and mean betweenness centrality are reproducible only when the network density is high.
- The intra subject split-half test-retest values of global graph measures decreases with the increase of density.

Weighted networks

- Global graph measures are reproducible for all the measures investigated.
- The intra subject split-half test-retest values of global graph measures were very low.
- The test-retest values of the mean of the global graph measures derived from subject-specific weighted networks for two independent groups varied between 7 and 17%.
- Communities are consistent for both intra-subject (in the split-half case) and inter-subject comparisons.
- The average global graph measures are not critically depending on the group size.
- The average global graph measures show robustness against missing nodes.

Group-based networks

Binary and weighted networks

- In the split-half case, all graph measures show test-retest variability $< 10\%$
- Hubs show a significant high consistency in the split-half case compared to the values obtained from random null networks.
- Communities show consistency for both the split-half case and when comparing independent groups
- A sufficiently large group size is required to obtain reliable results.
- Global efficiency and characteristic path length are more robust for the group size.
- Global efficiency, characteristic path length, mean local efficiency and clustering coefficient are more robust against missing nodes compared to the mean betweenness centrality

Binary networks

- Test-retest variability of global graph measures decreases as the network becomes more dense.

Weighted networks

- The global efficiency and the characteristic path length have the smallest overall test-retest variability.

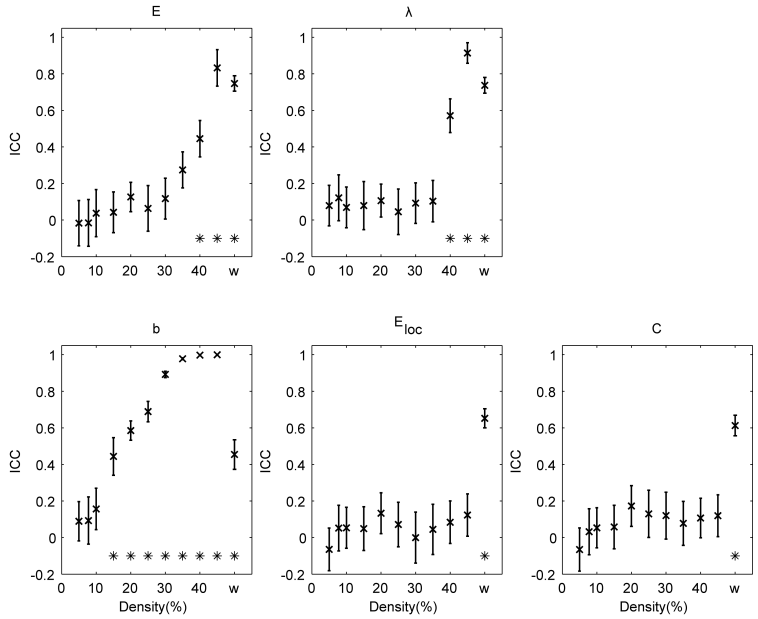

Figure 4.1: Reproducibility at the individual level. ICC for the global efficiency (E), the characteristic path length (λ), the mean betweenness centrality (b), the mean local efficiency (E_{loc}) and the mean clustering coefficient (C). The results are shown for binary (over a range of densities) and weighted (w) networks. Error bars denote the standard deviation. Values significantly ($p_{cor} < 0.05$) higher than 0.4 are indicated with *.

local efficiency. Weighted global graph measures show significant ($p_{cor} < 10^{-8}$) reproducibility ($ICC > 0.4$) for all the measures investigated (figure 4.1).

As can be expected, reproducibility at the nodal level exhibits heterogeneity across graph measures and nodes (see table S1). Efficiency E_i and average path length L_i are the most reproducible nodal graph measures (although only in 2 nodes a significant ($p_{cor} < 0.05$) ICC value > 0.4 was found) in contrast to the betweenness centrality b_i which is the least reproducible one. In case of weighted local graph measures, we observed the following range of averaged (across subjects) ICC values: $0.03 \leq E_i \leq 0.45$; $0.01 \leq L_i \leq 0.44$; $0.03 \leq b_i \leq 0.32$; $3 \times 10^{-4} \leq E_{loc,i} \leq 0.36$ and $0.02 \leq C_i \leq 0.38$.

The intra subject split-half test-retest values (TRT) for global graph measures are shown for binary and weighted networks (figure 4.2). The test-retest values of global graph measures decreases with the increase of density in case of binary networks (for all global graph measures under investigation $p_{cor} < 10^{-10}$). For weighted networks, the test-retest values were excellent ($< 5\%$): E:1.12% ($p_{cor} < 10^{-10}$); λ: 1.11% ($p_{cor} < 10^{-10}$); b: 4.09% ($p_{cor} < 10^{-4}$); E_{loc}: 1.93% ($p_{cor} < 10^{-10}$) and C: 2.40% ($p_{cor} < 10^{-10}$).

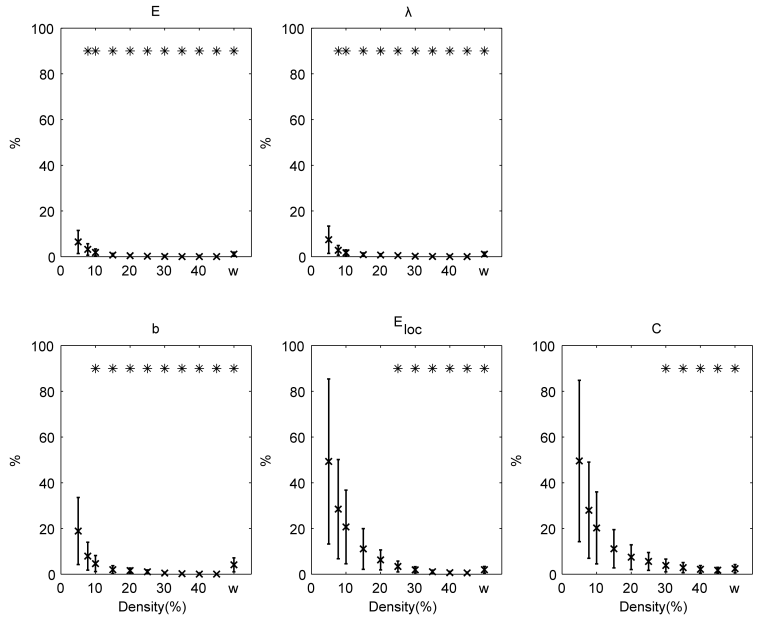

Figure 4.2: Intra-subject split-half test-retest variability (%). The results are shown for binary (over a range of densities) and weighted (w) networks. Error bars refer to the standard deviation across all randomization and subjects. E: global efficiency; λ: the characteristic path length; b: the mean betweenness centrality; E_{loc}: the mean local efficiency; C: the mean clustering coefficient. Test-retest variabilities significantly ($p_{cor} < 0.05$) lower than 10% are indicated with *.

In table 4.2, we show the comparison of the global graph measures derived from subject-specific weighted networks for the two independent groups. The values in the current group are significantly different from those obtained in our previous study (Vandenberghe et al., 2013) and the test-retest values of the mean of the global graph measures derived from subject-specific weighted networks for two independent groups varied between 7 and 17% (table 4.2).

Table 4.2: Comparison of global graph measures derived from subject-specific weighted networks between two independent groups.

	Current study mean ± std	Previous study (Vandenberghe et al., 2013) mean ± std	TRT of the mean %
mean clustering coefficient	0.588 ± 0.020	0.520 ± 0.022	12
characteristic path length	1.444 ± 0.028	1.544 ± 0.034	7
global efficiency	0.739 ± 0.014	0.690 ± 0.016	7
mean local efficiency	0.629 ± 0.018	0.566 ± 0.020	11
mean betweenness centrality	0.0057 ± 0.0003	0.0067 ± 0.0004	17

TRT: test-retest variability

4.3.2 Reproducibility for group-based graph measures

Test-retest variability for the different global graph measures are shown for the *split-half* case (figure 4.3) and the *between-independent groups* case (figure 4.4) for binary and weighted networks.

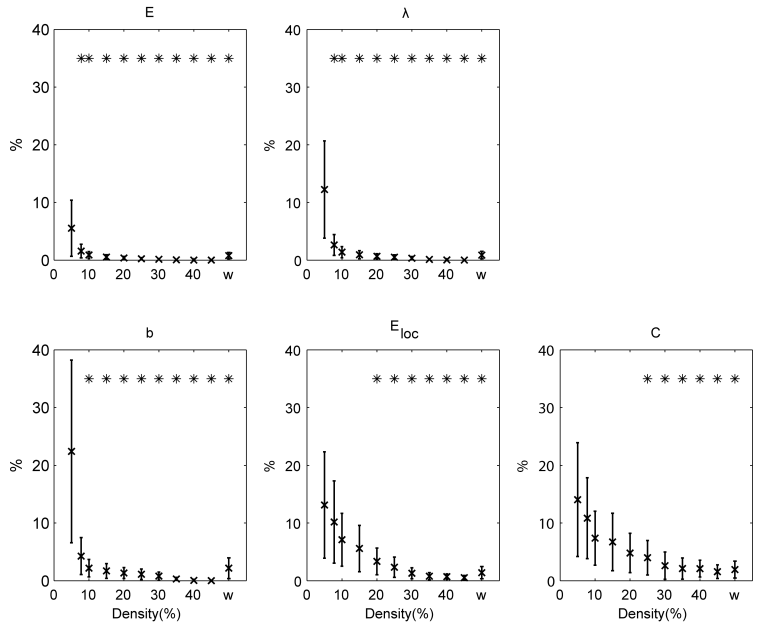

Figure 4.3: Test-retest variability (%) for the split-half case. The results are shown for binary (over a range of densities) and weighted (w) networks. Error bars refer to the standard deviation. E: global efficiency; λ: the characteristic path length; b: the mean betweenness centrality; E_{loc}: the mean local efficiency; C: the mean clustering coefficient. Test-retest variabilities significantly ($p_{cor} < 0.05$) lower than 10% are indicated with *.

In the *split-half* case (figure 4.3), all graph measures show a significantly ($p_{cor} < 10^{-5}$) small test-retest variability ($< 10\%$) for binary (with densities $\geq 25\%$) and weighted networks. The global graph measures showing the smallest overall test-retest variability are the global efficiency and the characteristic path length. For binary networks, test-retest variability of global graph measures decreases as the network becomes more dense (for all global graph measures under investigation: $p_{cor} < 10^{-10}$). When looking at the local graph measures (table 4.3), we observe that the efficiency and average path length in the majority of nodes show a significantly ($p_{cor} < 0.05$) small test-retest variability ($< 10\%$) for both binary (with densities $\geq 10\%$) and weighted networks. On the other hand, betweenness centrality has the largest test-retest variability. In the *between-independent groups* situation, there was a trend that the test-retest variability

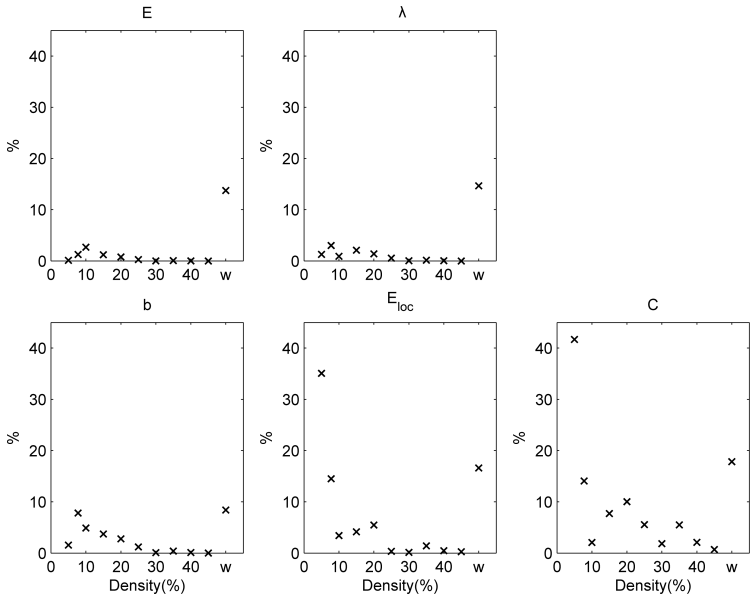

Figure 4.4: Test-retest variability (%) between independent groups for binary (over a range of densities) and weighted (w) networks. E: global efficiency; λ: the characteristic path length; b: the mean betweenness centrality; E_{loc}: the mean local efficiency; C: the mean clustering coefficient.

of global graph measures in case of binary networks (figure 4.4) decreases as the network becomes more dense (for all global graph measures under investigation: uncorrected $p < 0.05$). Furthermore, the test-retest variability for graph measures of weighted networks in this situation are mostly above 10%. When looking at the local graph measures (table 4.4), we observe that the efficiency and average path length in the majority of nodes show small test-retest variability ($< 10\%$) for binary networks with densities $\geq 15\%$.

4.3.3 Hubs and communities

We analysed the hubs and community structure for binary and weighted networks at the individual and group-averaged level.

At the group-averaged level, table 4.5 shows the co-occurrence of hubs H_C in the *split-half* case and in the comparison between independent groups. For binary and weighted networks, hubs show a significant ($p_{cor} < 0.05$) high consistency in the *split-half* case compared to the values obtained from random null networks. However, when comparing two independent groups the consistency of the hubs is clearly reduced.

The results for the consistency of the community structure are given in table 4.6 as the mean pSI for both binary and weighted networks. Communities show

Table 4.3: The split-half case: the test-retest variability of local graph measures across densities

% of nodes with a significant ($p_{cor} < 0.05$) test-retest variability $< 10\%$

Density%	5	7.8	10	15	20	25	30	35	40	45	w
node degree	28	9	7	0	0	0	0	2	0	0	98
cluster coefficient	9	0	0	0	0	0	4	12	37	75	98
average path length	0	53	91	95	98	100	100	100	100	100	100
efficiency	23	65	89	95	96	100	100	100	100	100	100
local efficiency	7	2	2	2	21	46	79	95	100	100	98
betweenness centrality	0	0	0	0	0	0	0	0	0	0	0

median test-retest variability (%)

Density%	5	7.8	10	15	20	25	30	35	40	45	w
node degree	15	18	18	16	16	15	14	13	12	11	5
cluster coefficient	56	41	31	24	20	16	13	10	9	7	6
average path length	15	8	6	5	4	4	3	3	3	3	3
efficiency	11	7	6	5	4	4	3	3	3	3	3
local efficiency	58	46	34	23	14	8	5	4	3	2	6
betweenness centrality	90	69	58	52	49	44	40	37	33	29	42

consistency for both the *split-half* case and when comparing independent groups, i.e. the pSI values are significantly different from those obtained from random null networks. When we look at groups of nodes which are consistently assigned (average value in the co-assignment matrix > 0.95) to the same module between the two independent groups at the density 7.8%, we find the following groups: 1) nodes in the dorsomedial prefrontal gyrus, the left superior frontal gyrus, the left supplementary motor area, the left anterior and the right cingulate gyrus; 2) nodes in the left inferior frontal gyrus pars orbitalis, the left posterior middle temporal gyrus, the left anterior and posterior superior temporal sulcus and the left supramarginal gyrus; 3) nodes in the left lingual gyrus, the left intraparietal sulcus and the left middle occipital gyrus; 4) nodes in the left superior frontal gyrus and the left medial frontal; 5) nodes in the right caudate, the left anterior thalamus and posterior thalamus; 6) nodes in the right inferior and middle occipital gyrus. At the individual level for weighted networks in the split-half case, the mean intra-subject co-occurrence of hubs H_C across all 54 subjects and 100 randomization is 0.32 ($p_{uncor} > 0.1$) while the mean inter-subject H_C across all pairs of subjects is 0.31 ($p_{uncor} > 0.1$). The mean intra-subject consistency of the community structure pSI across all 54 subjects and 100 randomization is 0.19 ($p_{cor} < 0.05$) while the mean inter-subject pSI across all pairs of subjects is 0.21 ($p_{cor} < 0.05$).

At the individual level for weighted networks in the comparison of two indepen-

Table 4.4: **Between independent groups: the test-retest variability of local graph measures across densities**

% of nodes with a test-retest variability $< 10\%$

Density%	5	7.8	10	15	20	25	30	35	40	45	w
node degree	26	18	25	19	16	16	23	21	26	35	25
cluster coefficient	7	7	12	14	19	19	32	53	53	75	26
average path length	23	47	46	60	65	72	79	84	81	75	30
efficiency	30	44	53	60	65	68	72	77	72	75	35
local efficiency	4	7	16	26	40	53	70	88	98	100	30
betweenness centrality	7	5	2	4	7	7	11	12	16	16	14

median test-retest variability (%)

Density%	5	7.8	10	15	20	25	30	35	40	45	w
node degree	40	40	29	25	27	29	24	20	18	16	18
cluster coefficient	129	73	57	26	26	20	13	9	9	6	19
average path length	18	11	11	8	7	7	5	4	4	5	16
efficiency	17	11	9	8	8	6	6	5	5	5	15
local efficiency	133	79	53	22	17	8	5	3	3	2	18
betweenness centrality	116	118	105	91	60	62	58	52	44	37	67

Table 4.5: Co-occurrence of hubs H_C.

Split-half case

Density%	5	7.8	10	15	20	25	30	35	40	45	w
H_C	**0.62**	**0.70**	**0.78**	**0.75**	**0.73**	**0.70**	**0.68**	**0.66**	**0.64**	**0.62**	**0.79**

Between-independent groups

Density%	5	7.8	10	15	20	25	30	35	40	45	w
H_C	0.43	0.32	**0.52**	0.31	0.31	0.30	*0.41*	0.30	0.34	0.40	*0.43*

Bold: Values which are significantly ($p_{cor} < 0.05$) different from the value obtained from null networks (see text). Italic: $p_{uncor} < 0.05$.

dent groups, the mean inter-subject H_C across all pairs of subjects was 0.31 for the current study and this was not significantly different from 0.32 obtained from the data of the previous study (Vandenberghe et al., 2013). However, the mean inter-subject pSI across all pairs of subjects was significantly ($p < 10^{-10}$) different: 0.21 for the current study versus 0.18 for the previous study (Vandenberghe et al.,

Table 4.6: Mean pSI

Split-half case

Density%	5	7.8	10	15	20	25	30	35	40	45	w
pSI	**0.31**	**0.35**	**0.40**	**0.42**	**0.42**	**0.47**	**0.50**	**0.56**	**0.54**	**0.49**	**0.50**

Between-independent groups

Density%	5	7.8	10	15	20	25	30	35	40	45	w
pSI	**0.14**	**0.13**	**0.15**	**0.18**	*0.14*	**0.29**	**0.23**	**0.35**	**0.33**	**0.37**	**0.44**

Bold: Values which are significantly ($p_{cor} < 0.05$) different from the value obtained from null networks (see text). Italic: $p_{uncor} < 0.05$.

2013).

4.3.4 Group size effect

For group based networks, the relative change of global graph measures as a function of group size are shown in figure 4.5 for networks with a density of 5%, 20%, 45% as well as for the weighted network. Overall, the relative difference in graph measures when taken the complete group (54 subjects) as the reference, decreases when the number of participants and/or the density increase. Furthermore, some binary graph measures are more robust for the group size: the absolute value of the relative error of global efficiency and characteristic path length are significantly ($p_{cor} < 0.05$) smaller than 10% even for smaller group sizes ($\geq$ 10 subjects) for all densities $\geq$ 7.8%. The mean betweenness centrality, the mean local efficiency and the mean clustering coefficient show a similar behaviour but for minimum group sizes of respectively 17, 38 and 44 subjects for a binary network at a density of $\geq$ 7.8%. At a density of 5%, the minimum group size to obtain relative errors significantly ($p_{cor} < 0.05$) smaller than 10% in absolute value, could only be determined for E, E_{loc}, C and λ and this size was respectively 42, 44, 44 and 49 subjects. For the weighted network, the minimum group size is 13, 14, 19, 20 and 23 for E, λ, b, E_{loc} and C respectively.

At the individual level for weighted networks, all the average global graph measures showed a small relative error ($< 5\%$ in absolute value, $p_{cor} < 0.05$) as a result of the smaller group size even for groups as small as 10 subjects (figure 4.6).

4.3.5 Network robustness

For group based networks, the robustness of graph measures in case we missed the least significant nodes is shown in figure 4.7 for binary (with an initial density of 5%, 20%, 45%) and weighted networks. The robustness depends on the network

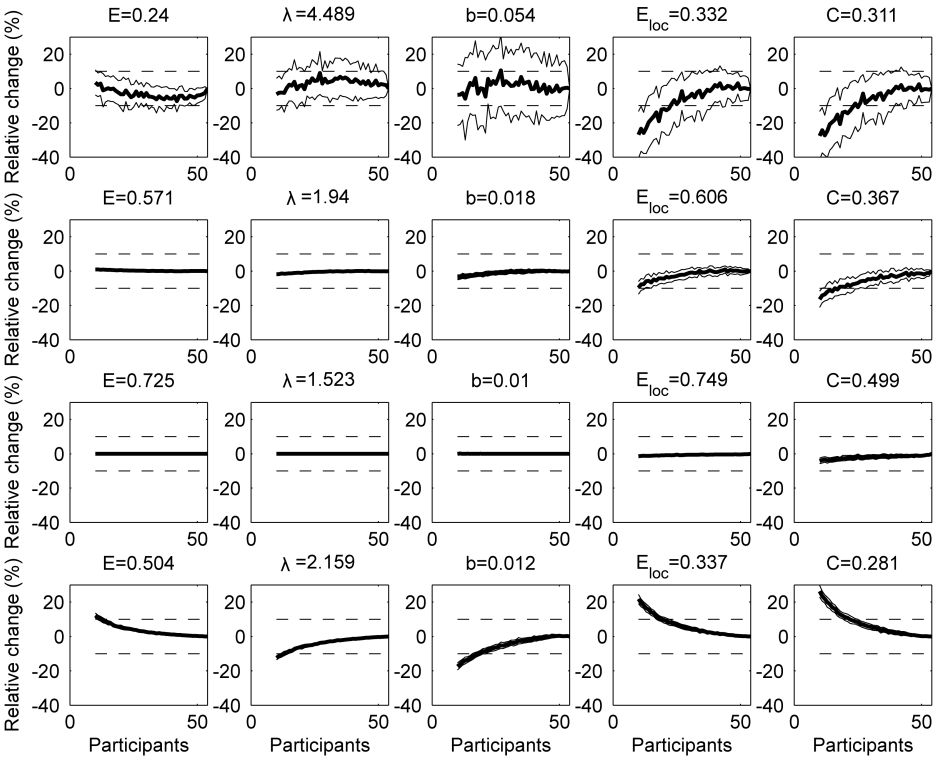

Figure 4.5: Group size effect for group based networks. The effect of group size for networks at a density of 5% (top row), 20% (second row), 45% (third row) and the weighted network (bottom row). A bootstrapping procedure was used (100 realizations) to randomly group the subjects with increasing group size. For graph measures the relative change (%) to the reference value (which is obtained when taking the complete group) are shown. Full lines denote the mean (bold) and ± standard deviation of the metric. Dotted lines represent a relative change of ± 10%. E: global efficiency; λ: the characteristic path length; b: the mean betweenness centrality; E_{loc}: the mean local efficiency and C: the mean clustering coefficient.

measure under investigation. Global efficiency, characteristic path length, mean local efficiency and clustering coefficient are more robust compared to the mean betweenness centrality.

At the individual level for weigthed networks, the robustness to missing nodes remains within 10% error ($p_{cor} < 0.05$) up to removal of the 8 least significant nodes (figure 4.8).

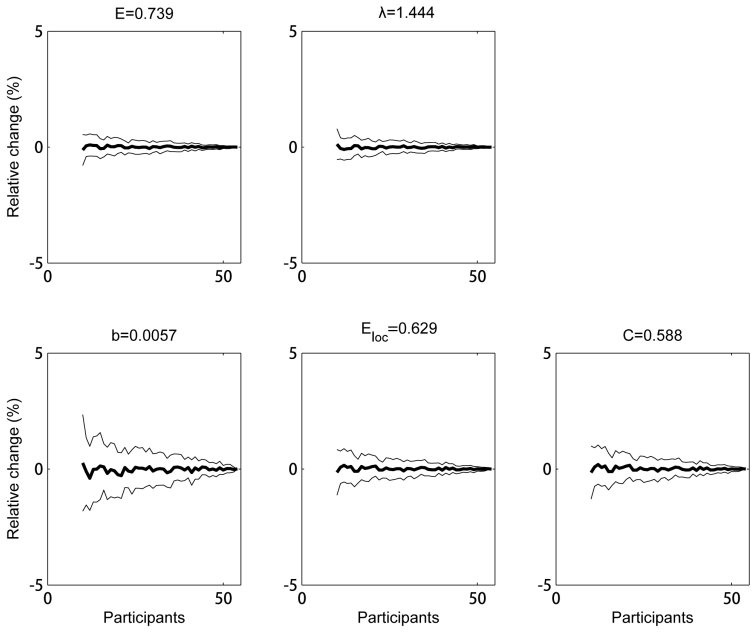

Figure 4.6: Group size effect for groups of individual networks. The average across subjects of the weighted graph measures determined from the individual's network is shown as function of group size. A bootstrapping procedure was used (100 realizations) to randomly group the subjects with increasing group size. For graph measures the relative change (%) to the reference value (which is obtained by averaging across all subjects) are shown. Full lines denote the mean (bold) ± standard deviation of the metric. Dotted lines represent a relative change of ± 10%. E: global efficiency; λ: the characteristic path length; b: the mean betweenness centrality; E_{loc}: the mean local efficiency and C: the mean clustering coefficient.

4.4 Discussion

In this work, reproducibility and robustness of the functional connectivity network associated with an associative-semantic task was examined by studying local and global graph measures, hubs and the community structure. The nodes of the associative-semantic network were taken from a previous study (Vandenberghe et al., 2013). The paradigm that we used gives a highly consistent activation pattern using univariate analyses and this is replicated in our and other centres (Vandenberghe et al., 1996; Vandenbulcke et al., 2007; Nelissen et al., 2007, 2011; Buckner et al., 2000; Van Doren et al., 2010; Seghier and Price, 2011; Whitney et al., 2011; Goldberg et al., 2007; Binder et al., 2009; Wagner et al., 1997). Furthermore, we have shown previously that the nodes have a low anatomical inter-subject variability (Dupont et al., 2008). This consistency and reproducibility

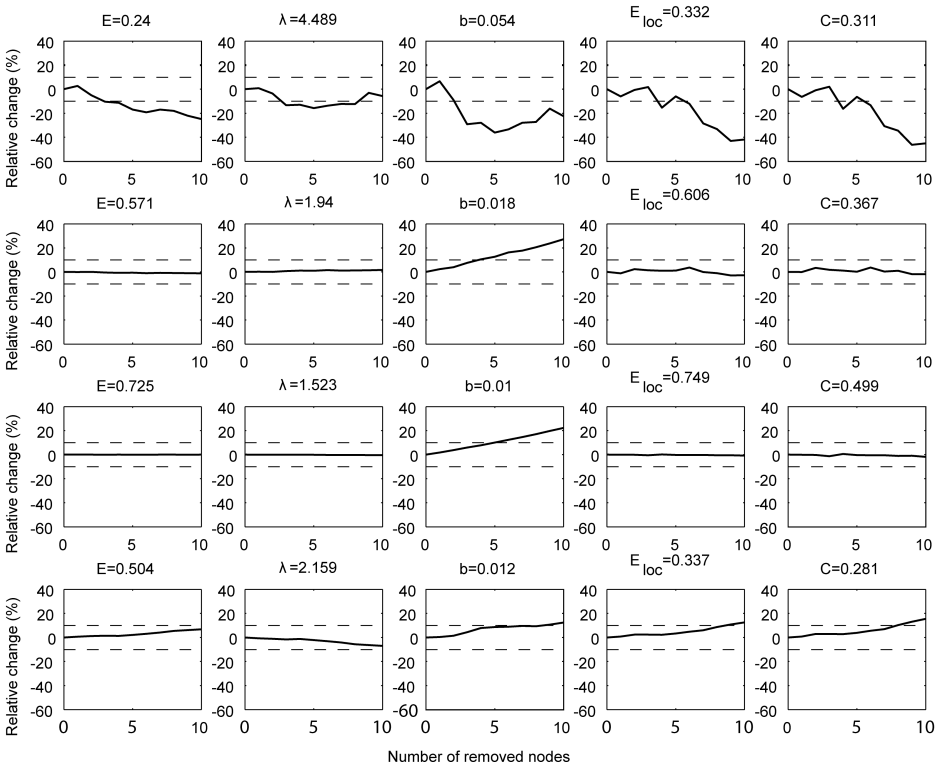

Figure 4.7: Robustness to missing nodes for networks with an initial density of 5% (top row), 20% (second row), 45% (third row) and the weighted network (bottom row). The relative change (%) to the value obtained when taking the intact network as the reference is shown. The nodes were removed based on their significance in the main effect of task (starting with the least significant ones). Dotted lines indicate the ± 10% interval. Relative changes significantly ($p_{cor} < 0.05$) lower than 10% in absolute value are indicated with *.

at the nodal level is essential when looking at the network measures.

4.4.1 Choice of connectivity measure

A network is dependent on the choice of the measure of connectivity between different brain regions. Many groups investigating functional networks in the human brain use the Pearson correlation coefficient (Schwarz and McGonigle, 2011; Hayasaka and Laurienti, 2010; van den Heuvel et al., 2008). Other similarity measures have also been used, including the correlation between wavelet components (Wang et al., 2013; Achard et al., 2006; Achard and Bullmore, 2007) and mutual information (Smith et al., 2011). However, constructing a network

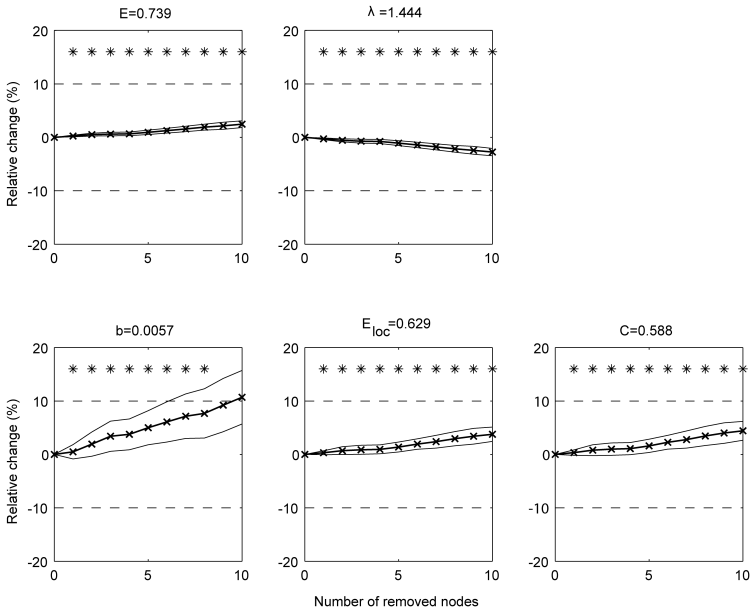

Figure 4.8: Robustness to missing nodes for individual weighted networks. The relative change (%) to the value obtained when taking the intact network as the reference is shown. The nodes were removed based on their significance in the main effect of task (starting with the least significant ones). Full lines denote the mean (bold) ± standard deviation of the metric across all subjects.

by correlation or mutual information does not necessarily imply that the functional connection between two nodes is direct. The distinction between direct and indirect functional relationships between areas is very important in terms of correctly estimating the network. Hence, partial correlation became a hot topic in recent years (e.g.(Marrelec et al., 2006; Soranzo and Altafini, 2007; Stifanelli et al., 2013)). Partial correlation provides a convenient summary of conditional independence and turns out to be an effective way to model the connectivity (Smith et al., 2011). In our work, partial correlations are used to remove mutual dependencies on common influences from other brain areas. By conditioning the dependencies between two nodes on other nodes, the functional connectivity (i.e. partial correlation) reflects a quantity that is more closely related to direct interaction, taking the analysis of functional connectivity closer to the characterization of functional interactions in terms of effective connectivity. It is data-driven in the sense that, unlike existing methods such as structural equation modelling (SEM) and dynamic causal modelling (DCM), it does not require any prior information regarding functional interactions.

4.4.2 Split-half variability versus comparison of two independent groups

In this work, we have studied two situations which reflect two complete different situations when looking at the variability of the measurement. The first situation is the one in which we have split the time series in two even parts to assess the split-half variability. This corresponds to a situation in which subjects are measured twice under almost similar conditions (i.e. exactly the same scanner, the same sequence, the same paradigm) within one session and assuming no time effects. The limitation of this approach is that we have violated the temporal order of the runs and that the number of runs in the newly composed parts is small. The other situation corresponds to the measurement of two independent groups on different scanners using a slightly different paradigm. As can be expected, the test-retest variability in the latter case is larger than the split-half variability in case of weighted networks and for most densities. The test-retest values of the mean of the global graph measures derived from subject-specific weighted networks for two independent groups varied between 7 and 17%. However, the values were significantly different between both groups most likely due to the inclusion of a null condition in the current study.

4.4.3 Reproducibility

For binary group based networks, we observed that the reproducibility improves when the density of the network increases. Networks with high density, weighted group based networks and weighted individual networks show all a very good reproducibility for the global graph measures. Only when we compared two independent groups, the weighted group based network showed a weaker reproducibility. Networks with low density (e.g. 5%) showed weak reproducibility and this was depending on the graph measure itself.

Local graph measures showed weak reproducibility in almost all situations for most nodes and therefore quantification of local graph properties needs to be interpreted with care.

4.4.4 Hubs and community structure

A node playing a pivotal role in the flow of information is called a hub but the operational definition of a hub differs between studies. In the current study, we have taken a similar approach as (van den Heuvel et al., 2010). We observe a high co-occurrence in the *split-half* case but a low co-occurrence for the comparison between independent groups. We also observe that the co-occurrence is relatively stable over the different densities and this is also the case for the weighted graph measures. The average inter-subject and intra-subject co-occurrence of hubs in case of individual weighted networks is somewhat lower and this is probably due to the higher variability which one can expect in individual networks compared to group based networks.

The community structure represents how nodes are separated into interacting (integrated) but distinct (segregated) functional modules. A major challenge in examining network module organization is the reproducibility of modules and how to measure this reproducibility. Several studies compared modularity Q and number of communities to achieve this goal (Schwarz and McGonigle, 2011; Wang et al., 2011; Braun et al., 2012). However, the value of Q only gives a sense of the network strength in dividing itself into modules. One could easily have two networks which may be considerably different, yet sharing the same number of communities and similar Q values. A more appropriate measure is to use scaled inclusivity which is a measure for the overlap of modules across networks while penalizing for disjunction of modules (Moussa et al., 2012; Steen et al., 2011). The calculation requires a final assignment of nodes to a community. In this work, we have extended this formula so that it is now directly based on the probabilistic co-assignment matrix without the need to assign each node to a community. In case the co-assignment matrix is binarized (which is similar to assigning each node to a community) it reduces to the original formula. We found that the reproducibility of the community structure of weighted group based networks was similar or even better compared to the values for dense binarized networks. When looking at the average intra- and intersubject probabilistic scaled inclusivity, we observed smaller values most likely again due to the higher variability which you can expect in individual networks compared to group based networks.

4.4.5 Group size effect

An important issue relates to the number of subjects required to obtain robust graph measures. In a recent study (Button et al., 2013), it was emphasized that a small sample size undermines the reproducibility of neuroscience. We found that in low density networks, a large number of subjects is required to obtain robust values and this depends on the graph measure under investigation (global efficiency and characteristic path being the most stable measures). The use of weighted graph measures leads to robust values. This is also true for the averaged graph measures in case of individual weighted networks.

4.4.6 Robustness against missing nodes

If we have not captured all nodes of the network, the question is in how far graph measures will be influenced. Indeed, some nodes are only weakly activated in an fMRI experiment and the choice of selection of inclusion of nodes can be based on a statistical criterion. We found that all graph measures, except the mean betweenness centrality, are robust even if we didn't include several of these weaker nodes.

4.4.7 Binary versus weighted networks

The popularity of binary network analysis may arise from the fact that in most cases it is simpler to characterize (Rubinov and Sporns, 2010). In our previous

study (Vandenberghe et al., 2013), we have binarized the network based on a statistical criterion (significant association values). If we would have applied the same criterion in our current study, we would have found much more significant connections (and therefore a higher density) because of the larger cohort size, the inclusion of a null condition and the use of an MRI scanner with a higher magnetic field. Networks with different densities can have different properties (Van Wijk et al., 2010). To overcome this problem, we used an equi-density thresholding (Achard and Bullmore, 2007; He et al., 2008) and we have studied the networks at different densities like most other studies (Achard and Bullmore, 2007; Hayasaka and Laurienti, 2010; Wang et al., 2010; Schwarz and McGonigle, 2011). Another problem with the use of a threshold to binarize the network is that a small change in the association (connectivity) strength can lead to a change in connectivity (just below versus just above a threshold).

To overcome these problems, one can define a weighted network. The question is then how to define these weights. Some groups take the connection with the highest connectivity value and set this to one and scale the remaining connections accordingly (van den Heuvel et al., 2010). This approach is straightforward and simple but it is also more sensitive to noise. We propose an approach which is based on the fact that the partial correlations were transformed to a Z-score using a Fisher r-to-Z transform and by applying a non-linear transform based on the cumulative distribution of the standard normal distribution. This approach is less sensitive to noise (or to outliers) in connection strength and it leads in a natural way to positive weights between 0 and 1.

4.4.8 Subject specific versus group based networks

When studying brain networks in a group of subjects we have two possible approaches: 1) define the network for each subject, calculate the variables of interest (e.g. network measures) and use these values for further analysis or 2) define the network based upon the group itself by e.g. averaging the association matrices across the subjects of the group and by calculating the network (and the corresponding measures) based upon this averaged association matrix. The first approach gives information about the individual variability and we can relate directly graph measures to other subject specific information. This is important especially in the light of comparing and quantifying networks in normals and patients. However, the disadvantage is that the results are more sensitive to noise in the measurements. On the other hand, the notion that averaging connection strengths across subjects summarizes the overall characteristics of the group is widely accepted (Rubinov and Sporns, 2011; Power et al., 2011).

Based on the ICC values and on the intra-subject test-retest results, weighted individual networks can be reliably determined. The fact that the identification of hubs and communities is more variable compared to the group based networks is less important since it may also be a result of subject specific behaviour and in that sense it may capture the underlying biological variability.

4.5 Conclusion

We have studied the reproducibility and robustness of various graph measures in group based and in individual binary and weighted networks derived from an fMRI experiment using an associative-semantic paradigm. We have shown that global graph measures exhibit a good reproducibility and robustness but the results depend on the graph measure itself and on the density in case of binary networks. Group based binary networks should be derived from groups of sufficient size and the lower the density the more subjects are required to obtain robust values. Local graph measures are very variable in terms of reproducibility and should be interpreted with care. For weighted networks, we found good reproducibility when using subject specific networks and this will allow us to relate network properties to individual subject information.

4.6 Supporting Information

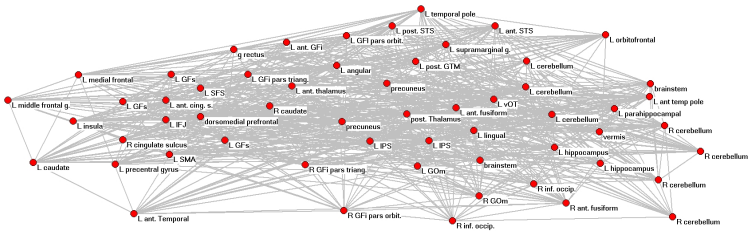

Figure S4.1: Graph of the associative-semantic network. The connection strength is determined by the partial correlation. Only connections which are significant at uncorrected $p < 0.05$ are shown. The density is 42.6%.

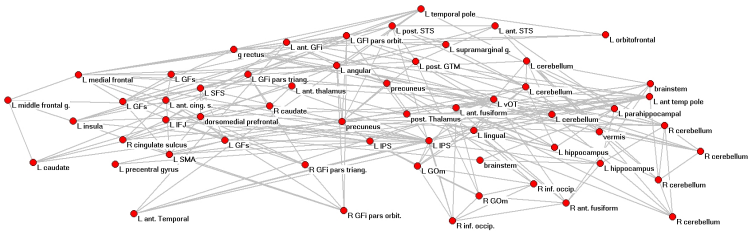

Figure S4.2: Graph of the associative-semantic network. The connection strength is determined by the partial correlation. Only connections which are significant at corrected (for the number of possible connections) $p < 0.05$ are shown. The density is 14%.

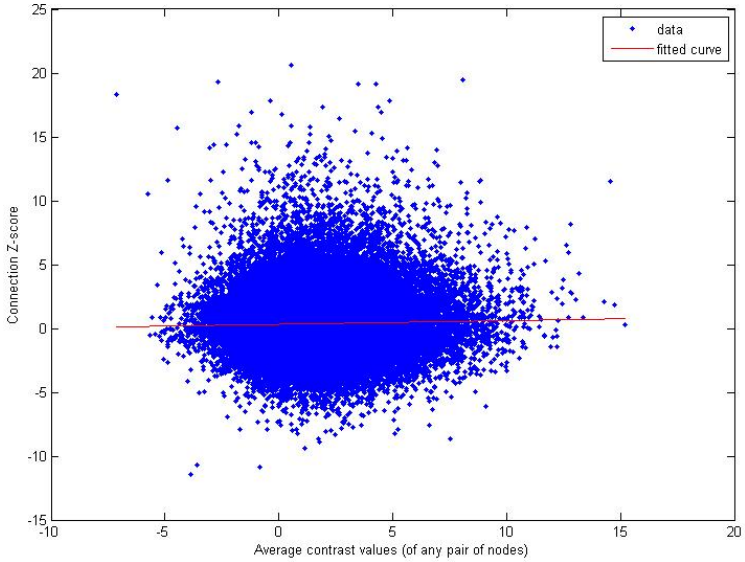

Figure S4.3: Correlation between the average contrast values (based on the beta values and the main contrast of task) of any pair of nodes and the strength of the functional connectivity (expressed as the Z-values obtained from the partial correlations after a Fisher r-to-z transform) between these nodes to investigate if there is a relation between GLM results and the likelihood of having an edge. Values are plotted for every connection and every subject. The correlation is weak ($r = 0.027$) but very significant ($p < 10^{-10}$).

Table S4.1 ICC values for each node for different graph measures at different densities and for the weighted network; http://journals.plos.org/plosone/article?id =10.1371/journal.pone.0115215

5

Generalization of clustering coefficient and local efficiency for fully weighted undirected networks

Abstract

Incorporating edge weights in the graph analysis, calls for generalizations of the graph metrics. However, the generalizations of clustering coefficient and local efficiency in literature are sensitive to the changes in edge weight. It is preferable that the generalization should possess three important properties: general versatility, weight-scale invariance and continuity. It is also preferable that the generalization be robust to the accumulation of noisy connections, which we call as overall robustness, especially for large scale fully weighted networks. In this study, we reviewed the existing generalization of clustering coefficient and local efficiency and proposed our generalizations. We evaluated our generalization by comparing the four properties with the existing ones in the simulated data as well as real world data. Our generalizations outperform existing ones in terms of general versatility, weight-scale invariance, continuity and overall robustness.

This chapter has been submitted for publication: *Yu Wang, Rik Vandenberghe, Patrick Dupont, Generalization of clustering coefficient and local efficiency for fully weighted undirected networks*

5.1 Introduction

A complex system can be modelled as a graph or network, which is composed of nodes and edges connecting them. Analysis over a wide range of complex systems has led to a fundamental insight: many complex systems often share certain topological characteristics and these can be captured by graph theoretical metrics (Barabasi and Oltvai, 2004; Amaral and Ottino, 2004; Zhang and Horvath, 2005; Bullmore and Sporns, 2009; Fornito et al., 2013). Take small worldness for example which has been found in many real world networks (He et al., 2007b; Opsahl and Panzarasa, 2009; Batalle et al., 2012; Vandenberghe et al., 2013), and which is an indication of the cost-efficiency of these networks.

While traditional graph analysis use binary edges to enhance contrast between strong and weak connections, there's an increasing demand of utilizing edge weight which entails potentially important information. Incorporating edge weights in the graph analysis, calls for generalizations of the graph metrics. While some of these measures can be naturally generalized to a weighted version, e.g., node degree to node strength, others cannot be generalized straightforwardly. The generalization of clustering coefficient and local efficiency, which are used to quantify small worldness (Watts and Strogatz, 1998; Achard and Bullmore, 2007; Batalle et al., 2012) is far from trivial.

The clustering coefficient reflects the tendency that neighbours of a node are also neighbours to each other (Rubinov and Sporns, 2010). The clustering coefficient is high in small world networks compared to random networks (Watts and Strogatz, 1998). Local efficiency is a measure for the fault tolerance of the system (Latora and Marchiori, 2003). A small world network features a local efficiency intermediate to that of regular (lattice) and random network (Achard and Bullmore, 2007; Batalle et al., 2012). The two measures are related in a way that the clustering coefficient in an undirected network is found to be a reasonable approximation of local efficiency (Latora and Marchiori, 2003).

Although it is straightforward to find the neighbours of a node, the question of how to define their weighted surrogates is far from obvious. Several generalizations are proposed (Barrat et al., 2004; Onnela et al., 2005; Zhang and Horvath, 2005; Saramäki et al., 2007; Opsahl and Panzarasa, 2009; Miyajima and Sakuragawa, 2014; Rubinov and Sporns, 2010). Different definitions capture slightly different aspects of the network, yet some of the existing generalizations are not designed for fully weighted networks (Rubinov and Sporns, 2010; Barrat et al., 2004; Onnela et al., 2005). These generalizations require the removal of the weak/noisy connections beforehand. A preferable solution is to adapt the formulas for a fully weighted network (Zhang and Horvath, 2005; Saramäki et al., 2007; Opsahl and Panzarasa, 2009; Miyajima and Sakuragawa, 2014).

A generalization should ideally satisfy some criteria as proposed by (Miyajima and Sakuragawa, 2014):

1. **General versatility:** If the input is given as a binary network, the output of the generalizations should give the same results as the binary version.

2. **Weight-scale invariance:** The graph measure is invariant to a global

scale factor for all edges.

3. **Continuity:** The graph measure should be continuous so that small changes in the edge value will lead to small changes in the graph measure.

However, in case of fully weighted networks, a fourth criterion should be satisfied:

4. Overall robustness: The graph measure should be robust to the accumulation of noisy connections. The contribution of weak/noisy connections to a graph measure is often negligible due to the small values. However, accumulation of weak connections may distort the characteristic of the graph metrics. The impact of weak/noisy connections may become important in a fully weighted network, especially when the network size is large.

In this paper, we first introduce existing generalizations and then we propose a generalization of the weighted clustering coefficient and local efficiency for fully weighted undirected networks with no self-connections. We evaluate our generalization in terms of general versatility, weight-scale invariance, continuity as well as overall robustness and compare it with existing generalizations. Finally, we apply the different generalizations on a well characterised network.

5.2 Methods

5.2.1 Existing generalizations

A good review of existing generalizations of the clustering coefficient and local efficiency can be found in (Miyajima and Sakuragawa, 2014). In that paper, the authors have investigated the general versatility, weight-scale invariance and continuity. Here, we will investigate also the fourth criterion of overall robustness. We first give a short description of the different generalizations which are currently available.

The (i, j)-th element a_{ij} of the adjacency matrix A is 1 if an edge between i and j exists, and 0 otherwise. In this work we assume that no self-connections are present, i.e. $a_{ii} = 0$. For a binary undirected network the clustering coefficient is given by:

$$C(i) = \frac{1}{k_i(k_i - 1)} \sum_{j,h;j\neq h} a_{ij}a_{ih}a_{jh} \tag{5.1}$$

with k_i the degree of node i. The node degree k_i is defined as the number of nodes connected to node i. The local efficiency is defined as:

$$E_{loc}(i) = \frac{1}{k_i(k_i - 1)} \sum_{j,h;j\neq h} a_{ij}a_{ih}[d_{jh}(G_i)]^{-1} \tag{5.2}$$

in which G_i is the subgraph consisting of the neighbours of i excluding node i, $d_{jh}(G_i)$ is the length of the shortest path between nodes j and h containing only neighbours of i. If no path containing these neighbours is found, $d_{jh}(G_i) = \infty$.

In a weighted network, we define the weight matrix W in which each element represents the weight between w_{ij} between node i and node j. All weights are assumed to have values between 0 and 1. If no connection is present, the weight is 0 (thus self-connections are assumed to have zero weight). The node degree k_i is calculated based on the presence of connections with non-zero weights irrespective of the amplitude. In case of a fully connected weighted network, i.e. $a_{ij} = 1$ if $i \neq j$, with N nodes, $k_i = N - 1$. The node strength which takes into account the weight of the connection, is defined by:

$$s_i = \sum_j w_{ij} \tag{5.3}$$

Note that for a binary network in which $w_{ij} = 1$ if a connection is present between nodes i and j and 0 otherwise, $s_i = k_i$.

Barrat et al. (2004) proposed a generalization by including the node strength s_i and the weight of connections from node i.

$$C^B(i) = \frac{1}{s_i(k_i - 1)} \sum_{j,h} \frac{w_{ij} + w_{ih}}{2} a_{ij} a_{ih} a_{jh}. \tag{5.4}$$

If the network is fully weighted, $C^B(i) = 1$ for all nodes i.

Onnela et al. (2005) proposed a weighted clustering coefficient based on the weighted triangles and this algorithm is used in the brain connectivity toolbox (Rubinov and Sporns, 2010).

$$C^O(i) = \frac{1}{k_i(k_i - 1)} \sum_{\substack{j,h \\ j \neq h}} (w_{ij} w_{ih} w_{jh})^{1/3} \tag{5.5}$$

Zhang and Horvath (2005) have defined, in their gene co-expression network analysis, a clustering coefficient for a fully weighted network.

$$C^Z(i) = \frac{\sum_{j,h;j\neq h} w_{ij} w_{ih} w_{jh}}{\sum_{j,h;j\neq h} w_{ij} w_{ih}} \tag{5.6}$$

Holme et al. (2007) have defined a similar definition as the previous one but normalized with $\max(w)$, the maximum edge weight of the network.

$$C^H(i) = \frac{1}{\max(w)} \frac{\sum_{j,h;j\neq h} w_{ij} w_{ih} w_{jh}}{\sum_{j,h;j\neq h} w_{ij} w_{ih}}. \tag{5.7}$$

Opsahl and Panzarasa (2009) proposed a generalization as

$$C^{Op}(i) = \frac{\sum_{j,h} f(w_{ij}, w_{ih}) a_{ij} a_{ih} a_{jh}}{\sum_{j,h;j\neq h} f(w_{ij}, w_{ih}) a_{ij} a_{ih}} \tag{5.8}$$

They proposed four methods to calculate $f(w_{ij}, w_{ih})$: arithmetic mean, geometric mean, maximum and minimum of the weights of the edges.

Miyajima and Sakuragawa (2014) extended the generalization of the cluster coefficient to the case of weighted directed networks using different functions (multiplication, geometric mean, minimum and harmonic mean). The case of multiplication and an undirected network, their generalization is the same as the one from Holme et al. (2007). For undirected networks, we give the other extensions below.
Geometric mean:

$$C^{M,gm}(i) = \frac{\sum_{j,h;j\neq h} \sqrt{\sqrt{w_{ij}w_{ih}}w_{jh}}}{\sum_{j,h;j\neq h} \sqrt{\sqrt{w_{ij}w_{ih}}\max(w)}} \tag{5.9}$$

Minimum:

$$C^{M,min}(i) = \frac{\sum_{j,h;j\neq h} \min(\min(w_{ij}, w_{ih}), w_{jh})}{\sum_{j,h} \min(\min(w_{ij;j\neq h}, w_{ih}), \max(w))} \tag{5.10}$$

Harmonic mean:

$$C^{M,hm}(i) = \frac{\sum_{j,h;j\neq h} \frac{2}{\frac{1}{\frac{2}{\frac{1}{w_{ij}}+\frac{1}{w_{ih}}}}+\frac{1}{w_{jh}}}}{\sum_{j,h;j\neq h} \frac{2}{\frac{1}{\frac{2}{\frac{1}{w_{ij}}+\frac{1}{w_{ih}}}}+\frac{1}{\max(w)}}} \tag{5.11}$$

A generalization of the local efficiency is given by Rubinov and Sporns (2010):

$$E^R_{loc}(i) = \frac{1}{k_i(k_i-1)} \sum_{j,h;j\neq h} (w_{ij}w_{ih}[d^w_{jh}(G_i)]^{-1})^{1/3} \tag{5.12}$$

where $d^w_{jh}(G_i)$ is the shortest distance between j and h, that contains only neighbours of i. The distance between nodes i and j in a network is defined as:

$$d^w_{ij} = \sum_{\substack{k,l \\ a_{kl}\in g^W_{i\leftrightarrow j}}} \frac{1}{w_{kl}} \tag{5.13}$$

with $g^W_{i\leftrightarrow j}$ the shortest weighted path between i and j.

5.2.2 Generalizations

Because not all measures are satisfying all criteria (see later) and to improve the robustness of these measures in case of fully weighted networks, we propose another generalization of the clustering coefficient as

$$C^W(i) = \frac{1}{\max(w)} \frac{\sum_{j,h}(\min(w_{ij}, w_{ih}, w_{jh}))^3}{\sum_{j,h}(\min(w_{ij}, w_{ih}))^2} \tag{5.14}$$

We extend the weighted local efficiency defined by (Rubinov and Sporns, 2010) to satisfy general versatility:

$$E_{loc}^{W}(i) = \frac{1}{\max(w)} \frac{\sum_{j,h}((\min(w_{ij}, w_{ih}))^3 [\tilde{d}_{jh}^{w}(N_i)]^{-1}}{\sum_{j,h}(\min(w_{ij}, w_{ih}))^2} \tag{5.15}$$

where $\tilde{d}_{jh}^{w}(N_i)$ is the adapted shortest distance between j and h.

The adapted shortest distance was calculated as follows:
1) Remove node i from the network. The weight of edge (j, h) in the remaining network is adapted to $\tilde{w}_{jh}$:

$$\tilde{w}_{jh} = \frac{w_{jh} w_{ij} w_{ih}}{(\max(w))^3} \tag{5.16}$$

2) The shortest distance $\tilde{d}_{jh}(N_i)$ in the adapted network was then calculated.

Weighting by $\max(w)$ makes the shortest distance invariant to the weight scale.

5.2.3 Evaluation of the generalizations

The general versatility can be proven mathematically by setting the weights to either 1 or 0 and show that the formula reduces to the one in case of binary networks. The weight-scale invariance can be proven by introducing a scaling factor and by showing that the generalizations are independent of this factor. Continuity depends on the continuity of the functions used in the generalization and especially the continuity when a small weight is approaching 0 could be a problem. In the latter case, setting a very small weight to zero would make a marked difference in the graph measure.

To evaluate the overall robustness, we start from a network and we add N_n nodes which all have noisy connections (i.e. with small weights ϵ) between each other and with all the nodes of the original network. Combined with the original network, we will call this the extended network N_{ext}. Theoretically, we should have the following property for the generalization: $M_{ext}(i) \to M(i)$ if $\epsilon \to 0$ for every node i of the original network in which $M_{ext}(i)$ and $M(i)$ are the generalizations of the clustering coefficient or the local efficiency of node i in respectively the extended and the original network. In practice, ϵ may have a small but non-zero value and therefore, we will also evaluate the overall robustness of the generalizations by calculating the error:

$$\Delta(\epsilon, N_n) = \sum_i \left(\frac{M(i) - M_{ext(\epsilon,N_n)}(i)}{M_{ext(\epsilon,N_n)}(i)} \right)^2 \tag{5.17}$$

for different values of ϵ and N_n.

5.2.4 Application to the associative-semantic network

An empirical network was taken to test the properties of the generalization. The associative-semantic network (ASN) is constructed from functional interactions between brain regions which are activated during the associative-semantic task

(Vandenberghe et al., 2013; Wang et al., 2014) measured using fMRI. The network has 57 nodes which are mostly located in the left hemisphere. The data are derived from an experiment in which 54 healthy elderly participants participated in an fMRI measurement on a 3T Philips system (Wang et al., 2014). The nodes were defined based on a previous experiment (Vandenberghe et al., 2013). Based on the average time series in these nodes, partial correlations were calculated. The weight of the edge between node i and j is calculated from the Fisher r-to-z transform z_{ij} of the partial correlation as:

$$w_{ij} = (2.\Phi(|z_{ij}|) - 1)^4. \tag{5.18}$$

where Φ is the cumulative distribution function of the standard normal distribution. The weights are a measure of the functional interaction between brain regions.

5.3 Results

5.3.1 General versatility

All the generalizations of the clustering coefficient lead to the standard formula in case of binary undirected networks as can be easily seen from the formulas (5.4-5.11,5.14), where $w_{ij} = a_{ij}$, $a_{ij} = 0$ or 1 and $s_i = k_i$.

However, the generalization of the local efficiency, introduced in equation 5.12, does not show this property because of the power $\frac{1}{3}$ and the fact that the distance can be larger than 1. In contrast, the generalization of the local efficiency proposed in this paper (equation 5.15) does show general versatility.

5.3.2 Weight-scale invariance

Weight-scale invariance means that if we multiply the weights by a factor, the measure should not change. This is the case for the generalizations of the clustering coefficient $C^B, C^H, C^{Op}, C^{M,gm}, C^{M,min}, C^{M,hm}$ and C^W but not for C^O and C^Z. This is also the case for the generalization of the local efficiency E^W_{loc} but not for E^R_{loc}.

5.3.3 Continuity

The node degree k_i is a discontinuous function for a weighted network since it will consider any node with a non-zero weight as a neighbour irrespective of the amplitude while if the weight becomes zero, the node degree will drop with 1. As a result, C^B, C^O and E^R_{loc} are not continuous. C^{Op} is also not continuous since in the numerator, only closed triangles will contribute no matter how small the weight of the third connection in the triangle is and the contribution depends only on the weights of the two other connections in the triangle. The other extensions $C^Z, C^H, C^{M,gm}, C^{M,min}, C^{M,hm}$ and C^W are all continuous.

5.3.4 Overall robustness

The generalizations for the nodal clustering coefficient or local efficiency have the property $M_{ext}(i) \to M(i)$ if $\epsilon \to 0$ for every node i of the original network in those cases which also showed continuity. However, the error $\Delta(\epsilon, N_n)$ is different among the different generalizations as will be shown in the example of the associative-semantic network (see below).

The results of each generalization for the four criteria is summarized in table 5.1.

Table 5.1: Properties of the different generalizations

Method	general versatility	weight scale invariance	continuity	overall robustness
C^B	x	x	-	-
C^O	x	-	-	-
C^Z	x	-	x	x
C^H	x	x	x	x
C^{Op}	x	x	-	-
$C^{M,gm}$	x	x	x	x
$C^{M,min}$	x	x	x	x
$C^{M,hm}$	x	x	x	x
C^W	x	x	x	x
E^R_{loc}	-	-	x	x
E^W_{loc}	x	x	x	x

x : YES and - : NO.

5.3.5 Application to the associative-semantic network

In this part, we will limit the analysis only to those generalizations which satisfied all four criteria (see table 5.1), i.e. C^H, $C^{M,gm}$, $C^{M,min}$, $C^{M,hm}$, C^W for the clustering coefficient and E^W_{loc} for the local efficiency. For comparison, we also include the generalizations C^O and E^R_{loc} used in the brain connectivity toolbox.

First, we compared the generalizations of the clustering coefficient in case of the fully weighted network and the weighted network after applying a soft-threshold to remove weak connections. An ideal generalization should not be affected too much by applying a soft-threshold. In figure 5.1 and table 5.2 the results are shown for different values for the soft-threshold leading to different densities of the network. Interestingly to note is that different generalizations also lead to different values of the local clustering coefficient (figure 5.1). Secondly, we compared the generalizations of the local efficiency in case of the fully weighted network and the soft-thresholded weighted network. The results are shown in figure 5.2 and table 5.3. If we look at the overall robustness of the generalizations of the local clustering coefficient and we plot the error Δ (formula 5.17) as function of the number of noisy nodes N_n with connection strength ϵ with each other node,

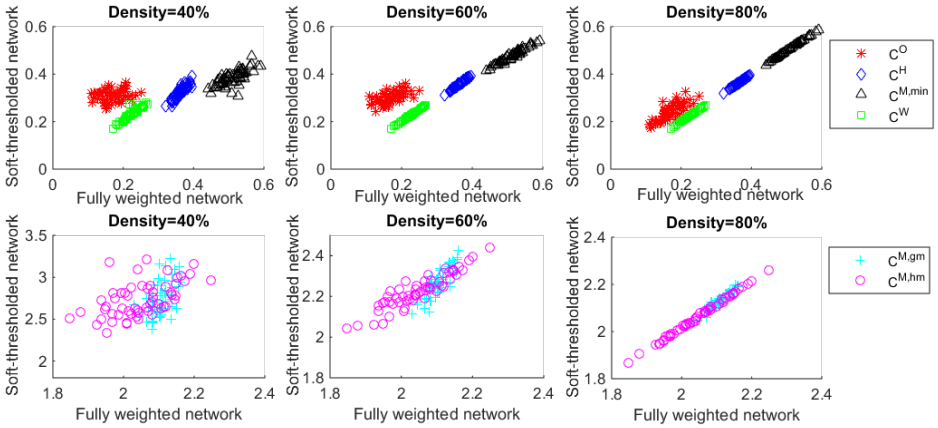

Figure 5.1: Scatter plot of the nodal clustering coefficient for different generalizations for nodes in the fully weighted network and the soft-thresholded weighted network (the latter leading to different densities).

Table 5.2: Correlation between the clustering coefficients calculated in each node for the fully weighted network and the soft-thresholded weighted network.

density (%)	40	60	80
C^O	0.21	0.57	0.81
C^H	0.91	1.00	1.00
$C^{M,gm}$	0.53	0.85	0.96
$C^{M,min}$	0.71	0.97	1.00
$C^{M,hm}$	0.54	0.92	1.00
C^W	0.93	1.00	1.00

Table 5.3: Correlation between the local efficiency calculated in each node for the fully weighted network and the soft-thresholded weighted network.

density (%)	40	60	80
E^R_{loc}	0.51	0.68	0.82
E^W_{loc}	0.97	1.00	1.00

we can observe that C^W leads to the lowest error for small connection strengths ϵ. Only in case of relatively large $\epsilon = 0.1$ $C^{M,hm}$ performs better (figure 5.3). A similar observation can be made for the local efficiency (figure 5.4) in which E^W_{loc} outperforms E^R_{loc} except in case of a high $\epsilon = 0.1$ and a large number of noisy nodes $N_n > 100$ (almost twice the amount of active nodes).

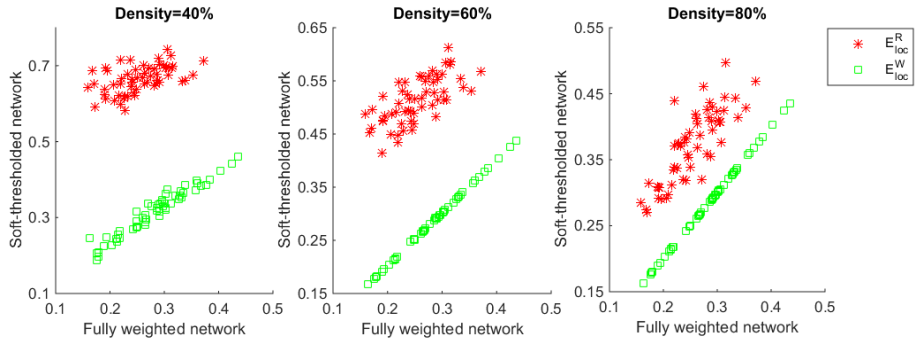

Figure 5.2: Scatter plot of the nodal local efficiencies for different generalizations for nodes in the fully weighted network and the soft-thresholded weighted network (the latter leading to different densities).

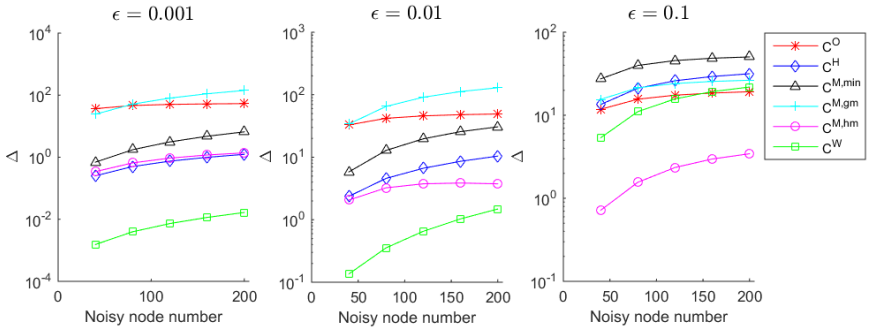

Figure 5.3: Error Δ of the overall robustness when adding N_n noise nodes with connection strength ϵ for different generalizations of the clustering coefficient.

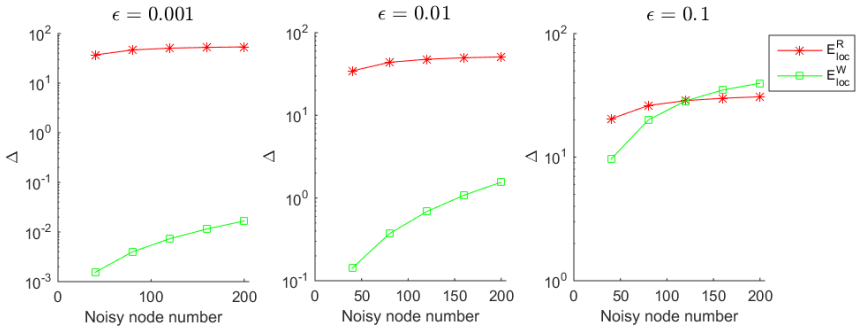

Figure 5.4: Error Δ of the overall robustness when adding N_n noise nodes with connection strength ϵ for different generalizations of the local efficiency.

5.4 Discussion

Despite of the growing interests in incorporating weight values into graph analysis, some of the generalizations still need improvements. Clustering coefficient and local efficiency are among them. In this paper, we focused on generalizations of these two measures in case of fully weighted network. We extended the criteria to quantify these generalizations to fully weighted network: general versatility, weight-scale invariance, continuity and overall robustness. The importance of these criteria becomes very clear in a fully weighted network. We evaluated all criteria for all generalizations under investigation and we measured and compared our generalizations using an empirical brain connectivity dataset. Several generalizations for the local clustering coefficient can be found in the literature but as we can see from table 5.1, some of these generalizations are not satisfying the weight scale invariance or continuity. The remaining existing generalizations (C^H, $C^{M,gm}$, $C^{M,min}$, $C^{M,hm}$ suffered from a relative large error (formula 5.17) in the overall robustness when applying to network. We found that our generalization outperformed the existing methods in terms of the four criteria mentioned before.

The existing generalization of the local efficiency E^R_{loc} doesn't satisfy general versatility. This might be problematic since one would expect that when using a network with only weights 0 and 1, the binary case and the weighted generalization would lead to the same result. This problem was not the case for the generalization we proposed (E^W_{loc}).

One limitation of our generalization is when the network is filled with only noisy nodes. In other words, none of the edges in the network is of any meaning. The binarization will force the network into a fully disconnected none without any problem in calculating clustering coefficient or local efficiency. However, in our generalization, it will obtain some value, based on the contrast of edges to the highest weight edge (which contains no useful information as well). However, given the fact that small value in weight doesn't necessarily mean weak or noisy, our generalization make sense in a way that it captures the relative difference in the edge topology of the network. Avoiding analysing meaningless networks with not even one strong connection is beyond the scope of this work and should be done before any network analysis.

The other limitation of our generalization is it is not fully exempted from the curse of weak edges and large network sizes, which means that it is not fully overall robust. Although we obtained low errors in overall robustness, this property does not hold when the network size increases dramatically. For example, if we simplify the edges in the network into two categories with either a strong edge (E_s) or a weak edge (E_w), the configuration of possible triangle distribution around node i can be depicted as figure 5.5. Our generalization can be simplified as

$$C^W(i) = \frac{1}{E_s} \cdot \frac{N_1 E_s^3 + (N_2 + N_3 + N_4 + N_5 + N_6) E_w^3}{(N_1 + N_2) E_s^2 + (N_3 + N_4 + N_5 + N_6) E_w^2} \tag{5.19}$$

in which N_i is the number of triangles of type i in the network as specified in figure 5.5.

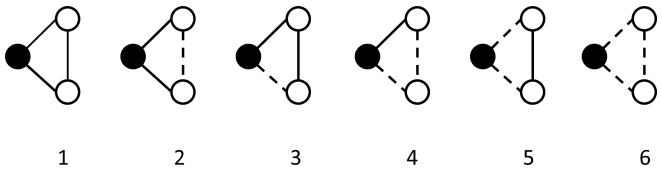

Figure 5.5: Six possible triangle configurations for the node filled in black. Normal and dashed line represent strong and weak edges, respectively.

As shown in the equation 5.19, N_1 and N_2 are relating to the strong connections with weight E_s. In the binary case, in which weak connections will be set to zero ($E_w = 0$), N_1 and N_2 are the only one which will have an effect on C. As the proportion $(N_3+N_4+N_5+N_6)/(N_1+N_2+N_3+N_4+N_5+N_6)$ increase drastically, the contribution of N_1 and N_2 to $C^W(i)$ will decrease accordingly. By using power 3 and 2 respectively in the numerator and denominator (equation 5.14), we enhance the contrast between contributions from strong and weak connections. Therefore, the generalization performs better compared to other generalizations when adding noisy nodes. One may argue that a further increase of the power may enhance the contrast even better to account for the accumulation contributions from weak connections. However, there's no free lunch on this planet. While the power enhances the contrast between strong and weak connections, it also enlarged the difference between strong and less strong connections, which is not what we want. In the extreme case, the clustering coefficient will be driven only by the strongest connections. The reason we are using 3 and 2 in the formula is that there are three edges in a triangles and two edges in the open triplet. However, when the network size increases dramatically, it might be a better choice to filter the noisy connections in advance to simplify the complexity of the network. We suggest a careful check before calculating the weighted graph metrics. This will exclude these extreme cases and avoid problems.

5.5 Conclusion

In this paper, we focused on generalizing the clustering coefficient and local efficiency to the case of a fully weighted network. Our generalizations outperform existing generalizations in terms of general versatility, weight-scale invariance, continuity and overall robustness.

Acknowledgments

This work was supported by Research Foundation Flanders (FWO) [G0660.09 & G0A0913N to RV and PD], KU Leuven [OT/12/097 to RV and PD], Federaal Wetenschapsbeleid belspo [IAP-VII P7/11] and Stichting voor Alzheimer Onderzoek (SAO11020 & 13007). YW has a grant from the Chinese Scholarship Council, and RV is a senior clinical investigator of the FWO.

6

Graph Analysis of the Associative-Semantic Network at Different Levels of Granularity

Abstract

Analysis and interpretation of graph analysis rely on the definition of the nodes. Integrating graph analysis across studies requires knowledge on the effect of nodes definition. While task-activated nodes constrain the focus on task-specific regions, functional parcellation approaches extend our view to whole-brain functional homogeneous regions. In this work, we address the effect of granularity by varying scales in the functional parcellation procedure and compare the results with task-activated regions-of-interests (ROI) as well as a more general whole brain ROI approach. A fully weighted graph analysis is performed per subject and per granularity level. Variations in granularity lead to discrepancies in the global graph measures of the functional network based on a task-based fMRI. Normalized global graph measures by equivalent random networks show reduced sensitivity to the granularity effect. The small world topology is preserved for all levels of granularity. We also found consistency across levels of granularity in part of the modular structure as well as for some hubs.

This chapter has been submitted for publication as: Yu Wang, Natalie Nelissen, Katarzyna Adamczuk, An-Sofie DeWeer, Mathieu Vandenbulcke, Stefan Sunaert, Rik Vandenberghe, Patrick Dupont. Graph Analysis of the Associative-Semantic Network at Different Levels of Granularity.

6.1 Introduction

Analysing graph theoretical measures has gained increasing interests in the neuroscience community. However, comparing graph metrics across studies can cause a problem because of the diversity in the procedures of defining the network. Graph metrics are strongly related to the network modelling method such as node definition and edge construction.

Nodes are defined using different approaches but these methods can be subdivided into two broad categories: a-priori defined or data driven methods. A-priori defined region of interest (ROI) based approaches are widely used to define the nodes of the network. Often ROIs are constructed as spheres around some central voxels which are selected based on a-priori knowledge (Power et al., 2011) or they are defined based on an independent experiment (Wang et al., 2014) or taken from an atlas such as the automatic anatomic labelling atlas (AAL) (van den Heuvel et al., 2010; Achard et al., 2006; Power et al., 2011). As a result, networks are constrained to these predefined regions. Data driven approaches have the advantage that they are based on the data itself and as a result lead to nodes which are functionally more homogeneous. Independent component analysis (ICA), which decomposes statistically independent components for brain functional networks, is one of the best-known methods (De Luca et al., 2006; Smith et al., 2009). However, there is no simple way to match ICA components across subjects because components do not have a natural ordering. In addition, group ICA analysis is often performed by concatenating or averaging time series across subjects. This procedure can only provide summarized components for the whole group by eliminating any idiosyncratic effects. Recently, Shen et al. proposed a group-wise parcellation scheme (Shen et al., 2013), which can simultaneously parcellate the group as well as individual network into subunits. The natural correspondence between group and individual subunits makes network analysis among individuals more straightforward. This is a relatively new technique for identifying connectivity-based subregions but it has already provided new insight into the functional segregation of brain networks. While originally described for resting state functional connectivity, the concept can also be applied to task-based functional connectivity analysis. As all the above methods focusing on a macroscopic view of brain connectivity, a voxel-wise approach zoom in the picture and gives insight on a finer resolution (Buckner et al., 2009; Cecchi et al., 2007; Eguluz et al., 2005; Hayasaka and Laurienti, 2010). All these approaches investigate brain networks at different scales, thus knowing the effect of granularity on the graph analysis will be the first step to move forward in integrating studies at different levels of granularity.

The goal of this paper is to investigate the effect of granularity of the nodes on the resulting graph measures as well as on the modular structure and the identification of hubs using task-fMRI data. More specifically, we used the associative-semantic paradigm, which activates a distributed set of brain areas that has been replicated across a wide range of studies (Vandenberghe et al., 1996; Vandenbulcke et al., 2007; Nelissen et al., 2007; Van Doren et al., 2010; Adamczuk et al., 2013). Analysing graph theoretical measures has proven to reveal novel

insights into the structure of the network for associative-semantic processing (Vandenberghe et al., 2013). Furthermore, we have shown that graph measures of weighted subject specific networks have a good reproducibility (Wang et al., 2014). To study the effect of granularity of the nodes on the graph measures, we will construct networks which differ in granularity based on a parcellation-based approach. For comparison, we will also include the network based on the task-activated ROIs as we used in our previous studies (Vandenberghe et al., 2013; Wang et al., 2014) and based on a more general whole brain ROI based approach. We will study global graph measures, the modular structure and hubs for each network.

6.2 Methods

6.2.1 Participants and experimental design

A group of 54 healthy elderly participants (age (mean ± std): 65.2 ± 5.6 yrs; 31 male) (Adamczuk et al., 2013) performed an associative-semantic judgement task. Twenty-eight subjects were scanned on a 3T Philips Intera system equipped with an 8-channel receive-only head coil (Philips SENSitivity Encoding head coil) and twenty-six subjects were scanned on a 3T Philips Achieva system equipped with a 32-channel receive-only head coil (Philips 10 SENSitivity Encoding head coil).

The design of the fMRI experiment was factorial (Vandenberghe et al., 1996; Vandenbulcke et al., 2007; Nelissen et al., 2007, 2011). The first factor, task, had two levels: associative-semantic versus visuoperceptual judgement. The second factor, input modality, also had two levels: pictures versus printed words. During a trial of the associative-semantic condition, a triplet of stimuli was presented for 5250 ms, one stimulus on top (the sample stimulus) and one in each lower quadrant (the test stimuli), at 4.6 eccentricity, followed by a 1500 ms interstimulus interval. Subjects had to press a left- or right-hand key depending on which of the two test stimuli matched the sample stimulus more closely in meaning. A given triplet was presented either as pictures or as words and this was counterbalanced across subjects. In the visuoperceptual control condition, a picture or word stimulus was presented in three different sizes (mean picture size was 3.7 and mean letter size 1.2). Subjects had to press a left- or right-hand key depending on which of the two test stimuli matched the sample stimulus more closely in size on the screen. An epoch, i.e. a block of trials belonging to the same condition, consisted of four trials (total duration 27 s). The fifth condition consisted of a resting baseline condition during which a fixation point was presented in the centre of the screen. During each fMRI run (5 runs in total), a series of the 5 epoch types, was replicated 3 times. The order of conditions was pseudorandom and differed across runs of the same subject. Subjects received a practice session before entering the scanner. In this session we determined which size difference (9%, 6%, 3%, or 1%) for the visuoperceptual conditions was needed for each individual subject to obtain comparable accuracies as for the associative-semantic conditions.

The protocol was approved by the Ethics Committee University Hospitals

Leuven (EudraCT: 2009-014475-45) and written informed consent was obtained from all subjects in accordance with the Declaration of Helsinki.

6.2.2 Preprocessing of the data

Image analysis was performed using Statistical Parametric Mapping (SPM8, Wellcome Department of Cognitive Neurology, London, UK. http://www.fil.ion.ucl.ac.uk/spm). Functional images of each subject were realigned to correct for small head motion during each run. The anatomical T1-weighted image was coregistered to the average of the realigned functional volumes and non-linearly normalized to Montreal Neurological Institute (MNI) space using the unified segmentation approach (Ashburner and Friston, 2005) and the resulting transformation was used to spatially normalize the functional images. The voxel size of the images in MNI space was 3x3x3 mm^3. Images were smoothed using a 6x6x6 mm^3 Full Width at Half Maximum (FWHM) Gaussian kernel. We also applied a temporal high-pass filter (cut-off 270s) and a low-pass filter consisting of the canonical hemodynamic response function. The epoch-related response was modelled by a canonical hemodynamic response function convolved with a boxcar.

For each subject, we extracted the time series after whitening, filtering and removing effects of no interest (session specific effects) using code from SPM8. Time series of different runs were concatenated. It is important to note that we used the whole time series, i.e. it included all the different conditions as well as the null condition.

6.2.3 Network modelling

ROI-based approach

Task-specific ROIs were taken from a previously published study on the associative-semantic network (Vandenberghe et al., 2013), namely fifty-seven spheres (radius 6 mm) for which the centres are located at least 20 mm apart. The spheres were centred on group-specific activation maxima (from the main effect of task) determined from this study. We will call the network consisting of these nodes R57.

We then used the whole brain coordinates spanning the cerebral cortex, subcortical structures, and the cerebellum taken from table S2 in (Power et al., 2011) and positioned spheres of 6 mm in these centre coordinates. These ROIs were merged with the associative-semantic activated regions in such a way that the latter regions were taken first followed by those spheres for which the centre was located at a distance of at least 20 mm from any other centre of the spheres. This resulted in a set of 85 ROIs (supplementary table 1). This network will be called R85.

The ROI analysis was restricted to grey matter voxels based on the a-prior grey matter map in SPM thresholded at 0.3.

Correlation-based parcellation

First, we select all voxels in grey matter (based on the a-priori grey matter map in SPM thresholded at 0.3) and obtain the voxel-wise Pearson correlation coefficient matrix between time series per hemisphere. Next, we applied the K-way group-wise parcellation algorithm (Shen et al., 2013) to the voxel-level correlation matrix for each hemisphere separately. The parcellation can segment the brain into subunits at both the group and individual level, under the assumption that the functional connectivity should share similar connectivity patterns. The procedure produces a brain parcellation composed of functional subunits. The parameter K (see below) controls the level of granularity.

Let $s = 1, \cdots, M$ denote the index of the subjects and N denotes the number of voxels. The algorithm starts by characterizing each individual network by a matrix X_s. The matrix X_s is a $N \times K$ matrix with columns constructed by the first K eigenvectors (ordered by decreasing eigenvalues) of the normalized correlation matrix. X_s is normalized such that each row has a unit norm. Thus X_s can represent a set of points in the unit sphere, which makes these points rotation-invariant. Taking advantage of this property, we can rotate the individual spheres to align the corresponding points from each subject to the same axes in the K dimensional space. The group K-way parcellation is formulated as minimizing $\sum_s \parallel Y - X_s R_s \parallel^2$ where $\parallel . \parallel$ denotes the Frobenius norm of a matrix, Y is the group-wise partition matrix and R_s is the rotation matrix for each subject. Y and R_s can then be solved iteratively. The individual parcellation for subject s can be obtained through $X_s R_s$. The straightforward correspondence between individual and group subunits is achieved by the fact that the whole parcellation is performed simultaneously. This procedure gives a nearly global-optimal solution combined with computational efficiency. Important to note is that the final group-wise parcellation may have less subunits compared to the initial K.

For each subject, we take the subject-specific subunits corresponding to the group-wise parcellation as the nodes of the network. These networks will be labelled Px with x the initial K per hemisphere in the parcellation procedure.

Functional connectivity

Based on the average time series, partial correlation coefficients between nodes were calculated. Partial correlation was used to obtain the degree of association between regions, with the effect of other regions removed (Marrelec et al., 2006; Smith et al., 2011).

The association strength is defined as the absolute value of the z-score which is calculated from the partial correlation using the Fisher r-to-z transform. We applied a nonlinear mapping of z score to weight (W) by calculating:

$$w_{ij} = [2\Phi(|z_{ij}|) - 1]^4. \tag{6.1}$$

where Φ is the cumulative distribution function of the standard normal distribution. This calculation of the weights differs from the one proposed in our previous paper (Wang et al., 2014) because the current definition is a further improvement

which prevents the weight distribution from skewing towards higher weights. All weights have values between 0 and 1.

6.2.4 Graph-theoretical analysis

This work will mainly focus on analysing weighted graphs at the individual level. Global measures include characteristic path length λ, mean clustering coefficient C, mean local efficiency E_{loc}, global efficiency E and mean betweenness centrality BC. Graph measures were calculated by using the brain connectivity toolbox (Rubinov and Sporns, 2010) (https://sites.google.com/a/brain-connectivity-toolbox.net/bct/Home) except for the weighted clustering coefficient and local efficiency because these measures require a thresholding of the weighted network something we tried to avoid. Therefore, we adapted the measures to take into account fully connected weighted networks even if the weights are very small for some connections (Wang et al., 2015b). We assume no self-connections, i.e. $w_{ii} = 0$.

The local (nodal) clustering coefficient for node i is calculated as:

$$C(i) = \frac{\sum_{j,h}(\min(w_{ij}, w_{ih}, w_{jh}))^3}{\max(\mathbf{w})\sum_{j,h}(\min(w_{ij}, w_{ih}))^2} \tag{6.2}$$

in which $\mathbf{w}$ represents the matrix of weights w_{ij} between node i and j.

The local efficiency is calculated as:

$$E^W_{loc}(i) = \frac{1}{\max(\mathbf{w})} \frac{\sum_{j,h}((\min(w_{ij}, w_{ih}))^3[\tilde{d}^w_{jh}(N_i)]^{-1}}{\sum_{j,h}(\min(w_{ij}, w_{ih}))^2} \tag{6.3}$$

where $\tilde{d}^w_{jh}(N_i)$ is the adapted shortest distance between j and h.
The adapted shortest distance was calculated as follows:
1) Remove node i from the network. The weight of edge (j, h) in the remaining network is adapted to $\tilde{w}_{jh}$:

$$\tilde{w}_{jh} = \frac{w_{jh}w_{ij}w_{ih}}{(\max(\mathbf{w}))^{\mathbf{3}}} \tag{6.4}$$

2) The shortest distance $\tilde{d}_{jh}(N_i)$ in the adapted network was then calculated.

One crucial step when studying the structure of networks is to identify underlying communities which are groups of related nodes or edges that correspond to functional units. To determine the community structure of the network, we used the algorithm of Newman (Newman, 2006a) as implemented in the Brain Connectivity Toolbox. For each network, a co-assignment matrix is obtained as an $N \times N$ matrix, where cell (i, j) is one if node i and node j are assigned to the same community.

The identification of hubs was based on a hub score (van den Heuvel et al., 2010; Vandenberghe et al., 2013), which is based on the ranking of nodes relative

to other nodes. We gave a score of 1 or 0 depending on whether or not the node belongs to the top 20% of nodes with 1) the highest node degree, 2) the highest betweenness centrality, 3) the lowest local cluster coefficient (limited to the top 80% of nodes with the highest weighted node degree), and 4) the lowest average path length. Nodes with a hub score ≥ 2 were considered hubs.

We also checked the small worldness of the network by two criteria (Watts and Strogatz, 1998; Achard and Bullmore, 2007; He et al., 2007b; Batalle et al., 2012). The first is to compare the clustering coefficient C and characteristic path length λ with the corresponding values of the equivalent random networks (labelled by $rand$): $C/C^{rand} > 1$ and $\lambda/\lambda^{rand} \approx 1$ (Watts and Strogatz, 1998; He et al., 2007b). The other more general criterion is to make sure that the global and local efficiency (E_{glob} respectively E_{loc}) lie between the extremes set by equivalent random and lattice (labelled by $latt$) networks: $E_{glob}^{latt} < E_{glob} < E_{glob}^{rand}$ and $E_{loc}^{latt} > E_{loc} < E_{loc}^{rand}$. It provides a view of how well the network balance local processing and global integration (Achard and Bullmore, 2007).

The equivalent random network has the same weight and strength (weighted node degree) distribution as the original network and is calculated using the brain connectivity toolbox. However, in the brain connectivity toolbox, lattice networks were calculated only for thresholded weighted networks. Therefore, we adapted the generation of a weighted equivalent lattice network to make it applicable to fully weighted networks as well. This was done using the following procedure: First, we generated a pseudo-distance matrix D in which the elements D_{ij} denote the pseudo-distance between i and j defined as the difference between the indices i and j after randomizing the indices). D will thus have the smaller values closer to its diagonal. Next, we applied the Markov-chain algorithm to swap edges in the network (Maslov and Sneppen, 2002; Sporns and Zwi, 2004) by selecting randomly four nodes i_1, i_2, j_1, j_2. If $w_{i_1j_1}D_{i_1j_1} + w_{i_2j_2}D_{i_2j_2} + w_{i_1j_2}D_{i_1j_2} + w_{i_2j_1}D_{i_2j_1} > w_{i_1j_1}D_{i_1j_2} + w_{i_2j_2}D_{i_2j_1} + w_{i_1j_2}D_{i_1j_1} + w_{i_2j_1}D_{i_2j_2}$, we rewire the edges among the four nodes so that the new weights will be set to $w_{i_1j_1}^{new} = w_{i_1j_2}$, $w_{i_1j_2}^{new} = w_{i_1j_1}$, $w_{i_2j_2}^{new} = w_{i_2j_1}$, $w_{i_2j_1}^{new} = w_{i_2j_2}$. This is repeated until the connection topology of the original matrix is latticed so that edges with high weight tend to have a short pseudo-distance.

6.2.5 Granularity effect on network properties

Graph measures depend on the network scale and degree distribution (Van Wijk et al., 2010) which requires some correction if we want to compare graph measures between networks at different scales of granularity. To solve this problem, graph measures are normalized via random networks (Stam, 2004; Smit et al., 2008). We calculated 100 random networks to determine the normalization factor.

The consistency of hubs across subjects can be shown by a probability hub map (HM). For each network, the probability hub map is created by calculating the proportion of subjects for which the node is considered a hub.

For communities, an overall probabilistic co-assignment matrix (P_{CM}) is generated by averaging the co-assignment matrices across subjects.

6.3 Results

6.3.1 Parcellation based on functional connectivity

We have tested different values of K to decompose the whole brain grey matter volume into functional homogeneous subunits, which are then treated as nodes in the subsequent analysis. As a result we obtained group-level parcellations with 56, 115, 183, 248 and 311 subunits in the whole brain for K (per hemisphere) = 50, 100, 150, 200 and 300), respectively (figure 6.1). With the increase of the parameter K, the parcellation shows a finer partition.

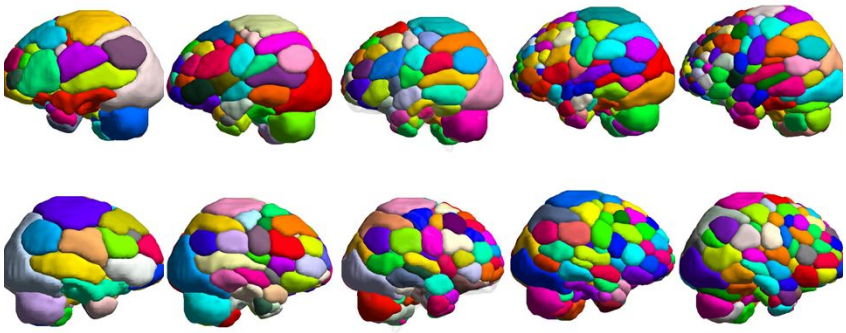

Figure 6.1: Rendered views of the parcellated brain (top: left hemisphere, bottom: right hemisphere). From left to right are group-level parcellation with 56, 115, 183, 248 and 311 subunits. Subunits are represented in different colours. The same colour is used for different parcels. Visualization using the BrainNet Viewer (http://www.nitrc.org/projects/bnv/).

6.3.2 Granularity effect on global graph metrics

Figure 6.2 shows the effect of granularity on the resulting global graph metrics. Figure 6.3 shows the global graph metrics after normalization by equivalent random networks across different levels of granularity. Although the raw graph metrics are different across different scales, the weighted global graph metrics normalized by equivalent random networks are similar across different granularity levels.

In addition, we use two different criteria to check the small world topology of the associative-semantic network (figure 6.4). The clustering coefficient and local efficiency were compared with parameters estimated by its equivalent random surrogates. In general, small worldness increases with the expansion of network size. $(C/C_{rand})/(\lambda/\lambda_{rand}) > 1$ across all models indicates a preserved small world property. This can be confirmed by global and local efficiency in comparison with the parameters obtained from the corresponding random and lattice networks: the

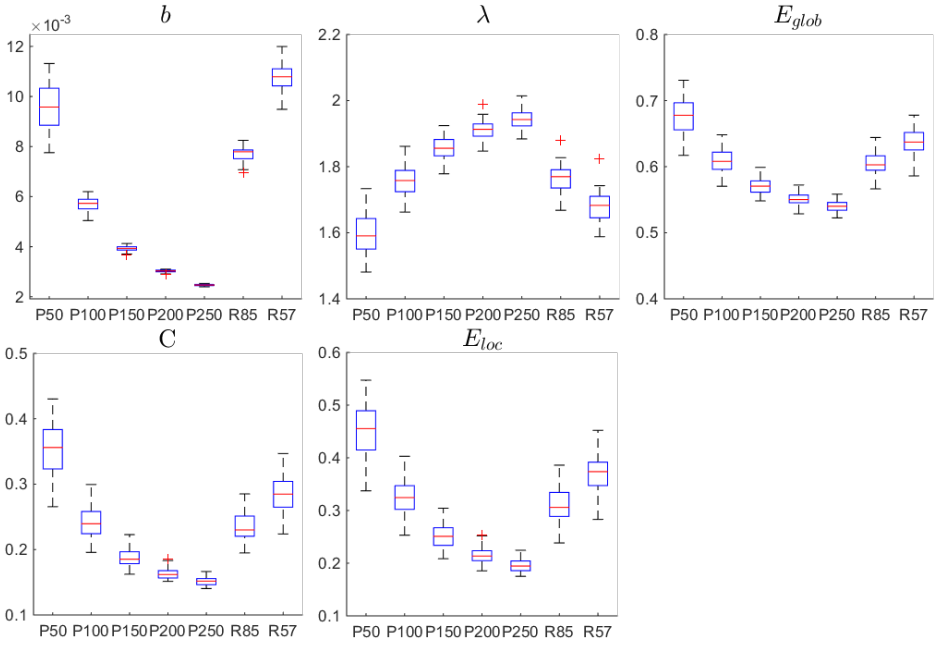

Figure 6.2: Graph metrics across scales. Individual graph metrics are shown for different levels of granularity for the fully weighted networks. On the x axis, we show the different networks. A Tukey boxplot is used to show the results across all subjects.

efficiency curves of the associative semantic network were intermediate between bounds set by random and lattice networks for all levels of granularity.

Normalization by random surrogates compensates for the differences in network size. However, when we look at networks of almost similar size (P50 with 56 nodes and R57 with 57 nodes), we can evaluate how critical the network metrics are depending on the node definition. Table 6.1 shows the mean values across all subjects obtained for both networks. When we compare the values using a paired t-test, we found that they all were statistically significantly different between both networks ($p_{corr} < 0.05$ corrected for the number of comparisons).

6.3.3 Granularity effect on the modular structure and hubs

The modular structure of each network was determined for each subject. The group-level probability co-assignment matrix is obtained by averaging the co-assignment matrices across subjects. When clustering the group-level probability co-assignment matrix, we can assign nodes to clusters by the Newman algorithm implemented in the brain connectivity toolbox (figure 6.5 for the parcellation based networks and figure 6.6 for the ROI based networks).

The clear clustering indicates that the modular structure of the functional

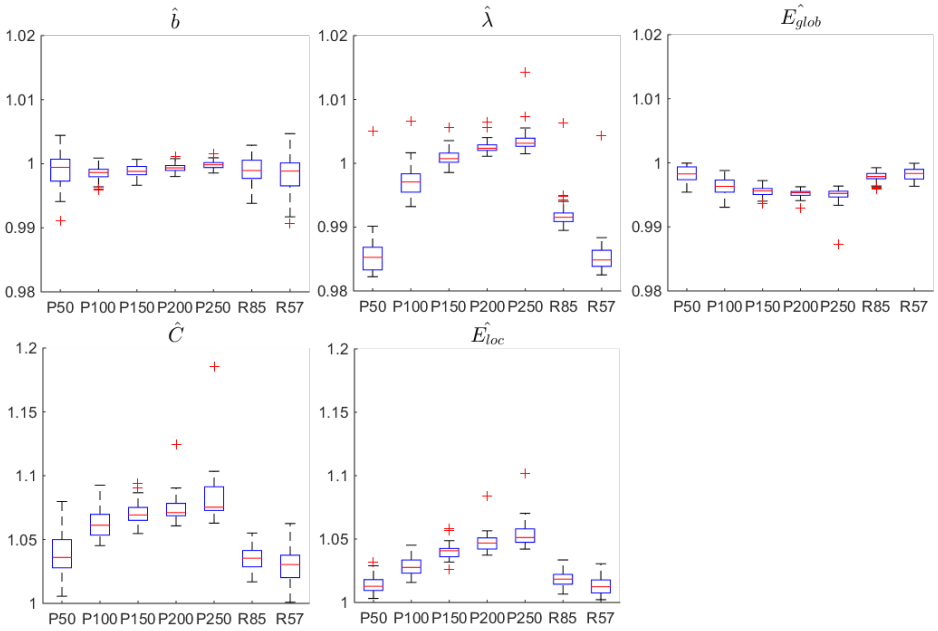

Figure 6.3: Normalized graph metrics across scales. Normalized individual graph metrics using random equivalent networks for different levels of granularity for the fully weighted networks. On the X axis, we show the different networks. A Tukey boxplot is used to show the results across all subjects.

	C	λ	E_{glob}	E_{loc}	BC
P50	**0.356**	**1.595**	**0.677**	**0.454**	**0.010**
R57	**0.287**	**1.679**	**0.639**	**0.374**	**0.011**

Table 6.1: Comparison of P50 and R57 networks. The mean of the graph metrics across all subject are shown for the clustering coefficient (C), the characteristic path length (λ), the local (E_{loc}) and global (E_{glob}) efficiency and betweenness centrality (BC). Significant differences ($p_{corr} < 0.05$ corrected for the number of comparisons, paired t test) between both networks are indicated in bold.

network is preserved despite the inter-individual variability. Projecting these clusters on the brain (figures 6.5 and 6.6), we can see this patterns remains quite constant across different granularity scales. However, the consistency across subjects decreases when the network size becomes larger as can be seen from the lower values in the group-level probability co-assignment matrix when K increases.

Hubs are more variable across subjects as can be seen by the relative low values in most hub regions (figure 6.7). However, some brain regions show clearly a higher consistency between subjects to be assigned as hub. For example, the

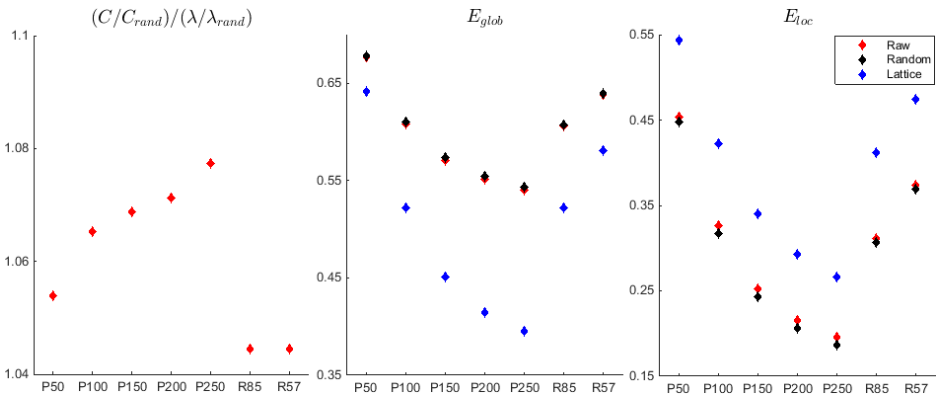

Figure 6.4: Preserved small world topology of the associative-semantic network across different granularity levels. Values shown are the mean values across subjects. Using fully weighted graph metrics, the associative-semantic network (ASN) shows preserved small worldness: $(C/C^{rand})/(\lambda/\lambda^{rand}) > 1$, $E_{glob}^{latt} < E_{glob} < E_{glob}^{rand}$ and $E_{loc}^{latt} > E_{loc} < E_{loc}^{rand}$. The random and lattice networks have the same weight distribution as the individual associative-semantic network.

left anterior inferior frontal gyrus, which is activated both for words and pictures (Goldberg et al., 2007), shows a high probability (> 0.65) in being assigned as hub across a range of parcellation-based approach ($K = 50, 100, 150, 200$) and a medium probability (> 0.4) in the ROI-based network. Interestingly, the hubs we identified in the task-specific region-based network (R57) are coinciding with the hubs of the whole-brain ROI-based network (R85). For example, left angular gyrus has been assigned as hub in 81% and 76% subjects in the R57 and R85 network respectively.

6.4 Discussion

6.4.1 Selection of nodes

The nodes are building blocks of complex networks. These nodes can be defined using an ROI-based or a data-driven approach. In this work we have evaluated a new data-driven method (Shen et al., 2013) which has the advantage that the parcellation of the brain is performed simultaneously at the group level and the subject specific level which makes the comparison of graphs across subjects straightforward. The data-driven approach was applied for different levels of granularity. In this way we were able to study the associative-semantic network at different levels of detail.

We have contrasted the results from the parcellation based networks with two ROI-based approaches in which ROIs were taken from a previous study (Vandenberghe et al., 2013) using the same paradigm (R57) or using these ROIs in

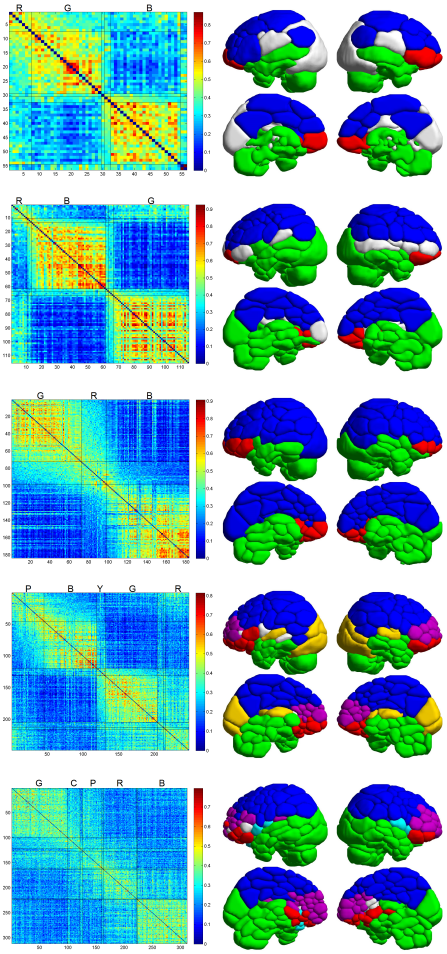

(a) K=50

(b) K=100

(c) K=150

(d) K=200

(e) K=250

Figure 6.5: Modular structure for parcellation based networks. Group-level probability co-assignment matrix (left column) and the projection of clusters of subunits onto a 3D brain surface using the BrainNet Viewer for a sagittal and medial view (right column) are shown across different levels of granularity. Letters on top of the probability co-assignment matrices correspond to colours of the clusters in the brain view: B: blue; C: cyan; G: green; P: purple; R: red; Y: yellow. Nodes belonging to small clusters are coloured as light grey (a small cluster contains less than 10 nodes and less than 10% of the total number of nodes).

combination with other ROIs located in the remaining of the brain (R85). The first network consists of only those nodes which were found active when subjects had to make an associative-semantic judgement in comparison to a visuoperceptual control task. However, the human brain is a highly incorporated system; all

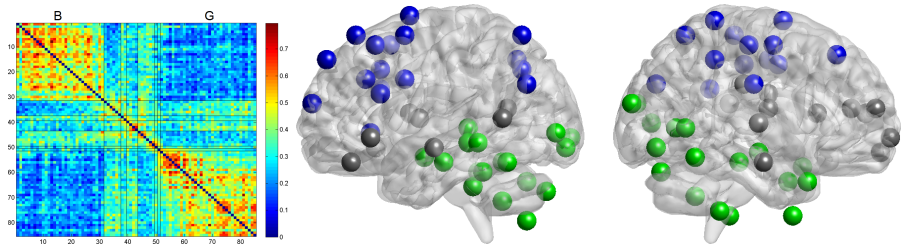

(a) R85

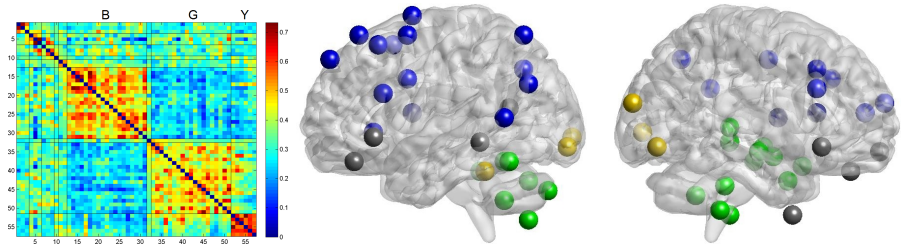

(b) R57

Figure 6.6: Modular structure for ROI-based networks. The averaged probability co-assignment matrices (left column) are shown for R85 (a) and R57 (b) with projection views on the left (middle column) and right (right column) hemispheres using the BrainNet Viewer. Letters on top of the probability co-assignment matrices correspond to colours of the clusters in the brain view: B: blue; G: green; Y: yellow. Nodes belonging to small clusters are coloured as grey (a small cluster contains less than 10 nodes and less than 10% of the total number of nodes).

cognitive tasks are embedded in the whole brain network. While task specific network reveals how information is processed among these regions, it also neglect the contribution of other regions which serve as general information processor other than specific to the task. This may account for some inconsistencies between structural and functional networks, especially when the edges are defined as partial correlation. The network R85 provides a more complete picture of the functional network underlying the associative-semantic processing.

As can be seen from the results, the hub distribution of the task-specific region-based network (R57) is coinciding with the hub distribution of the whole-brain ROI-based network (R85). Furthermore, task-activated nodes are not locally clustered, instead, it ensembles a similar modular structure as the R85 network. In other words, the task-activated nodes feature the whole-brain network structure, which indicates that the focus of the brain was in performing the tasks.

As shown in our work, different node definitions lead to different networks which capture distinct levels of the underlying process. While variations of graph metrics at the global level induced by the node definition can be removed partly by normalization procedures, at the nodal level it will play an important role

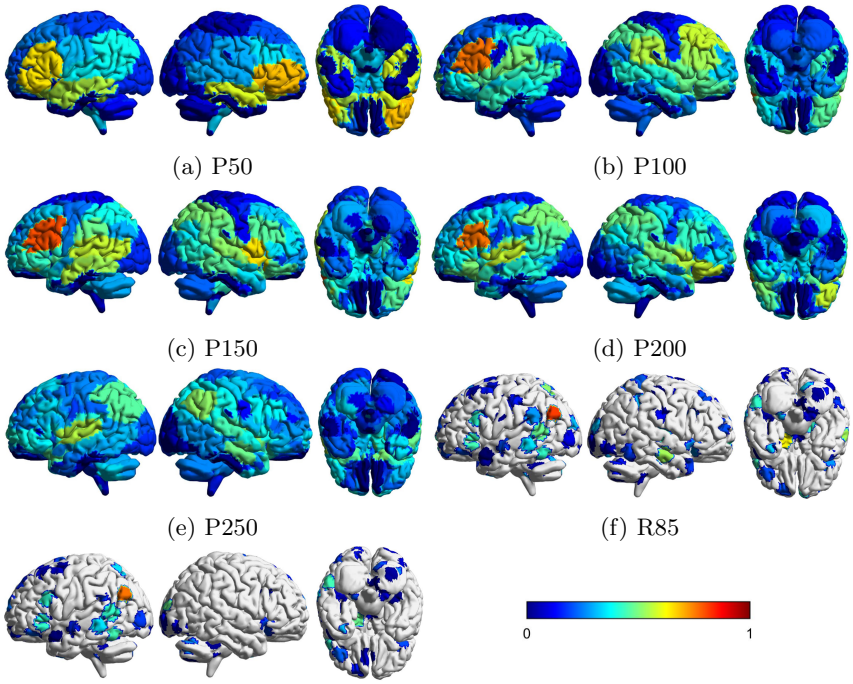

(a) P50 (b) P100

(c) P150 (d) P200

(e) P250 (f) R85

(g) R57

Figure 6.7: Hubmap shows the percentage of each node which was assigned as hub across all subjects. Panels (a)-(e) show the hubmap for the parcellation-based networks. Panels (f) and (g) show hubmaps for the ROI based networks R85 and R57 respectively.

and this can have an impact on e.g. the identification of hubs. Selection of nodes should be grounded and constrained by neurobiological assumptions and principles. Multiple-model network analysis is helpful to better understand the underlying brain networks.

6.4.2 Fully weighted networks

Many graph analysis focused on binary network topology, which requires a threshold to convert the continuous edges to either 1 or 0. The binarized network has a straightforward interpretation. However, there is no consensus on choosing the threshold. Furthermore, a small change in the connection strength may lead to a drastic change in the binarized matrix (just below or above a threshold). In order to fully capture the richness of the data, there is a growing interest in investigating weighted networks instead. Retaining strength of the supra-threshold connections helps in alleviating the tension but the question remains how to select the threshold (Nakamura et al., 2009; Wang et al., 2010). In practice, many studies have therefore examined results over a range of thresholds (Achard and

Bullmore, 2007; Hayasaka and Laurienti, 2010; Wang et al., 2010; Schwarz and McGonigle, 2011; Wang et al., 2014).

One of the most noteworthy strengths of the current study is that it analyses functional network based on a well-defined weight, which is a nonlinear transformation of the partial correlation. Weights are assumed to be normalized, such that $0 \leq w \leq 1$ (Rubinov and Sporns, 2010). Partial correlation coefficients, which are selected as the quantification of connections in the network, range from -1 to 1. Taking the absolute value makes it a potential candidate for the weights. To make inference of the population partial correlation, we used a Fisher r to z transformation by accounting for the differences in sample size between subjects. The resulted z scores thus are normally distributed with mean relating to population partial correlation and standard error as 1. In our previous study, we mapped the z score to weight by taking the area under the cumulative distribution function curve of the z score. However, this procedure shifted the resulted weight distribution towards the right. To solve this problem, we took a power 4 of the previously defined weight definition. The final weight distribution thus enhanced the contrast between the strongest and weakest connection by forcing the former closer to 1 and the latter nearer to 0. Moreover, this procedure keeps the "intermediate strong" connections, which are neither too strong nor too weak. Our procedure is better than a linear transformation from z score to weight, which is often implemented by using the maximum and minimum z score, in a way that it is less sensitive to the noise in the data.

6.4.3 Comparing graph metrics across different granularity levels

Despite the flux of interest in analysing networks using graph metrics, the problem of comparing networks differing in granularity has received little attention. Because of the size and degree dependency of graph metrics, comparing graph metrics across networks differing in size or (weighted) degree distribution become less intuitive. Fixing edge density of the binary network is one approach to account for the granularity-dependence. This is criticized by manipulating data by over- or under- estimating the real network (Ponten et al., 2010; Van Wijk et al., 2010) which may lead to undetected or spurious connections, especially when comparing graphs in different pathological conditions. Using weighted networks instead of binary networks would not suffer from this drawback. However, the scale-dependency remains.

A further step to take is to use random surrogates to compensate for the scale-dependency as used by many groups (Stam, 2004; Smit et al., 2008). While the random surrogates do remove discrepancies induced by scale difference, it is sensitive to the threshold chosen in the binary case. The combination of a weighted network analysis and the use of equivalent random networks removes the granularity dependency of graph metrics in our analysis.

Despite of the differences in network scale, the modular structure of the functional network remains quite constant. However, the consistency across

subjects decreases when the network size becomes larger by zooming in the granularity.

The hub distribution reflects the nodal characteristics and presents a higher variation across subjects. However, some brain regions show clearly a higher consistency between subjects to be assigned as hub. For example, the left anterior inferior frontal gyrus shows a high probability (> 0.65) in being assigned as hub across a range of parcellation-based approach ($K = 50, 100, 150, 200$) and a medium probability (> 0.4) in the ROI-based network. However, it is assigned as hub in only 33% of subjects when $K = 250$. This can be explained by the fact that for high values of K, there might be a problem of over-fitting. Also, inter-subject variability will play an important role when the nodes of the network become smaller.

The hubs we identified in the task-specific region-based network (R57) are coinciding with the hubs of the whole-brain ROI-based network (R85). Left angular gyrus has been assigned as hub in 81% and 76% subjects in the R57 and R85 network respectively. The angular gyrus is one of the areas that are regularly damaged in patients with aphasic stroke in the middle cerebral artery territory and with impaired semantic control (Jefferies and Lambon Ralph, 2006; Noonan et al., 2010; Corbett et al., 2009, 2011).

6.4.4 Preserved small world structure

A hallmark of many brain connectivity studies is their effort to analyse the small-world property of the network (Stam, 2004; Achard et al., 2006; Smit et al., 2008; He et al., 2007b; Batalle et al., 2012). The small world topology is often characterized by a higher number of clustering coefficient and a comparable value for the characteristic path length compared with random networks (Watts and Strogatz, 1998). A more general criterion that quantifies the small worldness is the comparison with both random and lattice surrogates (Achard and Bullmore, 2007; Batalle et al., 2012). The interest in small-world topology for brain network organization arises from its ability to support cost-efficiency information processing (Achard and Bullmore, 2007; Bullmore and Sporns, 2012) and to provide robustness against a pathological attack (Achard et al., 2006).

However, the small-worldness is sensitive to noise for empirical binary networks. For instance spurious random links, which are originated from inappropriate binarization, will fabricate small-worldness (Varoquaux and Thirion, 2012). Furthermore, the small worldness decreases when the network density increases in case of binary graphs, and can even be disrupted when the network density is high (Achard and Bullmore, 2007; He et al., 2007b). Given these pitfalls, weighted network analysis has the advantage that no specific threshold for binarization needs to be chosen. Unfortunately, the weighted version of clustering coefficient and local efficiency implemented in the brain connectivity toolbox (Onnela et al., 2005; Rubinov and Sporns, 2011) is not appropriate for fully weighted networks. For this reason, we have used another generalization for these metrics (Wang et al., 2015b).

By comparing the weighted clustering coefficient and the characteristic path

length between the associative semantic network and random networks, we showed the small worldness across all levels of granularity. Furthermore, our results of local and global efficiency show that values for the associative-semantic network are located in between the values for random and lattice networks for all levels of granularity. These results are indicative of a high global integrated and locally clustered cost-efficient system (Power et al., 2011; Bullmore and Sporns, 2012).

Our work is the first one to report small worldness in a fully weighted network for different levels of granularity.

6.5 Conclusion

Graph measures of the fully weighted associative-semantic network using task-based fMRI are depending on the granularity level. When normalized by equivalent random networks, this dependency is greatly diminished. The network showed small world topology for all levels of granularity. We also found consistency across levels of granularity in part of the modular structure as well as for some hubs.

Acknowledgements

This work was supported by Research Foundation Flanders (FWO) [G0660.09 & G0A0913N to RV and PD], KU Leuven [OT/12/097 to RV and PD], Federaal Wetenschapsbeleid belspo [IAP-VII P7/11] and Stichting voor Alzheimer Onderzoek (SAO11020 & 13007). YW has a grant from the Chinese Scholarship Council, KA is a doctoral fellow of the FWO and RV is a senior clinical investigator of the FWO.

6.6 Supporting Information

Table S6.1: MNI coordinate for the R85 network. Nodes in bold are the ones which are also used in R57.

ROI	x	y	z	ROI	x	y	z
R cerebellum	12	-81	-36	**precuneus**	-3	-57	15
L GFI.pars.triang	-51	21	24	**dorsomedial.prefrontal**	-3	15	54
L vOT	-54	-57	-18	**R cerebellum**	30	-69	-54
L ant.GFi	-39	39	-18	**L GFI.pars.orbit**	-54	27	-3
L ant.fusiform	-36	-42	-24	**L lingual**	-15	-93	-9
L IFJ	-39	6	33	**L post.GTM**	-63	-39	-6
L GFs	-33	6	60	**L post.STS**	-60	-54	9
L cerebellum	-15	-54	-18	**L IPS**	-24	-66	39
L SFS	-24	24	54	**R cerebellum**	36	-69	-30
L GFs	-9	54	45	**L insula**	-30	27	0
L GFs	-9	36	60	**L angular**	-48	-69	30
R caudate	12	3	12	**R Inf.occip**	27	-96	-3
L SMA	-9	3	72	**R ant.fusiform**	33	-39	-24
vermis	6	-54	-42	**L IPS**	-30	-66	60
R GFi.pars.orbit	42	24	-9	**precuneus**	-3	-63	45
L parahippocampal	-36	-18	-18	**brainstem**	0	-36	-33
L GOm	-39	-87	0	**L ant.thalamus**	-12	-3	9
post.Thalamus	-3	-33	3	**L hippocampus**	-30	-33	-6
L ant.STS	-57	-12	-9	**R GFi.pars.triang**	45	21	27
L hippocampus	-15	-6	-15	**L ant.Cing.sulcus**	-9	30	33
L medial.frontal	-9	63	18	**R Cing.sulcus**	9	21	39
L ant.temp.pole	-33	6	-51	**brainstem**	3	-15	-12
L cerebellum	-21	-33	-51	**R Inf.occip.**	42	-78	-9
L cerebellum	-30	-54	-39	**L orbitofrontal**	-15	60	-12
L temporal.pole	-54	12	-21	**L precentral.gyrus**	-33	-9	45
R GOm	30	-93	18	**R cerebellum**	21	-39	-48
L Ant.Temporal	-30	3	-30	**L caudate**	-15	21	12
L SupraMarginal	-60	-45	27	**L middle.frontal**	-24	51	12
R Parahippocampal	18	-27	-18	L Parietal.Inf	-54	-24	42
R Postcentral	21	-42	69	L Postcentral	-21	-30	60
R Postcentral	42	-21	54	R Insula	36	-9	15
L Postcentral	-54	-9	24	L Cing.Mid	-9	-3	42
L SMA	12	0	69	R Temporal.Sup	57	-15	6
L Rolandic.Oper	-39	-33	18	R SupraMarginal	60	-18	30
R Frontal.Mid.Orb	6	66	-3	R Temporal	45	15	-30
R Frontal.Sup	24	33	48	L Cing.Ant	-3	42	15
R Temporal.Mid	66	-12	-18	L Calcarine	-9	-81	6
R Lingual	21	-66	3	L Occipital.Mid	-24	-90	18
R Cuneus	15	-78	30	R Temporal.Inf	57	-54	-15
L Cerebelum.Crus	-18	-75	-24	R SupraMarginal	48	-42	45
R Frontal.Sup	30	57	15	Mid cing.	3	-24	30
R Precuneus	9	-60	60	R Temporal.Mid	45	-60	3
R Precentral	30	-6	54				

Abbreviations: L: left; R: right; GFI: inferior frontal gyrus; triang: triangularis; vOT: ventral occipitotemporal transition zone; IFJ: left inferior frontal junction; GTM: middle temporal gyrus; STS: superior temporal sulcus; IPS: intraparietal sulcus; SFS: superior frontal sulcus; GFs: superior frontal gyrus; SMA: supplementary motor area; GOm: middle occipital gyrus; inf. inferior; occip: occipital; ant: anterior; cing: cingulate; temp: temporal; Mid: middle; Oper: operculum; orbit: Orbitalis; post: posterior; sup: superior.

7

Functional connectivity and graph characterization in early-stage Alzheimer's disease

Abstract

Alzheimer's disease (AD) related graph alteration has been studied in resting-state functional network as well as structural network. But our understanding of the disease related network alteration in task-based conditions remains incomplete. Graph analysis is thus applied to task-based data. Twelve right-handed patients who were in an early disease stage and twelve age-, gender-, education level-matched controls were instructed to do a associative-semantic task during functional magnetic resonance imaging (fMRI). We adapted the group K-way algorithm in order to get subject specific adaptations of the K-way parcellations based on an independent group. Four node sets which vary in granularity have been investigated. Fully weighted network is constructed per individual and per node sets. The task-based functional network analysis shows an increased connectivity, preserved global network topology characteristics in early-stage AD compared to matched healthy elderly controls.

This chapter is in preparation for publication as: Yu Wang, Natalie Nelissen, Katarzyna Adamczuk, An-Sofie DeWeer, Mathieu Vandenbulcke, Stefan Sunaert, Rik Vandenberghe, Patrick Dupont. Functional connectivity and graph characterization in early-stage Alzheimer's disease.

7.1 Introduction

Over the last decade, the use of graph theory to characterize structural and functional networks of the human brain has gained an increasing interest. There are more and more efforts made to decipher AD at the system level using the graph theoretical approaches. Although the application is still in its infancy, there are already striking differences among the studies. For example, not only increases in the clustering coefficient and characteristic path length of the structural network in AD compared with normal controls have been reported (He et al., 2008; Yao et al., 2010) but also decreases (Tijms et al., 2013) or no change in these measures have been found. For the functional connectivity, there are also some controversial findings on the fluctuation of graph metrics related to disease. For example, AD related decreases of the clustering coefficient have been reported using different techniques such as fMRI (Supekar et al., 2008; Qin et al., 2015; Brier et al., 2014; Toussaint et al., 2014), MEG (Stam et al., 2009) or FDG-PET (Seo et al., 2013)). But other studies found no difference (Stam et al., 2007). Inconsistencies can be found for the characteristic path length as well: AD related increase of characteristic path length have been reported using fMRI (Qin et al., 2015; Wang et al., 2013), MEG (Stam et al., 2009) and EEG (Stam et al., 2007). In contrast, no differences (Catricalà et al., 2015; Brier et al., 2014) and AD related decreases (Buldú et al., 2011) for characteristic path length are also reported.

There are several potential reasons which can account for the variability. Some of these inconsistencies may arise from the differences in nature of the underlying biological substrates (e.g. networks based on blood oxygen level-dependent (BOLD) task or resting state fMRI, diffusion MRI (white matter fiber tracks) or structural MRI (cortical thickness)). The differences in network function may also play a role: while a resting state functional network measures the spontaneous fluctuations of the signal, a task-based network quantifies targeted interactions between regions (Catricalà et al., 2015; Buldú et al., 2011). Furthermore, group differences are depending on the choices made when constructing the network (Phillips et al., 2015). The field is filled with diversities in defining nodes and quantifying interactions between nodes. Nodes can be defined as regions of interest based on meta-analysis (Brier et al., 2014), as regions which are functional activated by a certain task (Vandenberghe et al., 2013), as regions defined by an atlas (Qin et al., 2015) or as regions based on a functional parcellation of the data (Wu et al., 2011). However, little effort is made in taking into account the individual functional and anatomical variability of the organization of the brain. Most studies use the same nodes across subjects by ignoring individual idiosyncratic effects. Recently, Shen et al. proposed a group-wise parcellation scheme (Shen et al., 2013), which enables the simultaneous parcellation of individual brains with respect to a group-level constraint. The interaction can be quantified as correlation (Catricalà et al., 2015; Phillips et al., 2015), partial correlation (He et al., 2008; Phillips et al., 2015), mutual information and synchronization likelihood (Buldú et al., 2011). The network can be binary (Catricalà et al., 2015) or weighted (de Haan et al., 2012; Buldú et al., 2011) and directed (Wu et al., 2011) or undirected (Wang et al., 2014).

The primary aim of this study is to address the possible re-organization in the whole-brain task-based functional connectivity of the associative-semantic network in Alzheimer's disease. To achieve this goal, we examined the functional connectivity for fully weighted networks based on nodes defined by adapting in a subject-specific way the functional parcellation of the whole brain using a similar task in an independent group of subjects. Networks are then constructed using partial correlations between pairs of average time series of the task-fMRI.

7.2 Methods

7.2.1 Task-fMRI data

The data were taken from an experiment published earlier (Nelissen et al., 2007). We excluded one patient from that study who was later on reclassified as primary progressive aphasia and another patient who was left-handed. We thus included 12 right-handed patients who filled the diagnostic criteria for clinically probable Alzheimer's disease (McKhann et al., 1984; Association et al., 1994) and who were in an early disease stage. The mean Mini Mental State Examination (MMSE) score (Folstein et al., 1975) of the patients was 24.6 (SD 2.7, range 19-28). Twelve cognitively intact controls, who were matched for gender, age, education level and handedness, underwent the same protocol. All controls were strictly free of psychotropic or vasoactive drugs, had a normal structural MRI and scored within the published norms on a standard conventional neuropsychological assessment. In table 7.1, the demographic data of two groups of subjects are listed.

	NC	AD
Age (years)	72 ± 7	73 ± 6
Education (years)	11.9 ± 2.3	11.9 ± 2.3
Gender (M/F)	5/7	5/7

Table 7.1: Demographic data

The fMRI experiment, image acquisition, analysis and preprocessing has been described in (Vandenberghe et al., 2013). In summary, the design of the fMRI experiment was factorial and has been described in detail before (Vandenberghe et al., 1996; Vandenbulcke et al., 2005, 2006; Nelissen et al., 2009, 2007; Adamczuk et al., 2013, 2014; Vandenberghe et al., 2013; Wang et al., 2014). The first factor, task, had two levels: associative-semantic versus visuoperceptual judgement. The second factor, input modality, had two levels: pictures versus printed words. A 1.5 tesla Siemens Sonata system (Siemens Medical Solutions, Erlangen, Germany) provided a T1-weighted structural volume as well as T2* echo-planar images (EPI). A total of 108 volumes were acquired during each run. Each run consisted of 3 replications of each of the 4 conditions. Subjects underwent 4 to 6 runs each. We used the normalized and smoothed data from previous studies (Nelissen et al., 2007) using Statistical Parametric Mapping (SPM2; Wellcome Department

of Cognitive Neurology, London, UK; http://www.fil.ion.ucl.ac.uk/spm). Using SPM8, we applied high-pass filtering (FWHM = 270 s) and low-pass filtering consisting of a canonical hemodynamic response function (hrf) to the data.

7.2.2 Node definition

We used a subject specific adaptation of the group K-way parcellation obtained in our previous study (Wang et al., 2015a) at 4 different scales (initial K = $50, 100, 150, 200$ per hemisphere). For the subject specific adaptation we adapted the algorithm of (Shen et al., 2013). This latter method combines a subject specific parcellation with a group based parcellation. In our approach we used the group based parcellation taken from an independent study (Wang et al., 2015a) and applied the K-way parcellation by keeping the group based parcellation constant. The subjects in the independent experiment (cohort size = 54) underwent the same paradigm except that a null condition was included in the experimental design and data were acquired on a 3T MRI scanner.

The subject specific partition will be evaluated in terms of overlap with the atlas parcellation and in terms of the functional homogeneity of each subunit. We expect some overlap between a parcel of the atlas and the subject specific adaptation of it (almost no overlap would mean that there is no longer a relation between the adapted subunit of a subject and the starting parcel of the atlas while perfect overlap would imply that no subject specificity is taken into account). We also expect that the functional homogeneity is increased when taking into account the subject specific subunit compared with the homogeneity of the corresponding parcel of the atlas.

We evaluated the overlap between the subject specific subunit and the corresponding parcel using the Dice coefficient, which is a measure of overlap. Given two sets A and B, the Dice coefficient is calculated as:

$$\text{Dice} = \frac{2|A \cap B|}{|A| + |B|} \tag{7.1}$$

where $|.|$ denotes the cardinality of the set. When the two sets completely overlap, the Dice coefficient is one and if there is no overlap, it will be zero.

The similarity silhouette (SIL) was chosen to evaluate the functional homogeneity. Let $S_k = v_1, \ldots, v_{n_k}$ be the set of voxels inside the k^{th} subunit and n_k is the size of S_k. The average similarity a_k of all voxels within the subunit is calculated as:

$$a_k = \frac{1}{n_k(n_k - 1)} \sum_{i,j \in S_k, i \neq j} s(v_i, v_j) \tag{7.2}$$

where $s(v_i, v_j)$ is the similarity measure between time series in voxel v_i and v_j. For this analysis we have chosen the Pearson correlation as similarity measure. Similarly, b_k is the average similarity between voxels within and outside the subunit S_k:

$$b_k = \frac{1}{n_k(N - n_k)} \sum_{i \in S_k} \sum_{j \notin S_k} s(v_i, v_j) \tag{7.3}$$

We then transform the average similarity measure to a distance measure:

$$Da_k = \frac{1 - a_k}{1 + a_k} \text{ and } Db_k = \frac{1 - b_k}{1 + b_k} \tag{7.4}$$

The silhouette (SIL) for the k^{th} subunit is given by:

$$\text{SIL}_k = \frac{Db_k - Da_k}{\max(Da_k, Db_k)} \tag{7.5}$$

Thus $-1 \leq \text{SIL}_k \leq 1$ and higher value of SIL_k indicates a better parcellation in terms of subunit homogeneity. On the other hand, negative values indicate an incorrect partition.

7.2.3 Network construction

Partial correlation coefficients between nodes were calculated based on the average time series to obtain the degree of association between regions, with the effect of other regions removed (Marrelec et al., 2006; Smith et al., 2011).

The association strength is defined as the absolute value of the z-score which is calculated from the partial correlation using the Fisher r-to-z transform. We applied a nonlinear mapping of z score to connection weight (w_{ij}) between nodes i and j by calculating (Wang et al., 2015a):

$$w_{ij} = (2\Phi(|z_{ij}|) - 1)^4. \tag{7.6}$$

where Φ is the cumulative distribution function of the standard normal distribution.

7.2.4 Graph characterization

This work will mainly focus on analysing weighted graphs at the individual level. Global measures include characteristic path length λ, mean clustering coefficient C, mean local efficiency E_{loc}, global efficiency E_{glob}, mean betweenness centrality b and average strength. Graph measures were calculated by using the brain connectivity toolbox (Rubinov and Sporns, 2010) (https://sites.google.com/a/brain-connectivity-toolbox.net/bct/Home,) except for the weighted clustering coefficient and local efficiency for which we used generalizations more suitable for fully weighted networks (Wang et al., 2015b). Weighted graph metrics are normalized by equivalent random networks, which have the same weight and strength (weighted node degree) distribution as the original network. Small worldness SW is quantified as:

$$\text{SW} = \frac{C/C^{rand}}{\lambda/\lambda^{rand}}. \tag{7.7}$$

7.2.5 Statistics

Paired t-tests were conducted to test the difference in regional homogeneity between the modified K-way parcellation method and a method in which we impose the group based parcellation without any adaptation.

Group differences in connectivity were tested with two-tailed t-tests for independent samples. Since the normality of the distribution of the brain topological graph metrics is yet unclear (Bullmore and Bassett, 2011; Meskaldji et al., 2013; Stam et al., 2009), we use a non-parametric random permutation test by permuting the group membership (10,000 permutations).

The significance level in all cases was set to $p < 0.05$ unless otherwise stated.

7.3 Results

7.3.1 Subject specific adaptation of the atlas

For the evaluation of the modified K-way parcellation, we limited this part of the analysis to the normal control subjects. The Dice coefficient is calculated to evaluate the overlap between each subunit of the group based parcellation and the corresponding subject specific adaptation of that subunit (figure 7.1). The average values for the Dice coefficient across all parcellations and subjects are between 0.5 and 0.7 for each level of K which is tested. This indicates that the subunits were adapted while preserving some overlap with the initial group based subunit. However, this is not sufficient. If the subject specific adaptation is an improvement the Silhouette values should improve compared to applying the group parcellation without adaptation. This is the case as can be seen in figure 7.2. The modified K-way parcellation method shows significantly better regional homogeneity compared to the approach of imposing the group based parcellation directly ($p_{corr} < 0.05$ Bonferroni corrected for the number of tests).

7.3.2 Network comparison

Connectivity

To test if differences exist between the AD group and the elderly controls at the level of the connections, we used a two-sample t-test of the z score of each connection. The distribution of significant ($p < 0.05$) connections between the two groups is shown in figure 7.3 in which we make a distinction between the type of the connection: intrahemispheric connections (left or right) or interhemispheric connections. We also indicate if connections are increased or decreased in the AD group compared to the control group. Visual inspection suggests that both increased and decreased connectivity exist all over the brain, mostly within the left hemisphere or between hemispheres. We also tested the difference in the amplitude of the connections (absolute Z score). The results are shown in figure 7.4. This shows that AD patients have more significant increased amplitudes in the connections mostly located in the left hemisphere or between hemispheres.

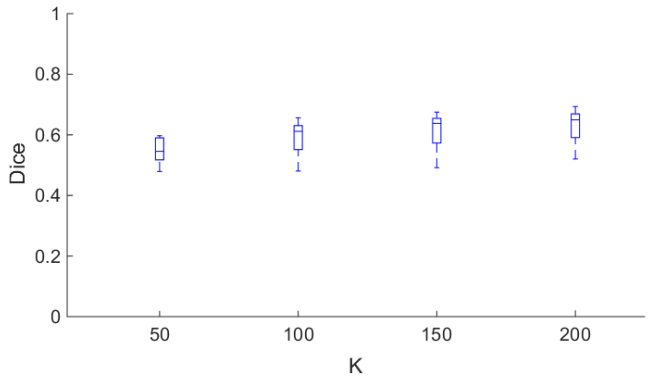

Figure 7.1: Overlap between the subunits obtained by the modified K-parcellation algorithm and the corresponding subunits of each group based parcellation. On the X-axis, the value of K (per hemisphere) used when applying the parcellation, is given. The overlap is evaluated by the Dice coefficient. Boxplots are given for the values measured in each subunit and for each subject.

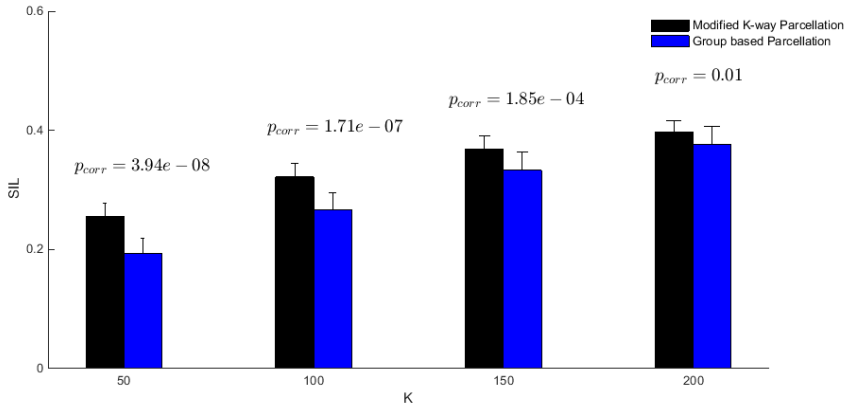

Figure 7.2: Comparison of the subunit homogeneity in terms of SIL between the modified K-parcellation method and the method applied by applying the group based parcellation directly. On the X-axis, the value of K (per hemisphere) used when applying the parcellation, is given. The error bar shows the variation of the average SIL (across all subunits) among all subjects. Significant differences between the two methods are indicated by the corrected p value on top.

However, some connections - mostly inter-hemispheric - show decreased amplitudes in the AD group compared to the normal controls.

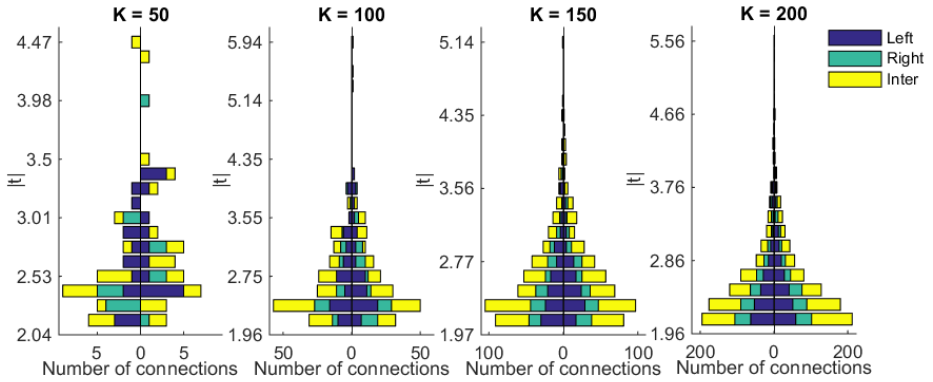

Figure 7.3: Histogram of between group differences in the connectivity Z score. X axis shows the number of connections per bin of the T-score. The left part shows the number of connections which are higher in AD patients compared to normal controls and the right part shows the reverse. Stacks in the bar indicate the number of intra-hemispheric connections (blue, left hemisphere; green, right hemisphere) and inter-hemispheric connections (yellow). Y axis shows the T-value of the two-sample t-test. The label on top refers to K (per hemisphere) used when applying the modified K-way parcellation.

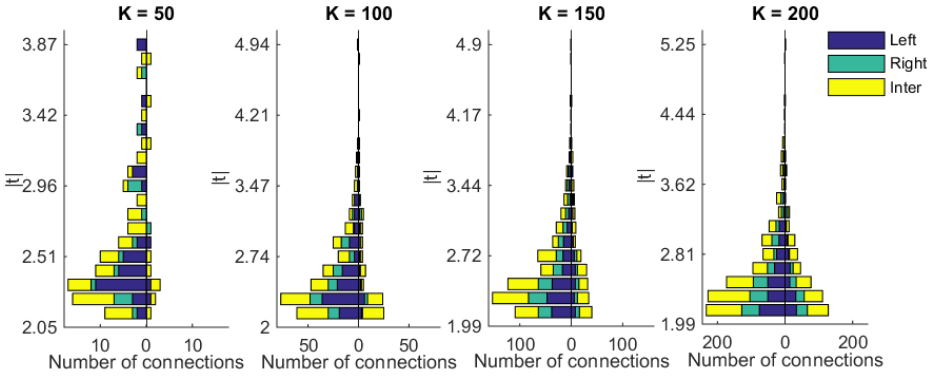

Figure 7.4: Histogram of between group differences in the amplitude of the connectivity Z score. X axis shows the number of connections per bin of the T-score. The left part shows the number of connections which are higher in AD patients compared to normal controls and the right part shows the reverse. Stacks in the bar indicate the number of intra-hemispheric connections (blue, left hemisphere; green, right hemisphere) and inter-hemispheric connections (yellow). Y axis shows the T-value of the two-sample t-test. The label on top refers to K (per hemisphere) used when applying the modified K-way parcellation.

We also calculated the mean of the amplitude of all connections in each subject and compared these values between both groups. We found that the mean value was significantly higher in the Alzheimer's disease group compared to the elderly normal controls for all the different atlases on which we applied the modified K-way parcellation method (figure 7.5).

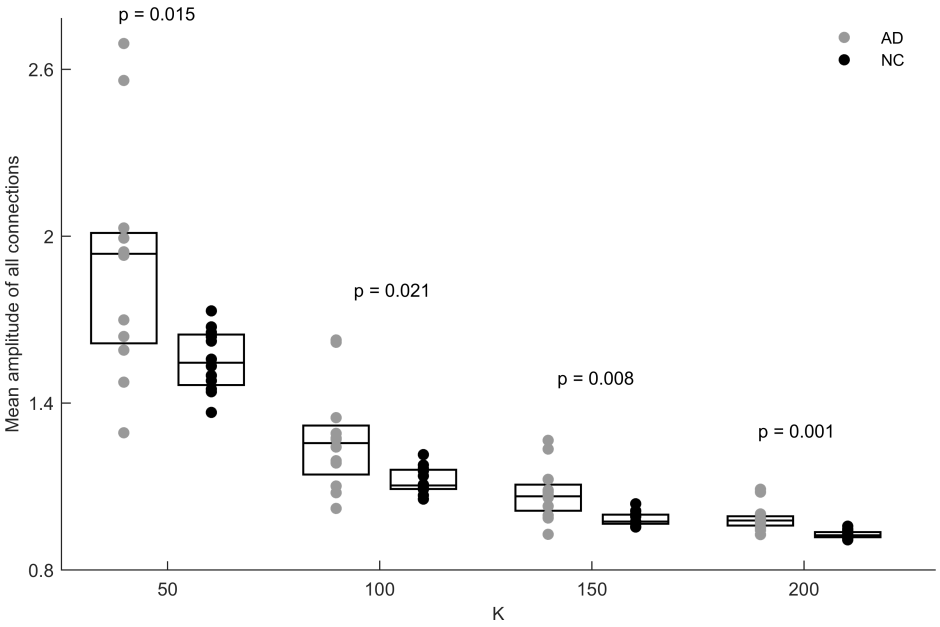

Figure 7.5: Mean amplitude of all connections within each subject. Boxplots and individual data points are shown for the AD patients (grey) or for the elderly controls (black). On the X-axis, the value of K (per hemisphere) used when applying the modified K-way parcellation, is given. P-values on top refer to the two sample t-test.

Global graph metrics

Figure 7.6 shows the results of the weighted graph analysis for each subject specific network for the two groups. The non-parametric permutation test reveals significant between group differences in which for the AD the betweenness centrality (b) and the characteristic path length (λ) is lower and the clustering coefficient (C), the local (E_{loc}) and global (E_{glob}) efficiency and network strength (S) are higher. However, when the graph metrics are normalized by equivalent random networks no differences between both groups were found (figure 7.7).

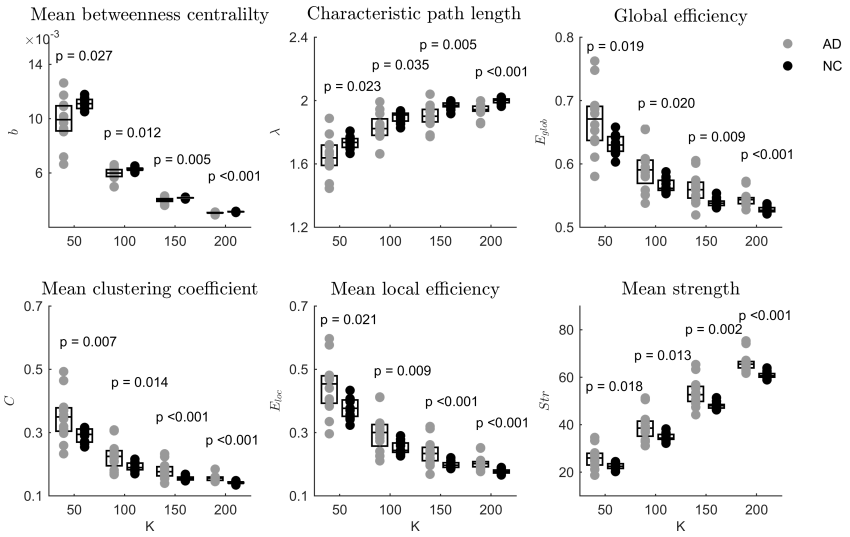

Figure 7.6: Individual graph metrics. Boxplots and individual data points are shown for the AD patients (grey) or for the elderly controls (black). On the X-axis, the value of K (per hemisphere) used when applying the modified K-way parcellation, is given. P-values on top refer to the non-parametric permutation test.

7.4 Discussion

In the present study, we attempt to address changes in the associative-semantic network related to AD pathology. When comparing our study with the existing literature, a few aspects need to be taken into account: 1) the results are based on a task-based fMRI with the associative-semantic network; 2) we are focussing on early-stage AD patients; 3) the nodes of the network were based on a new modified K-way parcellation method; 4) network measures were calculated based on partial correlations transformed to connection weights and the calculations were performed on the fully weighted graph.

7.4.1 Node definition

There is a significant inter-subject variability in the structural and functional organization of the brain even after warping all brains to the same common space. Many anatomical registration studies have shown mismatches in brain regions between subjects (Uylings et al., 2005). When comparing normal controls and patients, it even becomes worse since patients may have an alteration in the functional-anatomical organization.

This work can be considered as a small step towards generalizing an individualized functional atlas starting from a population based a-priori parcellation. We proposed a new modified K-way parcellation method to obtain individualized

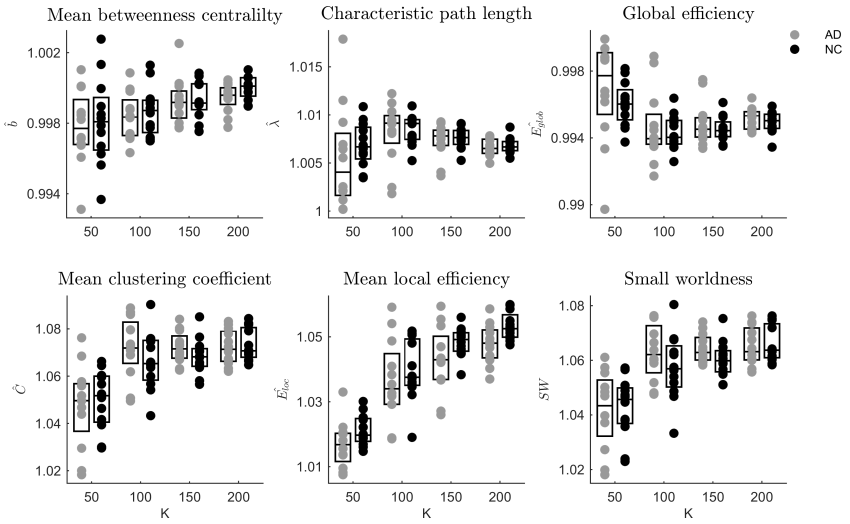

Figure 7.7: Normalized individual graph metrics. Boxplots and individual data points are shown for the AD patients (grey) or for the elderly controls (black). On the X-axis, the value of K (per hemisphere) used when applying the modified K-way parcellation, is given. P-values on top refer to the non-parametric permutation test.

whole brain functional homogeneous subdivisions by registering the data of each subject to a reference population atlas (Shen et al., 2013). The method differentiates itself from literature in terms of incorporating population consistency and individual specificity.

Shen et al. proposed two methods when comparing network level organization between normal controls and patients (Shen et al., 2013). One is to apply the control group parcellation to the patient data directly but when comparing the results between both groups the control group has an advantage because they have contributed to group based parcellation which is used. To overcome this problem, we have used the group based parcellation taken from an independent experiment.

The other way they suggest is to subdivide each group separately and compare the parcellation directly to examine the different organization in terms of subunits. This idea is interesting in understanding the reorganization, but it could complicate the interpretation of the subsequent network analysis of the brain since there is no natural correspondence between the group-level parcellations if they are obtained separately. Finding corresponding subunits faces difficulties which arise from an unequal number of subunits.

It is known that brain function act as a multi-level organization. Multi-scale analysis as provided by the group-wise K-way parcellation can show a more complete image by looking at different levels of granularity. Therefore, we presented results for different values of K which represent these granularity levels.

7.4.2 Group differences

Network changes related to AD pathology were examined in terms of functional connectivity and weighted graph theoretical measures in the present study.

First, an increase in global network connectivity/strength was observed in patients with early-stage AD. Although a connectivity/strength decrease has been reported in studies of AD patients across different modalities (Qin et al., 2015; Wu et al., 2011; Stam et al., 2009), a global increase is also found at lower-frequencies (0.01 to 0.05 Hz) using fMRI (Supekar et al., 2008). This inconsistency may result from the clinical heterogeneity of the AD patients. Most studies focused on advanced AD patients. Because of the severity of the brain atrophy, most of these studies are analysing resting-state networks. The popularity of resting-state analysis roots in the fact that it can be collected and compared across research sites, especially for patients with neurodegeneration (Turk-Browne, 2013). Despite these advantages, resting state fMRI cannot replace task-based fMRI when studying cognitive processes in the brain. In this study, the subjects involved are early-stage AD patients with the ability to complete the associative-semantic tasks (although the response time was longer and the accuracy lower compared to normal controls). The increase rather than decrease in connectivity may reflect the plasticity of brain. The higher strength can also be related to a higher demand of energetic cost which is needed to compensate for the lost functionality. The increase in functional connectivity of patients with AD is consistent with the global increase found in amnestic MCI patients using task-based MEG data (Buldú et al., 2011).

Second, our patients with AD showed a significant group-difference in clustering coefficient, characteristic path length, betweenness centrality and local and global efficiency. It should be addressed that the graph metrics are closely related to the main network characteristics: the number of nodes and edges, edge weight distribution as well as the size of the connected component (Meskaldji et al., 2013; Stam et al., 2009; Bassett et al., 2012; Ginestet and Simmons, 2011). For example, a lower level of weight will give rise to smaller global clustering coefficient irrespective of network topology. Thus changes in graph metrics may be dominated by differences of the connectivity level instead of the real topological alteration between AD and NC. In order to capture the "pure" changes between groups, we normalized graph metrics by individual weighted null networks (using equivalent random networks with the same weighted strength distribution). As a result, none of these differences remained significant. This suggests that the overall network topology is still maintained for the diseased brain. The same is true for the small worldness of the brain.

7.5 Conclusion

We adapted the group K-way algorithm in order to keep the group parcellation fixed so that it can be taken from an independent study while allowing subject specific adaptations of the parcellations. Furthermore, the task-based associative-

semantic network shows an increased connectivity and preserved global network topology in early-stage AD compared to matched healthy elderly controls.

Acknowledgements

This work was supported by Research Foundation Flanders (FWO) [G0660.09 & G0A0913N to RV and PD], KU Leuven [OT/12/097 to RV and PD], Federaal Wetenschapsbeleid belspo [IAP-VII P7/11] and Stichting voor Alzheimer Onderzoek (SAO11020 & 13007). YW has a grant from the Chinese Scholarship Council, KA is a doctoral fellow of the FWO and RV is a senior clinical investigator of the FWO.

8 Conclusions and further research

In this final chapter, the most important findings of the presented work will be briefly recapitulated in Section 8.1 and suggestions for future research directions are given in Section 8.2.

8.1 General Conclusion

Characterizing a meaningful spatial-temporal picture of the working brain by a graph theoretical approach requires a series of steps that need to be carefully considered. Throughout the whole doctoral project, we focused on the explicit associative-semantic processing of words and pictures which activates a distributed set of brain areas. In our lab we have already a long tradition to study this processing in normal subjects as well as in different patient populations (Nelissen et al., 2007; Van Doren et al., 2010; Adamczuk et al., 2013). Until recently, these studies were mainly focusing at the regional level, less is known about how information is integrated and transferred between regions. Brain network analysis is a promising tool to investigate cognitive processes (Rubinov and Sporns, 2010). The associative-semantic network consists of a large number of nodes and an even exponentially larger number of possible functional connections. Given the extent of the network and the significant lacunae that remain in our knowledge about its internal connectivity structure, we applied graph analysis to characterize and examine the structure of this network.

We started with conducting a group-level binary graph network analysis in chapter 3. A modularity analysis discerned 4 communities: one corresponded to the classical perisylvian language system, including superior temporal sulcus (STS), middle temporal gyrus (GTm) and pars triangularis of the inferior frontal gyrus (GFi), among other nodes. A second subsystem consisted of left ventral occipital temporal transition zone (vOT) and anterior fusiform gyrus along with hippocampus and intraparietal sulcus. The two subsystems were linked through a unique connection between vOT and GTm, which were hubs with a high

betweenness centrality compared to STS and GFi which had a high local clustering coefficient. In addition, the binary network exhibited small-world characteristics, which is a sign of economical and efficient information exchange(Achard and Bullmore, 2007).

Then, we moved a further step to look at reproducibility and robustness of graph metrics at both the group and individual level for binary as well as weighted networks. Only a few studies, to our knowledge, rely on a common area of activation across a group of subjects consider the individual variability and reliability of activity across the whole brain volume. Little research has investigated network reproducibility under different experimental conditions. Applying reliability and robust algorithms to achieve the above goals is the one of the main task of this work. With the data from different experimental design readily available, we were able to examine the reliability of the extracted networks across subjects in several levels. We have shown that global graph measures exhibited a good reproducibility and robustness but the results depend on the graph measure itself and on the density in case of binary networks. Group based binary networks should be derived from groups of sufficient size and the lower the density the more subjects were required to obtain robust values. Local graph measures were very variable in terms of reproducibility and should be interpreted with care. For weighted networks, we found good reproducibility when using subject specific networks and this made us focus on weighted individual global graph metrics in the following chapters.

As being discussed through the whole thesis, finding appropriate sets of nodes in the network connectivity analysis is the first step to go. However, the choice is not that trivial to make.

We have examined several definitions of nodes in the thesis. In chapter 3 and 4, we took the regions which are activated the most during the task. In this condition, we were investigating the information flow among these nodes. Partial correlations measure the pairwise linear relationship between multiple brain regions by removing the common linear influences of all other regions included in the analysis. However, it cannot be ruled out that other brain regions, which are not included in the analysis, may still drive the behaviour and the connectivity of network under investigation. In such a case, these driving regions were not detected using fMRI which is not very likely although not impossible. When using a whole brain-wide connectivity analysis this issue is partially resolved. In chapter 6, we applied functional homogeneous subunits as whole brain-wide nodes in the network analysis by the group-wise parcellation scheme which has been proposed to simultaneously parcellate the group as well as individual networks into subunits (Shen et al., 2013). The procedure created individualized parcellations which have natural correspondence among individuals. It made network analysis among individuals more straightforward. While this relatively new technique for identifying connectivity-based subregions was originally described for resting state functional connectivity, we applied it to task-based functional connectivity. In chapter 7, we adapted the group K-way parcellation algorithm in order to keep the group parcellation fixed so that it can be taken from an independent

study while allowing subject specific adaptations of the K-way parcellations. By comparing the resulted graph characteristics, we were able to investigate the granularity effect on the network properties. As shown in our work, different node definitions captured distinct levels of the underlying process. Despite of the variations induced by the granularity level, there were preserved global properties of the functional connectivity pattern: small world topology, normalized global graph metrics and part of the hub regions and modular structure.

The most suitable model you can choose is determined by the research question. After all, brain network analysis is grounded and constrained by neurobiological assumptions and principles. Multiple-model network analysis might also be helpful to understand the underlying brain activity interaction better. The brain is organized as multiple functional brain systems, e.g. visual, auditory, motor, language, etc. However, the human brain is a highly integrated system; all cognitive tasks are embedded in the whole brain network. In this work we compared network characteristics between the task-specific associative semantic network (R57) and the global whole brain network (R85 and parcellation-based) in Chapter 6 and 7. Future work regarding understanding of how functional brain systems are embedded in the global organization of the brain will be of great interest.

Besides the effort made to investigate node definition variation, we did also work to improve the contribution of edges connecting nodes. Many graph metrics were designed to investigate binary network topology, which requires a threshold to convert the continuous functional connections to either 1 or 0. The binarization procedure reduces the computation burden and has straightforward interpretation. However, there is no consensus on choosing the threshold. Graph network measures are dependent on the threshold selected and maybe unstable across threshold (Garrison et al., 2015). Thus caution should be taken when binarizing functional connectivity data and interpreting binary graph results. This renders weighted graph analysis as an alternative. Being exempt of imposing an arbitrary threshold, weighted graph preserve all edges. In chapter 4, we started to use weighted graph analysis. We proposed a non-linear transformation to convert partial correlation to network weight which ranges from 0 to 1. This approach enhanced the contrast between the strongest and weakest connection while keeping medium connections, which is neither too strong nor too weak. Our procedure was better than a linear transformation from z score to weight, which is often implemented by using the maximum and minimum z score, in a way that it is less sensitive to the noise in the data, especially when the high z score is caused by noise. Our proposed measures may obviate the need for these arbitrary analyses and open the way toward more sound and reliable network characterizations. Furthermore, we developed generalizations of clustering coefficient and nodal efficiency for fully weighted network in chapter 5. Our approach outperformed existing generalizations in terms of general versatility, weight-scale invariance, continuity and overall robustness.

Evidences on changing features of brain networks for pathology attacks are appropriate sets also of interests to us. In the end, the procedures developed in earlier chapters were applied to patients with Alzheimer's disease as well

as normal elderly healthy controls to extract more information of the network. Given the contradictions of the graph finding in the literature, this study tried to compare the graph alterations in patients compared to controls by conducting the fully weighted, multiple-granularity network analysis using task-based fMRI data. We found an increased connectivity and preserved global network topology characteristics in early-stage AD compared to matched healthy elderly controls.

8.2 Future direction

Several aspects which may influence the graph network analysis have been presented in the thesis and their strengths and limitations have been illustrated. Nevertheless, as a flourishing field, there are still a lot of open issues which haven't been addressed. Here we discuss several important issues which might be interesting and important in the future work. First, the signs of the connections need to be incorporated appropriately to make a distinction between two different function interactions: cooperation or inhibition. Second, hierarchical modularity analysis renders multiple spatial views of brain structure, ranging from coarse clustering to much more fine-grained grouping. Third, large-scale voxel-based analysis may give us insight at the smallest resolution. In addition, integrating the functional network with the structure network can be beneficial to single-modal analysis.

8.2.1 Negative or positive?

Interactions between nodes in complex networks often vary in sign from positive to negative. It is suggested that there are inherent distinction of positive and negative connections in network organization: while the former suggests cooperation between nodes, the latter points to inhibition (Fornito et al., 2012; Fox et al., 2005; Rubinov and Sporns, 2011; Sonuga-Barke and Castellanos, 2007).

However, graph theoretic measures often require the connections between nodes to be positive (Rubinov and Sporns, 2011). This necessitates taking the absolute value (Sala-Llonch et al., 2014; Fornito et al., 2013; Muller and Meyer, 2014), looking at positive and negative network separately (Schwarz and McGonigle, 2011), transferring negative to negligible positive connections (Schwarz and McGonigle, 2011) or discarding negative connections (Fornito et al., 2013; Vaessen et al., 2014). The idea of neglecting negative connections or transforming them to negligible positive assume that negative connections in fMRI data may be artefacts as a result of pre-processing techniques. However, it is shown that probably not all negative connections are artefacts; instead they may play an important role in behaviour with neurophysiologic origin (Fornito et al., 2013; Rubinov and Sporns, 2011). Treating positive and negative connections differently is another alternative. However, it artificially separates the complete information to two parts which will complicate the interpretation of the results. Throughout the entire thesis, we have been using the absolute values of partial correlation to

quantify interactions between nodes. This procedure preserved the interaction amplitude by neglecting the intrinsic difference of signs of the connections.

While sign information was not incorporated into graph theoretic measures, people started to take it into account when partitioning the network into modular (Muller and Meyer, 2014; Rubinov and Sporns, 2011). However, there's still room for improvement of modular detection algorithm to incorporate signs as the existing ones give non-stable partitions over runs.

Generalizations of existing formula for graph theoretic measures that can account for signed weights, and which are applicable to fully weighted network, will be an interesting topic for the future work.

8.2.2 Modularity hierarchy

Compared to graph measures which evaluate information integration, the focus of information segregation demands more the detection of modular structures. Segregation patterns of brain networks have been back-boned by strong evidences: modularity structures have been reported from non-human data (Schwarz et al., 2008; Hilgetag et al., 2000) to human anatomical and functional data (Salvador et al., 2005; Meunier et al., 2009a; Ferrarini et al., 2009; Bassett et al., 2008). However, most studies focused on studying the community structure at one particular level, neglecting the possible hierarchical organization over different levels. In fact, clear evidence for hierarchical modularity ("modules-within-modules") has been reported in brain networks (Zhou et al., 2006; Meunier et al., 2009b). Hierarchical modularity helps to zoom in and out the underlying structure and provides a complete view of brain connectivity. Furthermore, it is speculated that there is a link between the topological modularity of adult brain networks and the embryonic modularity of the developing nervous system (Meunier et al., 2009b). Increased computational burden, which is the product of broadening our horizon to multiple levels, might be one limitation which hinders the application of hierarchical organization studies. Algorithms to derive hierarchical modularity present an interesting focus for future studies. For example, in the link community detection procedure, the network is partitioned hierarchically by looking at the relations of edges (Ahn et al., 2010). These algorithms are worth attention to the neuroimaging field and may improve the comparison of modular structures given the inter-subject and inter-group variability.

8.2.3 Voxel-based analysis

Although modelling the same biological system, the human brain, striking differences have been reported, for example the distribution of node degree k and their ability to localize nodes with interesting characteristics in the brain space (Bullmore and Sporns, 2009). Furthermore, voxel-based network analysis by treating each voxel as a node (Hayasaka and Laurienti, 2010) is reported to be better in localization of highly connected nodes or hubs within the anatomical areas identified by region-based analysis. However, calculating the partial correlation via the direct calculation of the inverse of the covariance matrix is no

longer feasible. In recent years a number of authors have proposed methods to estimate the covariance inverse (Meinshausen and Bühlmann, 2006; Friedman et al., 2008; Songsiri and Vandenberghe, 2010; Stifanelli et al., 2011). For example, the graphical lasso algorithm (Friedman et al., 2008) can be used to get the large scale partial correlation network. There's a regularization parameter ρ to control the trade-off between the sparsity of solution and data fit. Specifically, when ρ is very large, then most entries of the estimated partial correlation matrix will be zero. Hence, a challenge in practice is how to select the value for ρ. There are several methods addressed to solve the problem, i.e. the stability selection method (Meinshausen and Bühlmann, 2010; Ji, 2011), the Bayes information criterion (BIC) (Songsiri and Vandenberghe, 2010), maximum a posteriori probability (MAP) and cross-validation method (Friedman et al., 2008). Another fact which may hinder individual level comparisons by voxel-based analysis is the high inter-subject variability. A promising approach is to impose a group-level graph constraint and estimate jointly multiple subject-specific models (Varoquaux and Thirion, 2012).

8.2.4 Integration of functional network with structural network

Another tempting direction to go is to integrate the functional and structural connectivity in order to take advantage of the edges of both techniques. For example, while fMRI is not sensitive enough to evaluate the microstructure of brain morphology, magnetic resonance diffusion tensor imaging (DTI) is an MRI technique that assesses and quantifies water diffusion in biological tissues at a microstructural level. Comparisons between anatomical and functional networks are encouraging and meaningful in some cases (e.g., modular structure analysis, (Zhou et al., 2006)). However, differences in frequency and spatial scales hinder straightforward global comparisons (Rubinov and Sporns, 2010) and make it still a current challenge to the neuroimaging field. For example, in the cross-correlation resting-state network analysis, structural connectivity serves as a basis for functional connectivity: the presence of strong connections is indicative of the existence of high weight functional connections between regions (Hagmann et al., 2008; Greicius et al., 2009; Honey et al., 2009; van den Heuvel et al., 2008, 2009). In contrast, a high functional connection is not necessarily a guarantee for the existence of anatomical connections (Hagmann et al., 2008; Greicius et al., 2009; Damoiseaux and Greicius, 2009; Honey et al., 2009). It is likely that many functional connections may be explained by indirect anatomical connections (Sporns, 2011). Thus functional networks are denser than structural counterparts. This discrepancy is likely to become more pronounced in larger networks, as anatomical connectivity in such networks becomes increasingly sparse, while functional connectivity remains comparatively dense. These discrepancies may be removed by using proper models in extracting network. For example, using the graphical lasso algorithm will help in obtaining a sparse partial correlation functional network. Future work relating structural connectivity to task-evoked

partial correlation functional network may provide further insight in the large scale brain communication. Furthermore, current non-invasive imaging techniques cannot capture neuronal connectivity. Invasive methods such as tract tracing help in revealing the ground truth of complex networks at the cellular level.

Bibliography

Achard, S., Bullmore, E., 2007. Efficiency and cost of economical brain functional networks. PLoS computational biology 3 (2), e17.

Achard, S., Salvador, R., Whitcher, B., Suckling, J., Bullmore, E., 2006. A resilient, low-frequency, small-world human brain functional network with highly connected association cortical hubs. J Neurosci 26 (1), 63–72.

Adamczuk, K., De Weer, A.-S., Nelissen, N., Chen, K., Sleegers, K., Bettens, K., Van Broeckhoven, C., Vandenbulcke, M., Thiyyagura, P., Dupont, P., Van Laere, K., M. Reiman, E., Vandenberghe, R., 2013. Polymorphism of brain derived neurotrophic factor influences β amyloid load in cognitively intact apolipoprotein e $\epsilon 4$ carriers. NeuroImage: Clinical 2, 512–520.

Adamczuk, K., De Weer, A.-S., Nelissen, N., Dupont, P., Sunaert, S., Bettens, K., Sleegers, K., Van Broeckhoven, C., Van Laere, K., Vandenberghe, R., 2014. Functional changes in the language network in response to increased amyloid β deposition in cognitively intact older adults. Cerebral Cortex, in press.

Ahn, Y.-Y., Bagrow, J. P., Lehmann, S., 2010. Link communities reveal multiscale complexity in networks. Nature 466 (7307), 761–764.

Albert, R., Barabási, A.-L., 2002. Statistical mechanics of complex networks. Reviews of modern physics 74 (1), 47–97.

Alexanderson, G., 2006. About the cover: Euler and königsbergs bridges: A historical view. Bulletin of the american mathematical society 43 (4), 567–573.

Amaral, L. A., Ottino, J. M., 2004. Complex networks. The European Physical Journal B Condensed Matter and Complex Systems 38 (2), 147–162.

Ashburner, J., Friston, K. J., 2005. Unified segmentation. NeuroImage 26 (3), 839–851.

Association, A. P., Association, A. P., et al., 1994. Diagnostic and statistical manual of mental disorders (DSM). Washington, DC: American psychiatric association, 143–7.

Barabasi, A.-L., Oltvai, Z. N., 2004. Network biology: understanding the cell's functional organization. Nature Reviews Genetics 5 (2), 101–113.

Barnes, K., Nelson, S., Cohen, A., Power, J., Coalson, R., Miezin, F., Vogel, A., Dubis, J., Church, J., Petersen, S., Schlaggar, B., 2012. Parcellation in left lateral parietal cortex is similar in adults and children. Cereb Cortex 22 (5), 1148–1158.

Barrat, A., Barthelemy, M., Pastor-Satorras, R., Vespignani, A., 2004. The architecture of complex weighted networks. Proceedings of the National Academy of Sciences of the United States of America 101 (11), 3747–3752.

Bassett, D. S., Brown, J. A., Deshpande, V., Carlson, J. M., Grafton, S. T., 2011. Conserved and variable architecture of human white matter connectivity. NeuroImage 54 (2), 1262–1279.

Bassett, D. S., Bullmore, E., Verchinski, B. A., Mattay, V. S., Weinberger, D. R., Meyer-Lindenberg, A., 2008. Hierarchical organization of human cortical networks in health and schizophrenia. The Journal of Neuroscience 28 (37), 9239–9248.

Bassett, D. S., Bullmore, E. T., 2009. Human brain networks in health and disease. Current Opinion in Neurology 22 (4), 340.

Bassett, D. S., Nelson, B. G., Mueller, B. A., Camchong, J., Lim, K. O., 2012. Altered resting state complexity in schizophrenia. NeuroImage 59 (3), 2196–2207.

Batagelj, V., Mrvar, A., 1998. Pajek-program for large network analysis. Connections 21 (2), 47–57.

Batalle, D., Eixarch, E., Figueras, F., Muñoz-Moreno, E., Bargallo, N., Illa, M., Acosta-Rojas, R., Amat-Roldan, I., Gratacos, E., 2012. Altered small-world topology of structural brain networks in infants with intrauterine growth restriction and its association with later neurodevelopmental outcome. NeuroImage 60 (2), 1352–1366.

Bernhardt, B., Chen, Z., He, Y., Evans, A., Bernasconi, N., 2011. Graph-theoretical analysis reveals disrupted small-world organization of cortical thickness correlation networks in temporal lobe epilepsy. Cereb Cortex 21 (9), 2147–2157.

Biggs, N., Lloyd, E. K., Wilson, R. J., 1986. Graph Theory, 1736-1936. Clarendon Press.

Binder, J. R., Desai, R. H., Graves, W. W., Conant, L. L., 2009. Where is the semantic system? a critical review and meta-analysis of 120 functional neuroimaging studies. Cereb Cortex 19 (12), 2767–2796.

Blondel, V. D., Guillaume, J.-L., Lambiotte, R., Lefebvre, E., 2008. Fast unfolding of communities in large networks. Journal of Statistical Mechanics: Theory and Experiment 2008 (10), P10008.

Braun, U., Plichta, M. M., Esslinger, C., Sauer, C., Haddad, L., Grimm, O., Mier, D., Mohnke, S., Heinz, A., Erk, S., et al., 2012. Test–retest reliability of resting-state connectivity network characteristics using fMRI and graph theoretical measures. NeuroImage 59 (2), 1404–1412.

Brier, M. R., Thomas, J. B., Fagan, A. M., Hassenstab, J., Holtzman, D. M., Benzinger, T. L., Morris, J. C., Ances, B. M., 2014. Functional connectivity and graph theory in preclinical Alzheimer's disease. Neurobiology of aging 35 (4), 757–768.

Brown, J. A., Terashima, K. H., Burggren, A. C., Ercoli, L. M., Miller, K. J., Small, G. W., Bookheimer, S. Y., 2011. Brain network local interconnectivity loss in aging APOE-4 allele carriers. Proceedings of the National Academy of Sciences 108 (51), 20760–20765.

Bruffaerts, R., Dupont, P., Peeters, R., De Deyne, S., Storms, G., Vandenberghe, R., 2013a. Right fusiform response patterns reflect visual object identity rather than semantic similarity. NeuroImage 83, 87–97.

Bruffaerts, R., Dupont, P., Peeters, R., De Deyne, S., Storms, G., Vandenberghe, R., 2013b. Similarity of fMRI activity patterns in left perirhinal cortex reflects semantic similarity between words. The Journal of Neuroscience 33 (47), 18597–18607.

Buchanan, C. R., Pernet, C. R., Gorgolewski, K. J., Storkey, A. J., Bastin, M. E., 2014. Test–retest reliability of structural brain networks from diffusion MRI. NeuroImage 86, 231–243.

Buckner, R. L., Koutstaal, W., Schacter, D. L., Rosen, B. R., 2000. Functional MRI evidence for a role of frontal and inferior temporal cortex in amodal components of priming. Brain 123 (3), 620–640.

Buckner, R. L., Sepulcre, J., Talukdar, T., Krienen, F. M., Liu, H., Hedden, T., Andrews-Hanna, J. R., Sperling, R. A., Johnson, K. A., 2009. Cortical hubs revealed by intrinsic functional connectivity: mapping, assessment of stability, and relation to Alzheimer's disease. J Neurosci 29 (6), 1860–1873.

Buldú, J. M., Bajo, R., Maestú, F., Castellanos, N., Leyva, I., Gil, P., Sendiña-Nadal, I., Almendral, J. A., Nevado, A., Del-Pozo, F., et al., 2011. Reorganization of functional networks in mild cognitive impairment. PLoS One 6 (5), e19584.

Bullmore, E., Sporns, O., 2009. Complex brain networks: graph theoretical analysis of structural and functional systems. Nat Rev Neurosci 10 (3), 186–198.

Bullmore, E., Sporns, O., 2012. The economy of brain network organization. Nat Rev Neurosci 13 (5), 336–349.

Bullmore, E. T., Bassett, D. S., 2011. Brain graphs: graphical models of the human brain connectome. Annual review of clinical psychology 7, 113–140.

Bundesen, C., Habekost, T., 2008. Principles of visual attention: Linking mind and brain. Oxford University Press.

Bundesen, C., Habekost, T., Kyllingsbæk, S., 2005. A neural theory of visual attention: bridging cognition and neurophysiology. Psychological review 112 (2), 291.

Button, K. S., Ioannidis, J. P., Mokrysz, C., Nosek, B. A., Flint, J., Robinson, E. S., Munafò, M. R., 2013. Power failure: why small sample size undermines the reliability of neuroscience. Nat Rev Neurosci 14, 365–376.

Buxton, R. B., 2009. Introduction to functional magnetic resonance imaging: principles and techniques. Cambridge university press.

Caspers, S., Eickhoff, S. B., Geyer, S., Scheperjans, F., Mohlberg, H., Zilles, K., Amunts, K., 2008. The human inferior parietal lobule in stereotaxic space. Brain Structure and Function 212 (6), 481–495.

Caspers, S., Geyer, S., Schleicher, A., Mohlberg, H., Amunts, K., Zilles, K., 2006. The human inferior parietal cortex: cytoarchitectonic parcellation and interindividual variability. NeuroImage 33 (2), 430–448.

Catricalà, E., Della Rosa, P. A., Parisi, L., Zippo, A. G., Borsa, V. M., Iadanza, A., Castiglioni, I., Falini, A., Cappa, S. F., 2015. Functional correlates of preserved naming performance in amnestic mild cognitive impairment. Neuropsychologia, in press.

Cecchi, G. A., Rao, A. R., Centeno, M. V., Baliki, M., Apkarian, A. V., Chialvo, D. R., 2007. Identifying directed links in large scale functional networks: application to brain fMRI. BMC Cell Biol 8 Suppl 1, S5.

Chertkow, H., Bub, D., Deaudon, C., Whitehead, V., 1997. On the status of object concepts in aphasia. Brain and language 58 (2), 203–232.

Cohen, L., Dehaene, S., Naccache, L., Lehéricy, S., Dehaene-Lambertz, G., Hénaff, M.-A., Michel, F., 2000. The visual word form area spatial and temporal characterization of an initial stage of reading in normal subjects and posterior split-brain patients. Brain 123 (2), 291–307.

Cohen, L., Lehéricy, S., Chochon, F., Lemer, C., Rivaud, S., Dehaene, S., 2002. Language-specific tuning of visual cortex? functional properties of the visual word form area. Brain 125 (5), 1054–1069.

Corbett, F., Jefferies, E., Ehsan, S., Ralph, M. A. L., 2009. Different impairments of semantic cognition in semantic dementia and semantic aphasia: evidence from the non-verbal domain. Brain 132 (9), 2593–2608.

Corbett, F., Jefferies, E., Ralph, M. A. L., 2011. Deregulated semantic cognition follows prefrontal and temporo-parietal damage: evidence from the impact of task constraint on nonverbal object use. Journal of Cognitive Neuroscience 23 (5), 1125–1135.

Cristescu, T. C., Devlin, J. T., Nobre, A. C., 2006. Orienting attention to semantic categories. NeuroImage 33 (4), 1178–1187.

Damoiseaux, J. S., Greicius, M. D., 2009. Greater than the sum of its parts: a review of studies combining structural connectivity and resting-state functional connectivity. Brain Structure and Function 213 (6), 525–533.

de Haan, W., van der Flier, W. M., Wang, H., Van Mieghem, P. F., Scheltens, P., Stam, C. J., 2012. Disruption of functional brain networks in Alzheimer's disease: what can we learn from graph spectral analysis of resting-state magnetoencephalography? Brain connectivity 2 (2), 45–55.

De Luca, M., Beckmann, C., De Stefano, N., Matthews, P., Smith, S. M., 2006. fMRI resting state networks define distinct modes of long-distance interactions in the human brain. NeuroImage 29 (4), 1359–1367.

Demb, J., Desmond, J., Wagner, A., Vaidya, C., Glover, G., Gabrieli, J., 1995. Semantic encoding and retrieval in the left inferior prefrontal cortex: a functional MRI study of task difficulty and process specificity. J. Neurosci. 15 (9), 5870–5878.

Démonet, J.-F., Thierry, G., Cardebat, D., 2005. Renewal of the neurophysiology of language: functional neuroimaging. Physiological reviews 85 (1), 49–95.

Derrfuss, J., Brass, M., Neumann, J., Von Cramon, D. Y., 2005. Involvement of the inferior frontal junction in cognitive control: Meta-analyses of switching and stroop studies. Human brain mapping 25 (1), 22–34.

Deuker, L., Bullmore, E. T., Smith, M., Christensen, S., Nathan ,P. J., Rockstroh, B., Bassett, D., 2009. Reproducibility of graph metrics of human brain functional networks. NeuroImage 47 (4), 1460–1468.

Di, X., Biswal, B. B., 2014. Identifying the default mode network structure using dynamic causal modeling on resting-state functional magnetic resonance imaging. NeuroImage 86, 53–59.

Dosenbach, N. U., Nardos, B., Cohen, A. L., Fair, D. A., Power, J. D., Church, J. A., Nelson, S. M., Wig, G. S., Vogel, A. C., Lessov-Schlaggar, C. N., et al., 2010. Prediction of individual brain maturity using fMRI. Science 329 (5997), 1358–1361.

Dupont P., Nelissen N., Vandenbulcke M., Vandenberghe R. 2008. The anatomical variability of the associative-semantic network. Program No. 868.18. 2008 Neuroscience Meeting Planner. Washington, DC: Society for Neuroscience, 2008. Online.

Eguluz, V. M., Chialvo, D. R., Cecchi, G. A., Baliki, M., Apkarian, A. V., 2005. Scale-free brain functional networks. Phys Rev Lett 94 (1), 018102.

Euler, L., 1741. Solutio problematis ad geometriam situs pertinentis. Commentarii academiae scientiarum Petropolitanae 8, 128–140.

Faria, A., Joel, S., Zhang, Y., Oishi, K., van Zjil, P., Miller, M., Pekar, J., Mori, S., 2012. Atlas-based analysis of resting-state functional connectivity: Evaluation for reproducibility and multi-modal anatomy-function correlation studies. NeuroImage 61, 613–621.

Ferrarini, L., Veer, I. M., Baerends, E., van Tol, M.-J., Renken, R. J., van der Wee, N. J., Veltman, D., Aleman, A., Zitman, F. G., Penninx, B. W., et al., 2009. Hierarchical functional modularity in the resting-state human brain. Human brain mapping 30 (7), 2220–2231.

Finn, J. D., 1974. A general model for multivariate analysis. Holt, Rinehart & Winston.

Folstein, M. F., Folstein, S. E., McHugh, P. R., 1975. Mini-mental state: a practical method for grading the cognitive state of patients for the clinician. Journal of Psychiatric Research 12 (3), 189–198.

Fornito, A., Bullmore, E. T., 2015. Reconciling abnormalities of brain network structure and function in schizophrenia. Current Opinion in Neurobiology 30, 44–50.

Fornito, A., Harrison, B. J., Zalesky, A., Simons, J. S., 2012. Competitive and cooperative dynamics of large-scale brain functional networks supporting recollection. Proceedings of the National Academy of Sciences 109 (31), 12788–12793.

Fornito, A., Zalesky, A., Breakspear, M., 2013. Graph analysis of the human connectome: promise, progress, and pitfalls. NeuroImage 80, 426–444.

Fox, M. D., Snyder, A. Z., Vincent, J. L., Corbetta, M., Van Essen, D. C., Raichle, M. E., 2005. The human brain is intrinsically organized into dynamic, anticorrelated functional networks. Proceedings of the National Academy of Sciences of the United States of America 102 (27), 9673–9678.

Freeman, L. C., 1977. A set of measures of centrality based on betweenness. Sociometry, 35–41.

Friedman, J., Hastie, T., Tibshirani, R., 2008. Sparse inverse covariance estimation with the graphical lasso. Biostatistics 9 (3), 432–441.

Garrison, K. A., Scheinost, D., Finn, E. S., Shen, X., Constable, R. T., 2015. The (in) stability of functional brain network measures across thresholds. NeuroImage, in press.

Ginestet, C. E., Simmons, A., 2011. Statistical parametric network analysis of functional connectivity dynamics during a working memory task. NeuroImage 55 (2), 688–704.

Goldberg, R. F., Perfetti, C. A., Fiez, J. A., Schneider, W., 2007. Selective retrieval of abstract semantic knowledge in left prefrontal cortex. J Neurosci 27 (14), 3790–3798.

Gong, G., He, Y., Concha, L., Lebel, C., Gross, D. W., Evans, A. C., Beaulieu, C., 2009. Mapping anatomical connectivity patterns of human cerebral cortex using in vivo diffusion tensor imaging tractography. Cereb Cortex 19 (3), 524–536.

Greicius, M. D., Supekar, K., Menon, V., Dougherty, R. F., 2009. Resting-state functional connectivity reflects structural connectivity in the default mode network. Cerebral cortex 19 (1), 72–78.

Griswold, M. A., Jakob, P. M., Heidemann, R. M., Nittka, M., Jellus, V., Wang, J., Kiefer, B., Haase, A., 2002. Generalized autocalibrating partially parallel acquisitions (grappa). Magnetic Resonance in Medicine 47 (6), 1202–1210.

Hagmann, P., Cammoun, L., Gigandet, X., Meuli, R., Honey, C. J., Wedeen, V. J., Sporns, O., 2008. Mapping the structural core of human cerebral cortex. PLoS Biol 6 (7), e159.

Hayasaka, S., Laurienti, P. J., 2010. Comparison of characteristics between region- and voxel-based network analyses in resting-state fMRI data. NeuroImage 50 (2), 499–508.

He, B. J., Shulman, G. L., Snyder, A. Z., Corbetta, M., 2007a. The role of impaired neuronal communication in neurological disorders. Current opinion in neurology 20 (6), 655–660.

He, Y., Chen, Z. J., Evans, A. C., 2007b. Small-world anatomical networks in the human brain revealed by cortical thickness from MRI. Cereb Cortex 17 (10), 2407–2419.

He, Y., Chen, Z., Evans, A., 2008. Structural insights into aberrant topological patterns of large-scale cortical networks in Alzheimer's disease. The Journal of neuroscience 28 (18), 4756–4766.

He, Y., Evans, A., 2010. Graph theoretical modeling of brain connectivity. Current opinion in neurology 23 (4), 341–350.

Heitger, M. H., Ronsse, R., Dhollander, T., Dupont, P., Caeyenberghs, K., Swinnen, S. P., 2012. Motor learning-induced changes in functional brain connectivity as revealed by means of graph-theoretical network analysis. NeuroImage 61 (3), 633–650.

Hellyer, P. J., Woodhead, Z. V., Leech, R., Wise, R. J., 2011. An investigation of twenty/20 vision in reading. The Journal of Neuroscience 31 (41), 14631–14638.

Hilgetag, C.-C., Burns, G. A., O'Neill, M. A., Scannell, J. W., Young, M. P., 2000. Anatomical connectivity defines the organization of clusters of cortical areas in the macaque and the cat. Philosophical Transactions of the Royal Society of London B: Biological Sciences 355 (1393), 91–110.

Hodges, J., Patterson, K., Oxbury, S., Funnell, E., 1992. Semantic dementia. progressive fluent aphasia with temporal lobe atrophy. Brain 115 (Pt 6), 1783–1806.

Holme, P., Park, S. M., Kim, B. J., Edling, C. R., 2007. Korean university life in a network perspective: Dynamics of a large affiliation network. Physica A: Statistical Mechanics and its Applications 373, 821–830.

Honey, C., Sporns, O., Cammoun, L., Gigandet, X., Thiran, J.-P., Meuli, R., Hagmann, P., 2009. Predicting human resting-state functional connectivity from structural connectivity. Proceedings of the National Academy of Sciences 106 (6), 2035–2040.

Hosseini, S., Black, J. M., Soriano, T., Bugescu, N., Martinez, R., Raman, M. M., Kesler, S. R., Hoeft, F., 2013. Topological properties of large-scale structural brain networks in children with familial risk for reading difficulties. NeuroImage 71, 260–274.

Howard, D., Patterson, K. E., 1992. The Pyramids and Palm Trees Test: A test of semantic access from words and pictures. Thames Valley Test Company.

Jefferies, E., Lambon Ralph, M., 2006. Semantic impairment in stroke aphasia versus semantic dementia: a case-series comparison. Brain 129 (8), 2132–2147.

Ji, S., 2011. Computational network analysis of the anatomical and genetic organizations in the mouse brain. Bioinformatics 27 (23), 3293–3299.

Jobard, G., Crivello, F., Tzourio Mazoyer, N., 2003. Evaluation of the dual route theory of reading: a metanalysis of 35 neuroimaging studies. NeuroImage 20 (2), 693–712.

Kaiser, M., Hilgetag, C. C., 2006. Nonoptimal component placement, but short processing paths, due to long-distance projections in neural systems. PloS Computational Biology 2 (7), e95.

Kamada, T., Kawai, S., 1989. An algorithm for drawing general undirected graphs. Information processing letters 31 (1), 7–15.

Karunanayaka, P., Eslinger, P. J., Wang, J.-L., Weitekamp, C. W., Molitoris, S., Gates, K. M., Molenaar, P., Yang, Q. X., 2014. Networks involved in olfaction and their dynamics using independent component analysis and unified structural equation modeling. Human brain mapping 35 (5), 2055–2072.

Kintali, S., 2008. Betweenness centrality: Algorithms and lower bounds. Arxiv preprint arXiv:0809.1906.

Latora, V., Marchiori, M., 2001. Efficient behavior of small-world networks. Phys Rev Lett 87 (19), 198701.

Latora, V., Marchiori, M., 2003. Economic small-world behavior in weighted networks. The European Physical Journal B Condensed Matter and Complex Systems 32 (2), 249–263.

Lauro-Grotto, R., Piccini, C., Shallice, T., 1997. Modality-specific operations in semantic dementia. Cortex 33 (4), 593–622.

Li, H., Xue, Z., Ellmore, T. M., Frye, R. E., Wong, S. T., 2014. Network-based analysis reveals stronger local diffusion-based connectivity and different correlations with oral language skills in brains of children with high functioning autism spectrum disorders. Hum Brain Mapp 35 (2), 396–413.

Li, L., Rilling, J., Preuss, T., Glasser, M., Damen, F., Hu, X., 2012. Quantitative assessment of a framework for creating anatomical brain networks via global tractography. NeuroImage 61 (4), 1017–1030.

Lindauer, U., Dirnagl, U., Füchtemeier, M., Böttiger, C., Offenhauser, N., Leithner, C., Royl, G., 2010. Pathophysiological interference with neurovascular coupling – when imaging based on hemoglobin might go blind. Frontiers in Neuroenergetics 2, 25.

Liu, J., Zhao, L., Nan, J., Li, G., Xiong, S., von Deneen, K. M., Gong, Q., Liang, F., Qin, W., Tian, J., 2013. The trade-off between wiring cost and network topology in white matter structural networks in health and migraine. Experimental Neurology 248, 196–204.

Liuzzi, A. G., Bruffaerts, R., Dupont, P., Adamczuk, K., Peeters, R., De Deyne, S., Storms, G., Vandenberghe, R., 2015. Left perirhinal cortex codes for similarity in meaning between written words: Comparison with auditory word input. Neuropsychologia, in press.

Lo, C.-Y., Wang, P.-N., Chou, K.-H., Wang, J., He, Y., Lin, C.-P., 2010. Diffusion tensor tractography reveals abnormal topological organization in structural cortical networks in Alzheimer's disease. The Journal of Neuroscience 30 (50), 16876–16885.

Ma, S., Calhoun, V. D., Eichele, T., Du, W., Adalı, T., 2012. Modulations of functional connectivity in the healthy and schizophrenia groups during task and rest. NeuroImage 62 (3), 1694–1704.

Marrelec, G., Kim, J., Doyon, J., Horwitz, B., 2009. Large-scale neural model validation of partial correlation analysis for effective connectivity investigation in functional MRI. Human brain mapping 30 (3), 941–950.

Marrelec, G., Krainik, A., Duffau, H., Plgrini-Issac, M., Lehricy, S., Doyon, J., Benali, H., 2006. Partial correlation for functional brain interactivity investigation in functional MRI. NeuroImage 32 (1), 228–237.

Martino, J., Brogna, C., Robles, S. G., Vergani, F., Duffau, H., 2010. Anatomic dissection of the inferior fronto-occipital fasciculus revisited in the lights of brain stimulation data. Cortex 46 (5), 691–699.

Maslov, S., Sneppen, K., 2002. Specificity and stability in topology of protein networks. Science Signalling 296 (5569), 910–913.

McKhann, G., Drachman, D., Folstein, M., Katzman, R., Price, D., Stadlan, E. M., 1984. Clinical diagnosis of Alzheimer's disease Report of the NINCDS-ADRDA Work Group under the auspices of Department of Health and Human Services Task Force on Alzheimer's Disease. Neurology 34 (7), 939–939.

Meinshausen, N., Bühlmann, P., 2006. High-dimensional graphs and variable selection with the lasso. The Annals of Statistics 34 (3), 1436–1462.

Meinshausen, N., Bühlmann, P., 2010. Stability selection. Journal of the Royal Statistical Society: Series B (Statistical Methodology) 72 (4), 417–473.

Meskaldji, D. E., Fischi-Gomez, E., Griffa, A., Hagmann, P., Morgenthaler, S., Thiran, J.-P., 2013. Comparing connectomes across subjects and populations at different scales. NeuroImage 80, 416–425.

Mesulam, M.-M., 1998. From sensation to cognition. Brain 121 (6), 1013–1052.

Mesulam, M., 2008. Representation, inference, and transcendent encoding in neurocognitive networks of the human brain. Annals of neurology 64 (4), 367–378.

Meunier, D., Achard, S., Morcom, A., Bullmore, E., 2009a. Age-related changes in modular organization of human brain functional networks. NeuroImage 44 (3), 715–723.

Meunier, D., Lambiotte, R., Fornito, A., Ersche, K. D., Bullmore, E. T., 2009b. Hierarchical modularity in human brain functional networks. Frontiers in Neuroinformatics 3,37.

Micheloyannis, S., Pachou, E., Stam, C. J., Breakspear, M., Bitsios, P., Vourkas, M., Erimaki, S., Zervakis, M., 2006. Small-world networks and disturbed functional connectivity in schizophrenia. Schizophr Res 87 (1-3), 60–66.

Micheloyannis, S., Vourkas, M., Tsirka, V., Karakonstantaki, E., Kanatsouli, K., Stam, C. J., 2009. The influence of ageing on complex brain networks: a graph theoretical analysis. Hum Brain Mapp 30 (1), 200–208.

Miyajima, K., Sakuragawa, T., 2014. Continuous and robust clustering coefficients for weighted and directed networks. arXiv preprint arXiv:1412.0059.

Molenberghs, P., Gillebert, C. R., Peeters, R., Vandenberghe, R., 2008. Convergence between lesion-symptom mapping and functional magnetic resonance imaging of spatially selective attention in the intact brain. The Journal of Neuroscience 28 (13), 3359–3373.

Moussa, M. N., Steen, M. R., Laurienti, P. J., Hayasaka, S., 2012. Consistency of network modules in resting-state fMRI connectome data. PLoS ONE 7 (8), e44428.

Muller, A. M., Meyer, M., 2014. Language in the brain at rest: new insights from resting state data and graph theoretical analysis. Frontiers in human neuroscience 8.

Nakamura, T., Hillary, F. G., Biswal, B. B., 2009. Resting network plasticity following brain injury. PloS one 4 (12).

Nelissen, N., Dupont, P., Vandenbulcke, M., Tousseyn, T., Peeters, R., Vandenberghe, R., 2011. Right hemisphere recruitment during language processing in frontotemporal lobar degeneration and Alzheimer's disease. J Mol Neurosci 45 (3), 637–647.

Nelissen, N., Pazzaglia, M., Vandenbulcke, M., Sunaert, S., Fannes, K., Dupont, P., Aglioti, S. M., Vandenberghe, R., 2010. Gesture discrimination in primary progressive aphasia: The intersection between gesture and language processing pathways. The Journal of Neuroscience 30 (18), 6334–6341.

Nelissen, N., Van Laere, K., Thurfjell, L., Owenius, R., Vandenbulcke, M., Koole, M., Bormans, G., Brooks, D. J., Vandenberghe, R., 2009. Phase 1 study of the pittsburgh compound B derivative ^{18}F-flutemetamol in healthy volunteers and patients with probable Alzheimer disease. J Nucl Med 50 (8), 1251–1259.

Nelissen, N., Vandenbulcke, M., Fannes, K., Verbruggen, A., Peeters, R., Dupont, P., Van Laere, K., Bormans, G., Vandenberghe, R., 2007. $A\beta$ amyloid deposition in the language system and how the brain responds. Brain 130 (8), 2055–2069.

Nelson, S. M., Cohen, A. L., Power, J. D., Wig, G. S., Miezin, F. M., Wheeler, M. E., Velanova, K., Donaldson, D. I., Phillips, J. S., Schlaggar, B. L., et al., 2010. A parcellation scheme for human left lateral parietal cortex. Neuron 67 (1), 156–170.

Newman, M. E., 2001. Who is the best connected scientist? A study of scientific coauthorship networks. Phys. Rev. E 64 (016131).

Newman, M., 2006a. Finding community structure in networks using the eigenvectors of matrices. Physical review E 74 (3), 036104.

Newman, M. E., 2006b. Modularity and community structure in networks. Proceedings of the National Academy of Sciences 103 (23), 8577–8582.

Niu, H., He, Y., 2013. Resting-state functional brain connectivity lessons from functional near-infrared spectroscopy. The Neuroscientist, 1073858413502707.

Niu, H., Li, Z., Liao, X., Wang, J., Zhao, T., Shu, N., Zhao, X., He, Y., 2013. Test-retest reliability of graph metrics in functional brain networks: a resting-state fNIRS study. PloS one 8 (9), e72425.

Noonan, K. A., Jefferies, E., Corbett, F., Ralph, M. A. L., 2010. Elucidating the nature of deregulated semantic cognition in semantic aphasia: Evidence for the roles of prefrontal and temporo-parietal cortices. Journal of Cognitive Neuroscience 22 (7), 1597–1613.

Onnela, J.-P., Saramäki, J., Kertész, J., Kaski, K., 2005. Intensity and coherence of motifs in weighted complex networks. Phys. Rev. E 71, 065103.

Opsahl, T., Panzarasa, P., 2009. Clustering in weighted networks. Social networks 31 (2), 155–163.

Owen, J. P., Ziv, E., Bukshpun, P., Pojman, N., Wakahiro, M., Berman, J. I., Roberts, T. P., Friedman, E. J., Sherr, E. H., Mukherjee, P., 2013. Test–retest reliability of computational network measurements derived from the structural connectome of the human brain. Brain connectivity 3 (2), 160–176.

Palla, G., Barabási, A.-L., Vicsek, T., 2007. Quantifying social group evolution. Nature 446 (7136), 664–667.

Palla, G., Derényi, I., Farkas, I., Vicsek, T., 2005. Uncovering the overlapping community structure of complex networks in nature and society. Nature 435 (7043), 814–818.

Penny, W. D., Stephan, K., Mechelli, A., Friston, K., 2004. Comparing dynamic causal models. NeuroImage 22 (3), 1157–1172.

Phillips, D. J., McGlaughlin, A., Ruth, D., Jager, L. R., Soldan, A., Initiative, A. D. N., et al., 2015. Graph theoretic analysis of structural connectivity across the spectrum of Alzheimers disease: the importance of graph creation methods. NeuroImage: Clinical, in press.

Poldrack, R. A., Mumford, J. A., Nichols, T. E., 2011. Handbook of functional MRI data analysis. Cambridge University Press.

Pons, P., Latapy, M., 2005. Computing communities in large networks using random walks. In: Computer and Information Sciences-ISCIS 2005. Springer, pp. 284–293.

Ponten, S., Daffertshofer, A., Hillebrand, A., Stam, C. J., 2010. The relationship between structural and functional connectivity: graph theoretical analysis of an EEG neural mass model. NeuroImage 52 (3), 985–994.

Power, J., Cohen, A., Nelson, S., Wig, G., Barnes, K., Church, J., Vogel, A., Laumann, T., Miezin, F., Schlaggar, B., et al., 2011. Functional network organization of the human brain. Neuron 72 (4), 665–678.

Power, J. D., Schlaggar, B. L., Lessov-Schlaggar, C. N., Petersen, S. E., 2013. Evidence for hubs in human functional brain networks. Neuron 79 (4), 798–813.

Price, C. J., Devlin, J. T., 2003. The myth of the visual word form area. NeuroImage 19 (3), 473–481.

Price, C. J., Devlin, J. T., 2011. The interactive account of ventral occipitotemporal contributions to reading. Trends in cognitive sciences 15 (6), 246–253.

Qin, Y., Li, Y., Zhang, S., Xiong, Y., Guo, L., Yang, S., Yao, Y., Li, W., Zhu, W., et al., 2015. Frequency-specific alterations of large-scale functional brain networks in patients with Alzheimer's disease. Chinese medical journal 128 (5), 602.

Ralph, M. A. L., Sage, K., Jones, R. W., Mayberry, E. J., 2010. Coherent concepts are computed in the anterior temporal lobes. Proceedings of the National Academy of Sciences 107 (6), 2717–2722.

Ramsey, J. D., Hanson, S. J., Hanson, C., Halchenko, Y. O., Poldrack, R. A., Glymour, C., 2010. Six problems for causal inference from fMRI. NeuroImage 49 (2), 1545–1558.

Rissman, J., Gazzaley, A., D'Esposito, M., 2004. Measuring functional connectivity during distinct stages of a cognitive task. NeuroImage 23 (2), 752–763.

Rogers, T. T., McClelland, J. L., 2004. Semantic cognition: A parallel distributed processing approach. MIT press.

Rosvall, M., Bergstrom, C. T., 2008. Maps of random walks on complex networks reveal community structure. Proceedings of the National Academy of Sciences 105 (4), 1118–1123.

Rubinov, M., Sporns, O., 2010. Complex network measures of brain connectivity: uses and interpretations. NeuroImage 52 (3), 1059–1069.

Rubinov, M., Sporns, O., 2011. Weight-conserving characterization of complex functional brain networks. NeuroImage 56 (4), 2068–2079.

Sala-Llonch, R., Junqué, C., Arenaza-Urquijo, E. M., Vidal-Piñeiro, D., Valls-Pedret, C., Palacios, E. M., Domènech, S., Salvà, A., Bargalló, N., Bartrés-Faz, D., 2014. Changes in whole-brain functional networks and memory performance in aging. Neurobiology of aging, in press.

Salvador, R., Suckling, J., Coleman, M. R., Pickard, J. D., Menon, D., Bullmore, E., 2005. Neurophysiological architecture of functional magnetic resonance images of human brain. Cereb Cortex 15 (9), 1332–1342.

Saramäki, J., Kivelä, M., Onnela, J.-P., Kaski, K., Kertesz, J., 2007. Generalizations of the clustering coefficient to weighted complex networks. Physical Review E 75 (2), 027105.

Sarubbo, S., De Benedictis, A., Maldonado, I. L., Basso, G., Duffau, H., 2013. Frontal terminations for the inferior fronto-occipital fascicle: anatomical dissection, DTI study and functional considerations on a multi-component bundle. Brain Structure and Function 218 (1), 21–37.

Schmahmann, J. D., Pandya, D., 2009. Fiber pathways of the brain. Oxford University Press.

Schwarz, A. J., Gozzi, A., Bifone, A., 2008. Community structure and modularity in networks of correlated brain activity. Magnetic resonance imaging 26 (7), 914–920.

Schwarz, A. J., McGonigle, J., 2011. Negative edges and soft thresholding in complex network analysis of resting state functional connectivity data. NeuroImage 55 (3), 1132–1146.

Seghier, M. L., Friston, K. J., 2013. Network discovery with large DCMs. NeuroImage 68. 181–191.

Seghier, M. L., Friston, K. J., Price, C. J., 2007. Detecting subject-specific activations using fuzzy clustering. NeuroImage 36 (3), 594–605.

Seghier, M. L., Price, C. J., 2011. Explaining left lateralization for words in the ventral occipitotemporal cortex. The Journal of Neuroscience 31 (41), 14745–14753.

Seo, E. H., Lee, D. Y., Lee, J.-M., Park, J.-S., Sohn, B. K., Lee, D. S., Choe, Y. M., Woo, J. I., 2013. Whole-brain functional networks in cognitively normal, mild cognitive impairment, and Alzheimers disease. PloS one 8 (1), e53922.

Shen, X., Tokoglu, F., Papademetris, X., Constable, R. T., 2013. Groupwise whole-brain parcellation from resting-state fMRI data for network node identification. NeuroImage 82, 403–415.

Shi, L., Wang, D., Chu, W. C., Liu, S., Xiong, Y., Wang, Y., Wang, Y., Wong, L. K., Mok, V. C., 2013. Abnormal organization of white matter network in patients with no dementia after ischemic stroke. PloS one 8 (12), e81388.

Shih, Y.-K., Parthasarathy, S., 2012. Identifying functional modules in interaction networks through overlapping markov clustering. Bioinformatics 28 (18), i473–i479.

Shrout, P. E., Fleiss, J. L., 1979. Intraclass correlations: uses in assessing rater reliability. Psychological bulletin 86 (2), 420.

Simon, H. A., 1996. The sciences of the artificial. MIT press.

Smit, D. J., Stam, C. J., Posthuma, D., Boomsma, D. I., De Geus, E. J., 2008. Heritability of small-world networks in the brain: A graph theoretical analysis of resting-state EEG functional connectivity. Human brain mapping 29 (12), 1368–1378.

Smith, S. M., Fox, P. T., Miller, K. L., Glahn, D. C., Fox, P. M., Mackay, C. E., Filippini, N., Watkins, K. E., Toro, R., Laird, A. R., et al., 2009. Correspondence of the brain's functional architecture during activation and rest. Proceedings of the National Academy of Sciences 106 (31), 13040–13045.

Smith, S. M., Miller, K. L., Salimi-Khorshidi, G., Webster, M., Beckmann, C. F., Nichols, T. E., Ramsey, J. D., Woolrich, M. W., 2011. Network modelling methods for fMRI. NeuroImage 54 (2), 875–891.

Songsiri, J., Vandenberghe, L., 2010. Topology selection in graphical models of autoregressive processes. The Journal of Machine Learning Research 11, 2671–2705.

Sonuga-Barke, E. J., Castellanos, F. X., 2007. Spontaneous attentional fluctuations in impaired states and pathological conditions: a neurobiological hypothesis. Neuroscience & Biobehavioral Reviews 31 (7), 977–986.

Soranzo, N. Bianconi, G., Altafini, C., 2007. Comparing association network algorithms for reverse engineering of large-scale gene regulatory networks: synthetic versus real data. Bioinformatics 23 (13), 1640–1647.

Sporns, O., 2011. Networks of the Brain. MIT press.

Sporns, O., 2013. Network attributes for segregation and integration in the human brain. Current opinion in neurobiology 23 (2), 162–171.

Sporns, O., Honey, C. J., Kötter, R., 2007. Identification and classification of hubs in brain networks. PloS one 2 (10), e1049.

Sporns, O., Zwi, J. D., 2004. The small world of the cerebral cortex. Neuroinformatics 2 (2), 145–162.

Stam, C., De Haan, W., Daffertshofer, A., Jones, B., Manshanden, I., Van Walsum, A. V. C., Montez, T., Verbunt, J., De Munck, J., Van Dijk, B., et al., 2009. Graph theoretical analysis of magnetoencephalographic functional connectivity in Alzheimer's disease. Brain 132 (1), 213–224.

Stam, C., Jones, B., Nolte, G., Breakspear, M., Scheltens, P., 2007. Small-world networks and functional connectivity in Alzheimer's disease. Cerebral cortex 17 (1), 92–99.

Stam, C. J., 2004. Functional connectivity patterns of human magnetoencephalographic recordings: a small-world network? Neuroscience letters 355 (1), 25–28.

Steen, M., Hayasaka, S., Joyce, K., Laurienti, P., 2011. Assessing the consistency of community structure in complex networks. Physical Review E 84 (1), 016111.

Stifanelli, P., Creanza, T., Anglani, R., Liuzzi, V., Mukherjee, S., Ancona, N., 2011. A comparative study of gaussian graphical model approaches for genomic data. Arxiv preprint arXiv:1107.0261.

Stifanelli, P. F., Creanza, T. M., Anglani, R., Liuzzi, V. C., Mukherjee, S., Schena, F. P., Ancona, N., 2013. A comparative study of covariance selection models for the inference of gene regulatory networks. Journal of biomedical informatics 46 (5), 894–904.

Supekar, K., Menon, V., Rubin, D., Musen, M., Greicius, M. D., et al., 2008. Network analysis of intrinsic functional brain connectivity in Alzheimers disease. PLoS Comput Biol 4 (6), e1000100.

Telesford, Q. K., Burdette, J. H., Laurienti, P. J., 2013. An exploration of graph metric reproducibility in complex brain networks. Frontiers in neuroscience 7, 67.

Telesford, Q. K., Morgan, A. R., Hayasaka, S., Simpson, S. L., Barret, W., Kraft, R. A., Mozolic, J. L., Laurienti, P. J., 2010. Reproducibility of graph metrics in fMRI networks. Frontiers in neuroinformatics 4, 117.

Thierry, G., Price, C. J., 2006. Dissociating verbal and nonverbal conceptual processing in the human brain. Journal of Cognitive Neuroscience 18 (6), 1018–1028.

Tijms, B. M., Möller, C., Vrenken, H., Wink, A. M., de Haan, W., van der Flier, W. M., Stam, C. J., Scheltens, P., Barkhof, F., 2013. Single-subject grey matter graphs in Alzheimer's disease. PloS one 8 (3), e58921.

Tijms, B. M., Seriès, P., Willshaw, D. J., Lawrie, S. M., 2012. Similarity-based extraction of individual networks from gray matter MRI scans. Cerebral Cortex 22 (7), 1530–1541.

Toussaint, P.-J., Maiz, S., Coynel, D., Doyon, J., Messé, A., de Souza, L. C., Sarazin, M., Perlbarg, V., Habert, M.-O., Benali, H., 2014. Characteristics of the default mode functional connectivity in normal ageing and Alzheimer's disease using resting state fMRI with a combined approach of entropy-based and graph theoretical measurements. NeuroImage 101, 778–786.

Turk-Browne, N. B., 2013. Functional interactions as big data in the human brain. Science 342 (6158), 580–584.

Uylings, H., Rajkowska, G., Sanz-Arigita, E., Amunts, K., Zilles, K., 2005. Consequences of large interindividual variability for human brain atlases: converging macroscopical imaging and microscopical neuroanatomy. Anatomy and embryology 210 (5-6), 423–431.

Vaessen, M., Hofman, P., Tijssen, H., Aldenkamp, A., Jansen, J., Backes, W., 2010. The effect and reproducibility of different clinical DTI gradient sets on small world brain connectivity measures. NeuroImage 51 (3), 1106–1116.

Vaessen, M. J., Jansen, J. F., Braakman, H. M., Hofman, P. A., De Louw, A., Aldenkamp, A. P., Backes, W. H., 2014. Functional and structural network impairment in childhood frontal lobe epilepsy. PloS one 9 (3), e90068.

van den Heuvel, M. P., Mandl, R. C., Stam, C. J., Kahn, R. S., Pol, H. E. H., 2010. Aberrant frontal and temporal complex network structure in schizophrenia: a graph theoretical analysis. The Journal of Neuroscience 30 (47), 15915–15926.

van den Heuvel, M. P., Stam, C. J., Boersma, M., Pol, H. H., 2008. Small-world and scale-free organization of voxel-based resting-state functional connectivity in the human brain. NeuroImage 43 (3), 528–539.

van den Heuvel, M., Mandl, R., Luigjes, J., Pol, H. H., 2008. Microstructural organization of the cingulum tract and the level of default mode functional connectivity. The Journal of neuroscience 28 (43), 10844–10851.

van den Heuvel, M. P., Mandl, R. C., Kahn, R. S., Pol, H., Hilleke, E., 2009. Functionally linked resting-state networks reflect the underlying structural connectivity architecture of the human brain. Human brain mapping 30 (10), 3127–3141.

Van Doren, L., Dupont, P., De Grauwe, S., Peeters, R., Vandenberghe, R., 2010. The amodal system for conscious word and picture identification in the absence of a semantic task. NeuroImage 49 (4), 3295–3307.

Van Doren, L., Schrooten, M., Adamczuk, K., Dupont, P., Vandenberghe, R., 2012. Chronometry of word and picture identification: Common and modality-specific effects. NeuroImage 59 (4), 3701–3712.

Van Wijk, B. C., Stam, C. J., Daffertshofer, A., 2010. Comparing brain networks of different size and connectivity density using graph theory. PLoS One 5 (10), e13701.

Vandenberghe, R., Geeraerts, S., Molenberghs, P., Lafosse, C., Vandenbulcke, M., Peeters, K., Peeters, R., Van Hecke, P., Orban, G., 2005. Attentional responses to unattended stimuli in human parietal cortex. Brain 128 (12), 2843–2857.

Vandenberghe, R., Gillebert, C., 2009. Parcellation of human parietal cortex: converging evidence from functional imaging in the intact human brain and patient lesion studies. Behav Brain Res 199, 171–182.

Vandenberghe, R., Price, C., Wise, R., Josephs, O., Frackowiak, R., 1996. Functional anatomy of a common semantic system for words and pictures. Nature 383 (6597), 254–256.

Vandenberghe, R., Wang, Y., Nelissen, N., Vandenbulcke, M., Dhollander, T., Sunaert, S., Dupont, P., 2013. The associative-semantic network for words and pictures: Effective connectivity and graph analysis. Brain Lang 127(2), 264–72.

Vandenbulcke, M., Peeters, R., Dupont, P., Van Hecke, P., Vandenberghe, R., 2007. Word reading and posterior temporal dysfunction in amnestic mild cognitive impairment. Cereb Cortex 17 (3), 542–551.

Vandenbulcke, M., Peeters, R., Fannes, K., Vandenberghe, R., 2006. Knowledge of visual attributes in the right hemisphere. Nat Neurosci 9 (7), 964–970.

Vandenbulcke, M., Peeters, R., Van Hecke, P., Vandenberghe, R., 2005. Anterior temporal laterality in primary progressive aphasia shifts to the right. Annals of neurology 58 (3), 362–370.

Varoquaux, G., Thirion, B., 2012. Statistical learning for resting-state fMRI: Successes and challenges. In: Machine Learning and Interpretation in Neuroimaging. Springer, pp. 172–177.

Vinckier, F., Dehaene, S., Jobert, A., Dubus, J. P., Sigman, M., Cohen, L., 2007. Hierarchical coding of letter strings in the ventral stream: dissecting the inner organization of the visual word-form system. Neuron 55 (1), 143–156.

Visser, M., Embleton, K., Jefferies, E., Parker, G., Ralph, M. L., 2010. The inferior, anterior temporal lobes and semantic memory clarified: novel evidence from distortion-corrected fMRI. Neuropsychologia 48 (6), 1689–1696.

Visser, M., Jefferies, E., Embleton, K., Lambon Ralph, M., 2012a. Both the middle temporal gyrus and the ventral anterior temporal area are crucial for multimodal semantic processing: distortion-corrected fMRI evidence for a double gradient of information convergence in the temporal lobes. Journal of Cognitive Neuroscience 24 (8), 1766–1778.

Visser, M., Ralph, M. L., 2011. Differential contributions of bilateral ventral anterior temporal lobe and left anterior superior temporal gyrus to semantic processes. Journal of Cognitive Neuroscience 23 (10), 3121–3131.

Wagner, A., Desmond, J., Demb, J., Glover, G., Gabrieli, J., 1997. Semantic repetition priming for verbal and pictorial knowledge: A functional MRI study of left inferior prefrontal cortex. J Cogn Neurosci 9 (6), 714–726.

Wang, J., Zuo, X., Dai, Z., Xia, M., Zhao, Z., Zhao, X., Jia, J., Han, Y., He, Y., 2013. Disrupted functional brain connectome in individuals at risk for Alzheimer's disease. Biological psychiatry 73 (5), 472–481.

Wang, J.-H., Zuo, X.-N., Gohel, S., Milham, M. P., Biswal, B. B., He, Y., 2011. Graph theoretical analysis of functional brain networks: test-retest evaluation on short- and long-term resting-state functional MRI data. PLoS One 6 (7), e21976.

Wang, L., Li, Y., Metzak, P., He, Y., Woodward, T. S., 2010. Age-related changes in topological patterns of large-scale brain functional networks during memory encoding and recognition. NeuroImage 50 (3), 862–872.

Wang, Y., Nelissen, N., Adamczuk, K., De Weer, A.-S., Vandenbulcke, M., Sunaert, S., Vandenberghe, R., Dupont, P., 2014. Reproducibility and robustness of graph measures of the associative-semantic network. PloS one 9 (12), e115215.

Wang, Y., Nelissen, N., Adamczuk, K., De Weer, A.-S., Vandenbulcke, M., Sunaert, S., Vandenberghe, R., Dupont, P., 2015a. Graph analysis of the associative-semantic network at different levels of granularity. *Submitted*.

Wang, Y., Vandenberghe, R., Dupont, P., 2015b. Generalization of clustering coefficient and local efficiency for fully weighted undirected networks. *Submitted*.

Watts, D. J., Strogatz, S. H., 1998. Collective dynamics of small-worldnetworks. Nature 393 (6684), 440–442.

Weber, M. J., Detre, J. A., Thompson-Schill, S. L., Avants, B. B., 2013. Reproducibility of functional network metrics and network structure: a comparison of task-related bold, resting asl with bold contrast, and resting cerebral blood flow. Cognitive, Affective, & Behavioral Neuroscience 13 (3), 627–640.

Wen, X., Rangarajan, G., Ding, M., 2013. Is granger causality a viable technique for analyzing fMRI data? PLoS One 8 (7), e67428.

Whitney, C., Kirk, M., O'Sullivan, J., Lambon Ralph, M. A., Jefferies, E., May 2011. The neural organization of semantic control: TMS evidence for a distributed network in left inferior frontal and posterior middle temporal gyrus. Cereb Cortex 21 (5), 1066–1075.

Whitney, C., Kirk, M., O'Sullivan, J., Lambon Ralph, M. A., Jefferies, E., 2012. Executive semantic processing is underpinned by a large-scale neural network: revealing the contribution of left prefrontal, posterior temporal, and parietal cortex to controlled retrieval and selection using TMS. J Cogn Neurosci 24 (1), 133–147.

Wise, R. J., Scott, S. K., Blank, S. C., Mummery, C. J., Murphy, K., Warburton, E. A., 2001. Separate neural subsystems within wernicke's area. Brain 124 (1), 83–95.

Woodhead, Z. V., Brownsett, S. L., Dhanjal, N. S., Beckmann, C., Wise, R. J., 2011. The visual word form system in context. The Journal of Neuroscience 31 (1), 193–199.

Wu, G.-R., Stramaglia, S., Chen, H., Liao, W., Marinazzo, D., 2013. Mapping the voxel-wise effective connectome in resting state fMRI. PloS one 8 (9), e73670.

Wu, X., Li, R., Fleisher, A. S., Reiman, E. M., Guan, X., Zhang, Y., Chen, K., Yao, L., 2011. Altered default mode network connectivity in Alzheimer's diseasea resting functional MRI and bayesian network study. Hum Brain Mapp 32 (11), 1868–1881.

Wylie, K. P., Rojas, D. C., Tanabe, J., Martin, L. F., Tregellas, J. R., 2012. Nicotine increases brain functional network efficiency. NeuroImage 63, 73–80.

Yao, Z., Zhang, Y., Lin, L., Zhou, Y., Xu, C., Jiang, T., Initiative, A. D. N., et al., 2010. Abnormal cortical networks in mild cognitive impairment and Alzheimer's disease. PLoS computational biology 6 (11), e1001006.

Yu, S. X., Shi, J., 2003. Multiclass spectral clustering. In: Computer Vision, 2003. Proceedings. Ninth IEEE International Conference on. IEEE, pp. 313–319.

Zalesky, A., Fornito, A., Bullmore, E., 2012. On the use of correlation as a measure of network connectivity. NeuroImage 60 (4), 2096–2106.

Zhang, B., Horvath, S., 2005. A general framework for weighted gene co-expression network analysis. Statistical applications in genetics and molecular biology 4 (1), 1544–6115.

Zhou, C., Zemanová, L., Zamora, G., Hilgetag, C. C., Kurths, J., 2006. Hierarchical organization unveiled by functional connectivity in complex brain networks. Physical review letters 97 (23), 238103.

Dankwoord

Five years ago, I was investigating aircraft data using Artificial Neural Networks (ANNs), which belong to a family of statistical learning algorithms inspired by the human central nervous system. Fascinated by the power of ANNs and, to be honest, tired of analysing aircraft data, I heard a voice: 'Why not investigate the real neural networks?' That's how the venture began. Passion kindled my enthusiasm for the project, but in itself it could never enable me to go through the significant challenge with ups and downs during the past four years. Prima facie, the credit goes to all those who in one way or another lent their hands in this venture.

> *"None of us got where we are solely by pulling ourselves up by our bootstraps."*
>
> –Thurgood Marshall

I am extremely thankful to Prof. Patrick Dupont, my promotor, for sharing his expertise, providing valuable guidance and offering encouragement. His selfless time and care were sometimes all that kept me going. His meticulous attention to detail drove me to gradually learn to punctuate prose. His constant encouraging words guided me through the difficulties and depressing moments. His timely reminders dragged me out of all the distractions.

I am also grateful to my co-promotor, Prof. Rik Vandenberghe for providing invaluable expertise in neuroscience and insight in integrating graph theory and associative semantic processing.

I have been fortunate to have received the help from the members of my thesis committee – Prof. Rufin Vogels, Prof. Stephan Swinnen, Prof. Daniele Marinazzo, Prof. Martijn van den Heuvel and Prof. Steven Dymarkowski – for their comments to elaborate this thesis and their participation in the examination. The timely feedback and suggestions from my internal jury members, Prof. Rufin Vogels and

Prof. Stephan Swinnen, have kept me on track in pursuing this PhD. It is also a great honour for me to have Prof. Daniele Marinazzo and Prof. Martijn van den Heuvel in my examining committee. The critical and constructive comments and suggestions I received have improved the work substantially. I would also like to thank Prof. Wim Vanduffel for chairing the thesis committee.

"Alone we can do so little; together we can do so much. "

—Helen Keller

Gratitudes go to all colleagues: Kate, François-Laurent, Jan, Jolien, Gabriella, Tatjana, Eshwar, Veerle, Maarten, Rose, Natalie C., Kim and Céline, for providing me with all the necessary data and the fantastic working atmosphere. During the instructive discussions in the office, the delicious moments during lunch and all the parties, and all the fun we have shared elsewhere, many of you are more than colleagues and have become true friends.

I would also like to take this opportunity to express my gratitude to all the department faculty members for their help and support.

"I cannot even imagine where I would be today were it not for that handful of friends who have given me a heart full of joy. Let's face it, friends make life a lot more fun."

–Charles R. Swindoll

Many friends have given their time generously to enrich my life besides research in Leuven. I am especially grateful to Yanyan and Hong, who made our apartment a home for the last three years. I also thank Sayuan, Tina, Jingjing and Yaojuan for sharing a lot of fun with me. With all the trips we had together, Lei Tian and Ling Tong, I am 100% sure that you are the best in shooting pictures of me and I am going to miss you (and your photos) so much. To all my friends in Leuven (Yejun Li, Zhe Li, Jun Li, Haihuai He, Zengjin Huang, Ting Yin, Pengcheng Yan, Xue Wang, Xiaocheng Zhao, Xinwu Wang, Xiaowen Chen, Beatrix-V.): thank you and good luck.

I place on record, my sincere thanks to my friends in China. Being thousands of miles away and seven hours apart, their support, help and love are however always there whenever needed. I owe many thanks to Pu Yang for his support and encouragement. I wish him all the best for the rest of his life.

"A man travels the world over in search of what he needs, and returns home to find it.

– George Moore

Without the unceasing encouragement, support and attention from my family, I would never have completed this. I am grateful to my parents for bearing with my stress and tension at the most daunting stages in this project. Mom and dad, you are and will always be a constant source of inspiration and guidance. My

dear sisters Fei Wang and Shan Wang, I owe too much to both of you ever since our childhood. Your courage to tackle every difficulty in life gives me the strength to hang in there whenever I am on the verge of giving up.

Finally, I am also grateful to my boyfriend, Tiannan, for there is no one like you to echo my thinkings, to cheer me up when I am down, to catch me when I am falling, to push me once I slack off, to inspire me when I am in chaos.

Curriculum vitae

Personal Data

Name: Yu Wang
Address: Herestraat 49, 3000 Leuven, Belgium
Email: yu.wang@med.kuleuven.be
Date of birth: June 22, 1987
Place of birth: Danfeng, China

Education

06/2012 - Present PhD student of Biomedical ScienceS at KU Leuven
10/2011 - 05/2012 International scholar at the laboratory for cognitive neurology, KU Leuven, Belgium
09/2009 - 3/2012 Master of Control Theory and Engineering at Northwestern Polytechnical University, China
09/2005 - 07/2009 Bachelor of Automation at Northwestern Polytechnical University, China

Publication list

Publication in peer-reviewed journals

Rik Vandenberghe, Yu Wang, Natalie Nelissen, Mathieu Vandenbulcke, Thijs Dhollander, Stefan Sunaert, Patrick Dupont (2013) The Associative-Semantic

network for Words and Pictures: Effective Connectivity and Graph analysis. Brain and Language 127(2): 264-72.

Yu Wang, Natalie Nelissen, Katarzyna Adamczuk, An-Sofie DeWeer, Mathieu Vandenbulcke, Stefan Sunaert, Rik Vandenberghe, Patrick Dupont (2014). Reproducibility and Robustness of Graph Measures of the Associative-Semantic Network. Plos One 9: e115215.

Journal articles submitted for publication

Yu Wang, Rik Vandenberghe, Patrick Dupont, Generalization of Clustering Coefficient and Local Efficiency for Fully Weighted Undirected Networks

Yu Wang, Natalie Nelissen, Katarzyna Adamczuk, An-Sofie DeWeer, Mathieu Vandenbulcke, Stefan Sunaert, Rik Vandenberghe, Patrick Dupont. Graph Analysis of the Associative-Semantic Network at Different Levels of Granularity.

Conference abstracts

Yu Wang, Katarzyna Adamczuk, An-Sofie De Weer, Stefan Sunaert, Rik Vandenberghe, Patrick Dupont. Combined Voxel- and Region- based Network Analysis of the Associative-semantic System. The Organization for Human Brain Mapping (OHBM) 2014.

Eshwar Gorakhnath Ghumare, Kathleen Vunckx, Karolien Goffin, Yu Wang, Wim Van Paesschen, Patrick Dupont. FDG-PET Based Connectivity in patients with Mesial Temporal Lobe Epilepsy with Hippocampal Sclerosis. The Organization for Human Brain Mapping (OHBM) 2014.

Yu Wang, Natalie Nelissen, Kate Adamczuk, An-Sofie De Weer, Mathieu Vandenbulcke, Stefan Sunaert, Rik Vandenberghe, Patrick Dupont. Reproducibility of Graph Measures and Functional Connectivity of the Associative-Semantic Network. The Organization for Human Brain Mapping (OHBM) 2013.

Rik Vandenberghe, Yu Wang, Natalie Nelissen, Mathieu Vandenbulcke Patrick Dupont. Effective Connectivity and Graph Analysis of the Associative-Semantic Network. Society for neuroscience (SFN) 2012.

FACULTY OF MEDICINE
DEPARTMENT OF NEUROSCIENCES
LABORATORY FOR COGNITIVE NEUROLOGY
Herestraat 49
B-3000 Leuven